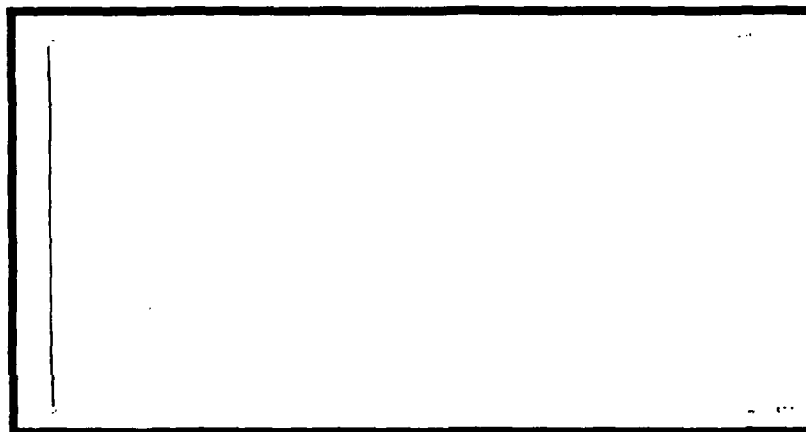AD-A202 724

DEPARTMENT OF THE AIR FORCE

AIR UNIVERSITY

AIR FORCE INSTITUTE OF TECHNOLOGY

Wright-Patterson Air Force Base, Ohio

DTIC
ELECTE
S
E
D

89   1   17   169

AFIT/GE/ENG/88D-41

ROBOTIC TACTILE SENSOR FABRICATED
FROM PIEZOELECTRIC
POLYVINYLIDENE FLUORIDE FILMS

THESIS

Rocky R. Reston
Captain, USAF
AFIT/GE/ENG/88D-41

AFIT/GE/ENG/88D-41

ROBOTIC TACTILE SENSOR FABRICATED FROM PIEZOELECTRIC

POLYVINYLIDENE FLUORIDE FILMS

THESIS

Presented to the Faculty of the School of Engineering

of the Air Force Institute of Technology

Air University

In Fulfillment of the

Requirements for the Degree of

Master of Science in Electrical Engineering

Rocky R. Reston, B.S.E.E.

Captain, USAF

December, 1988

Approved for public release; distribution unlimited

Acknowledgements

Throughout this effort, many people have provided me with assistance in a wide variety of forms. Foremost among them has been my thesis advisor, Maj Edward S. Kolesar. His ideas and technical direction were thought provoking and a source of inspiration; and his skills at finding "just the right phrase" helped to improve the quality of this work. I also appreciate the advice given to me by the other members of my committee, Dr. Matthew Kabrisky, Col Charles Hatsell, and Capt Billy Hodges. I would also like to thank Mr. Donald Smith and Mr. William Troop for their assistance with the equipment in the Cooperative Electronics Laboratory.

Finally, I want to thank my wife, ████ for her patience, understanding and support, and my parents for their guidance and confidence.

Table of Contents

List of Figures

List of Tables

Glossary

A . . . . Area of a Sensor Electrode

AFIT . . . . Air Force Institute of Technology

c . . . . Stiffness Coefficient

C . . . . Coulombs

°C . . . . Degrees Centigrade

CAD . . . . Computer Aided Design

CIF . . . . Caltech Intermediate Form

cm . . . . Centimeters

CMOS . . . . Complementary Metal-Oxide-Semiconductor

d . . . . Piezoelectric Strain Constant

DC . . . . Direct Current

E . . . . Electric Field

F . . . . Force

F . . . . Farads

°F . . . . Degrees Fahrenheit

g, gm . . . . Grams

GND . . . . Ground

GPIB . . . . General Purpose Instrumentation Bus

HCl . . . . Hydrochloric Acid

HP . . . . Hewlett Packard

Hz . . . . Hertz

IC . . . . Integrated Circuit

k . . . . Electro-Mechanical Coupling Factor

Kg . . . . Kilograms

$K\Omega$ . . . . Kilo-Ohms

l . . . . Length of Dipole

LED . . . . Light Emitting Diode

m . . . . Meters

Magic . . . . VLSI CAD Layout Tool

MHz	Mega-Hertz
MIT	Massachusetts Institute of Technology
mm	Millimeters
MOSFET	Metal-Oxide-Semiconductor Field Effect Transistor
MOSIS	Metal-Oxide-Semiconductor Implementation Service
MPa	Mega-Pascals
N	Newtons
$NaKC_4H_4O_6{\cdot}4H_2O$	Rochelle Salt
NASA	National Aeronautic and Space Administration
p	Dipole Observation Point
P	Polarization
pF	Pico-Farads
PC	Printed Circuit
PVDF	Polyvinylidene Fluoride
q	Charge Generated by PVDF Film
Q	Fundamental Unit of Charge
r	Distance Between p and the Dipole Center
$\hat{r}$	Polar Coordinate Unit Vector
RC	Resistance-Capacitance
RTV	Room Temperature Vulcanizing
s	Elastic Compliance Coefficient
S	Strain
SEM	Scanning Electron Microscope
Spice	Simulation Program with IC Emphasis
t	PVDF Film Thickness
V	Volts
V_{bias}	Bias Voltage
V_{dd}	Amplifier Supply Voltage
V_{ds}	Drain-Source Voltage
V_g	Gate Voltage

VLSI . . . . Very Large Scale Integration

V_{source} . . . . Electrometer Source Voltage

X . . . . Stress

ϵ . . . . Dielectric Constant (Permittivity)

ϵ_r . . . . Permittivity Relative to Free Space

ϵ_0 . . . . Permittivity of Free Space

μm . . . . Microns

Ω . . . . Ohms

θ . . . . Angle Between the Axis of a Dipole and the
Radial to the Point of Observation

$\hat{\theta}$ . . . . Polar Coordinate Unit Vector

AFIT/GE/ENG/88D-41

Abstract

The purpose of this research effort was to design, fabricate and test a robotic tactile sensor fabricated from polyvinylidene fluoride (PVDF) films coupled to a silicon substrate containing active amplification circuitry. The integrated circuit incorporated 25 sensor electrode pads (0.6mm×0.6mm each) arrayed in a 5×5 grid with a spacing of 0.6mm between electrodes (this corresponds to a spatial resolution four times greater than the human fingertip). The on-board amplification circuitry consisted of a dual MOSFET amplifier (with a gain of 5) for each sensor electrode.

Four different sensor configurations were fabricated and tested. The configurations varied only in the thickness of the PVDF film used (25μm, 40μm, 52μm, and 110μm). The individual elements of each of the sensor configurations were tested and the sensor based on the 25μm thick film was considered the optimal sensor of the four. This decision was based on its superior biasing ability and its linear operation over the test loading range (0.8g to 76g). Additionally, there was essentially no coupling between nearest neighbors for all of the sensor configurations. A group loading test (where multiple elements were loaded) was also performed, but problems with obtaining a consistent no-load output across the entire array prevented a true picture of the performance of the sensor. Methods for improving the tactile sensor (including a means for obtaining a consistent no-load output across the entire array) are discussed in the final chapter.

ROBOTIC TACTILE SENSOR FABRICATED FROM PIEZOELECTRIC POLYVINYLIDENE FLUORIDE FILMS

I. Introduction

Motivation

Traditionally, robots are used in very controlled and defined environments (1:177). However, in future military and industrial applications, robots "should be able to adapt to any work environment because it is often not practical to adapt the environment to them" (1:177). The two most important senses a robot should possess are vision and touch (1:177). In fact, developing the tactile sense for robots is one of NASA's highest priorities (2:17). Several approaches have been investigated to implement tactile sensing (optical, piezoresistive, capacitive, etc.) (2:18-19). Among these is a tactile sensor based on the piezoelectric effect observed in poled polyvinylidene fluoride (PVDF) (3:53).

Last year, Capt Pirolo investigated the response of several sensor array electrode configurations fabricated from PVDF film. This research effort will be concerned with extending Capt Pirolo's work by reducing the overall size of the sensor arrays to approximate that of the adult fingertip, enhancing the sensor's spatial resolution, and increasing the sensor's sensitivity by integrating

the PVDF film with the gate electrode contact of a metal-oxide-semiconductor field effect transistor (MOSFET).

Summary of Current Knowledge

Three fundamental approaches have been implemented to realize tactile sensors: optical, piezoresistive, and piezoelectric (1:184). The optical and piezoresistive approaches have been studied for some time (as witnessed by their commercial availability) (4:50). Recently, however, tactile sensors based on the piezoelectric effect found in certain ferroelectric polymers (primarily PVDF) have received more attention (4:46). Naturally, each of these three approaches have their respective advantages and disadvantages which, in turn, are based on their fundamental approach for converting a force into an electrical signal.

Optical Tactile Sensors. The operation of a typical optical tactile sensor is based on modulating a light source with an opaque shutter (1:186;5:13). Shown in Figure 1-1 is an optical sensor in a relaxed and loaded state. In the relaxed state, the shutter does not interfere with light transmission between the photo emitter and the photo detector. Under a load, however, the amount of light reaching the photo detector is reduced in proportion to the amount that the shutter is displaced. Thus, an electrical signal is generated which is proportional to the amount of the applied force (1:186;5:10).

Two of the major disadvantages of optical tactile sensors are the linearity and flexibility of the elastomeric surface (4:47). In an experimental sensor designed at MIT, the elastomer "broke down after a few hundred cycles of operation and permitted a dynamic range (maximum to minimum loading in

the sensor's linear region) of only 18 to 1 [N]" (4:47). A major advantage, however, is that they are currently commercially available (4:50;5:10).
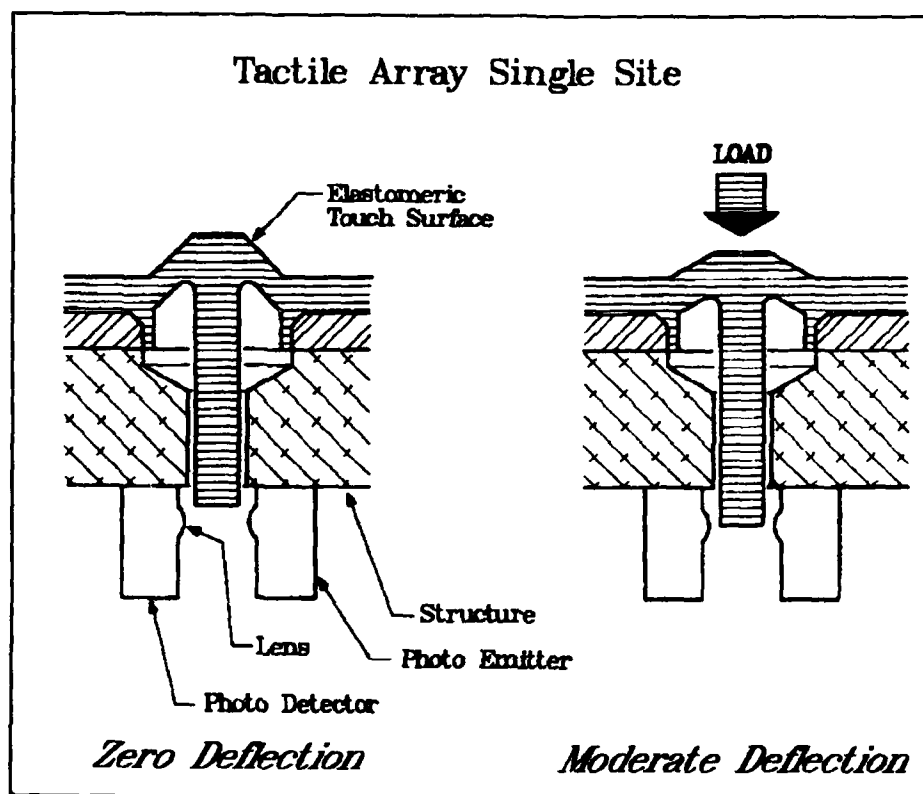
Figure 1-1. Optical Tactile Sensor (5:13).

Piezoresistive Tactile Sensors. Piezoresistive sensors are based on the principle that the resistance of certain materials change when pressure is applied to them (1:193;4:48). In the example shown in Figure 1-2, the actual sensing element is the silicon diaphragm. The resistance of this diaphragm can be measured between the two gold-plated pads. The major disadvantages of piezoresistive tactile sensors include: high electrical noise, moderate

hysteresis, low sensitivity, and long response time constants (4:48). Again, a major advantage is that they are commercially available (1:185;4:50)
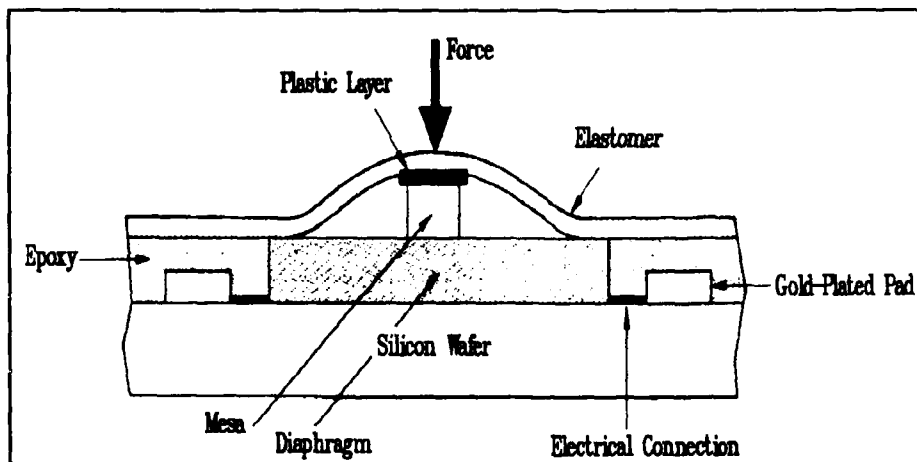
Figure 1-2. Piezoresistive Tactile Sensor (4:51).

Piezoelectric Tactile Sensors. Although optical and piezoresistive sensors are commercially available, their disadvantages prompted the investigation of an alternative sensing technique. An experimental tactile sensor (developed at the University of Pisa) that showed great promise was based on the piezoelectric effect (see Table 1-1) (1:198). Since this research is concerned with developing piezoelectric tactile sensors, they are discussed in detail in Chapter II. However, some of the major advantages of piezoelectric tactile sensors include: high durability, low cost, high conformality, and high spatial resolution (1:196). The major disadvantage, though, is that static pressures are difficult to measure with piezoelectric tactile sensors because induced charges tend to dissipate after a short period of time which results in a limited steady-state response (1:196).

Problem Statement

A piezoelectric tactile sensor using PVDF film will be fabricated from a two-dimensional array of aluminum electrodes that also serve as the gate electrode contacts to discrete MOSFETs. The MOSFET electrode arrays will be designed using in-house computer-aided design (CAD) tools, and then fabricated by the Metal-Oxide-Semiconductor Implementation Service (MOSIS), a cooperative group of silicon foundries which fabricate integrated circuits for education and research. The fabricated circuits will then be coupled to a homogeneous sample of the piezoelectric PVDF film. The resulting tactile sensors (which differ by the PVDF film thickness used) will be tested and their performance compared.

Table 1-1. Tactile Sensor Comparison (1:185).

Approach	Spatial Resolution	Sensitivity	Range	Status
Optical	1.8 mm	3 gm	0-681 gm	Commercial
Resistive	1.3 mm	230 gm	0.2-5 Kg	Commercial
Resistive	2 mm	10 gm	10-1K gm	Commercial
Piezoelectric	3 mm	20 gm	20-80K gm	Experimental

Assumptions

The following assumptions were made:

1. The ICs fabricated by MOSIS, although manufactured by a specific, undetermined vendor, are representative of all the MOSIS vendors.

2. Electrical fringing effects can be neglected when the electrode separations are 5 times greater than the PVDF film thickness.

3. The average spatial resolution of the human fingertip, as reported in the literature, establishes the minimum sensor element density.

4. The thickness of the adhesive used to attach the PVDF film to the IC is negligible so that the electrical effects of the PVDF film dominate.

Scope

This research will be limited to an investigation and performance characterization of the pressure sensitivity and coupling (mechanical and electrical) of several sensor configurations. The critical variables will be the PVDF film thickness and electrode spacing (by examining the response between neighbors of varying distance). Other parameters, such as temperature, electrode size, and long-term performance will be left to future studies.

Approach

The basic approach consists of three fundamental stages: design, fabrication, and performance evaluation. The general steps are listed below.

Design.

Design of the Sensor Electrode Array. The overall dimensions of the electrode array will be 6000×6000μm (due to chip size constraints). Each square electrode (since the VLSI CAD program, Magic, only deals with rectangles, circular objects are very difficult to construct) will be separated (edge-to-edge) from neighboring electrodes by a minimum of 600μm (so fringing effects can be neglected). A 5×5 electrode array, given these restrictions, will have a spatial resolution approximately 4 times greater than that of the adult human fingertip (6:205). MOSIS fabricated MOSFETs will have their gates

1-6

connected to the electrodes, and their drains and sources connected to external pads. An additional pad will permit external biasing of the sensing electrode to establish a consistent initial condition on the PVDF film (which was a possible cause of the fluctuations reported in Pirolo's research) (7:5.9-5.11).

Design of the Loading Test Probe. This probe will be used to compare the force and pressure sensitivity of the tactile sensors (1g to 100g weight distributed over the 0.36mm^2 surface area of each electrode). This situation correlates with pressures spanning of 0.28 N/cm^2 to 28 N/cm^2.

Fabrication. Both the integrated circuits and the loading test probe will be fabricated by outside agencies. The ICs will be fabricated by MOSIS using the design created with Magic (8). The loading test probe will be fabricated by the AFIT Model Shop. The tactile sensors will be constructed using four basic steps: charge removal, adhesive application, compression baking, and bias voltage connection.

Test and Evaluation. The performance of the sensor arrays will be tested with the mechanical load test probe and the electrometer (the data will be recorded on a data collection computer using a GPIB interface). The first phase of evaluation will characterize the performance of the integrated circuits. In the second phase, the PVDF will be tested to insure that it generates the proper signals. The third phase will focus on the evaluation of the performance of the assembled tactile sensors (both individual elements and coupling effects between elements).

Through these tests, the pressure sensitivity of individual sensor elements will be quantified, the coupling (electrical and mechanical) between them will

be established, the feasibility of using the MOSFETs as high impedance amplifiers will be documented, and the effectiveness of using an external biasing voltage to minimize transitory sensor instability will be explored. The majority of the data will be statistically analyzed and presented in a graphical format.

Order of Presentation

Background information on piezoelectricity and piezoelectric materials is discussed in Chapter II. Chapter III develops and extends the general approach discussed in this chapter into more detailed steps which includes the design rationale. Test and evaluation results and analysis are presented in Chapter IV. Chapter V summarizes the test and evaluation results to develop conclusions and recommendations concerning this research.

II. Background

Introduction

Scope. Since the purpose of this thesis effort is to design a robotic tactile sensor based on the piezoelectric effect, a fundamental understanding of piezoelectricity, and piezoelectric materials (specifically polyvinylidene fluoride) is critical. In this chapter, piezoelectricity is introduced with some basic definitions and a brief history. Following this discussion, the two fundamental piezoelectric theories (atomic and macroscopic) are presented so that the diverse family of piezoelectric materials can be addressed. From this discussion, the advantages of polyvinylidene fluoride (PVDF) film are compared to the requirements for a robotic tactile sensor, and an example of a PVDF film tactile sensor design is examined.

Motivation. Perhaps one of the most unusual aspects of piezoelectric materials is their versatility. They can function in three very different modes: generator, motor, and capacitor (9:1). When used as a generator, the piezoelectric material can change mechanical energy into electrical energy. When used as a motor, it can convert electrical energy into mechanical energy. Finally, since piezoelectric materials are dielectrics, they can be used as capacitors to store electrical energy.

Definitions. Before proceeding, two definitions are necessary. First, piezoelectricity is defined by W. G. Cady as:

> . . . electric polarization produced by mechanical strain in crystals belonging to certain classes, the polarization being proportional to the

strain and changing sign with it. This statement defines the direct piezoelectric effect. Closely related to it is the converse effect . . . whereby a piezoelectric crystal becomes strained, when electrically polarized, by an amount proportional to the polarizing field [10:4].

A related term, pyroelectricity, is defined as "a state of electric polarity produced on certain crystals by change of temperature. . ." (10:4). An understanding of pyroelectricity is not essential to understanding piezoelectricity, but it does have some historical significance.

History. The history of piezoelectricity actually began with the initial discovery of pyroelectricity in 1703 when Dutch merchants brought tourmaline crystals back from Ceylon (10:1). Tourmalines are very pyroelectric, so when they were placed in hot ashes, the ashes would stick to the crystals' surface. After a period of time, the crystals would cool down and repel the ashes (10:1). This peculiar behavior earned the tourmaline crystal the name "Ceylon magnet" (10:1). In 1824, Brewster, who had been examining similar behavior in crystals other than tourmaline, began using the term "pyroelectricity" to describe this action (10:1).

It was not until 1880, however, that the Curie brothers (Jacques and Pierre), who were investigating the relationship between pyroelectricity and crystal symmetry, found a similar relationship with pressure (9:2;10:2). Thus, they became the "fathers" of piezoelectricity.

The Curie brothers initially discovered that an electric field was generated by an applied mechanical stress (or the direct piezoelectric effect). In 1881, Lippman proposed the converse effect, which was immediately verified by the Curies (9:2;10:4).

In the following years, a number of scientists began refining the theory of piezoelectricity. Foremost among them was Woldemar Voigt who, in 1910, published his celebrated work, *Lehrbuch der Kristallphysik*, where he showed which of the 32 crystal classes would be piezoelectric (and what piezoelectric constants would be nonzero) (10:5).

Once the piezoelectric effect had been quantified for a number of materials (particularly quartz and rochelle salt), other scientists began applying the piezoelectric effect to solve various problems. One of the first scientists to find a practical application for piezoelectricity was Langevin. During World War I, he developed a way of locating submarines by interrogating submersed objects with high frequency (ultrasonic) waves. Consequently, he provided the groundwork for the science of ultrasonics (9:2;10:5).

After Langevin, there was a flurry of activity and research associated with piezoelectric crystals, ceramics, and organic materials. This research culminated in the piezoelectric thin film materials that are finding their way into a plethora of applications today (11:2-3).

Piezoelectricity

In order to gain an appreciation for the operation of piezoelectric devices, it is necessary to have an understanding of both the physics describing the piezoelectric effect (atomic analysis), and the origin of the piezoelectric constants (macroscopic analysis). The treatment here will be necessarily simplified and condensed. A more thorough analysis can be found in W. G. Cady's book, *Piezoelectricity* (10).

Atomic Analysis. Fundamental to an understanding of the atomic analysis of the piezoelectric effect is the concept of a center of inversion (or a center of symmetry) (7:2.7;9:1;12:7). A center of inversion permits non-piezoelectric crystals to maintain an overall neutral charge when stressed (see Figure 2-1a). Thus, the basic reason why certain crystals are piezoelectric is that they lack this center of inversion (7:2.7;9:1;12:7). When pressure is applied to an asymmetric crystal, the crystal becomes polarized and creates an electric field (see Figure 2-1b) (7:2.7).
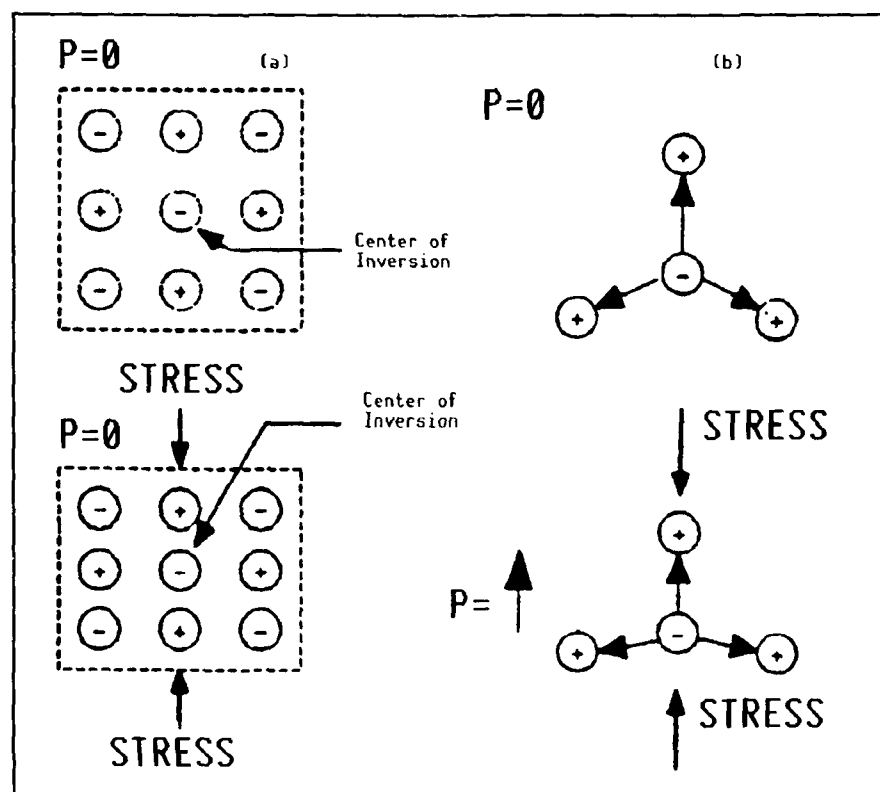
Figure 2-1. Concept of a Center of Inversion in a Crystalline Structure. (a) Crystal with a Center of Inversion, and (b) Crystal without a Center of Inversion (7:2.7).

Dipole Theory. From a mathematical perspective, an explanation for the electric field generated in Figure 2-1b can be constructed from simple dipole theory using the dipole element depicted in Figure 2-2.
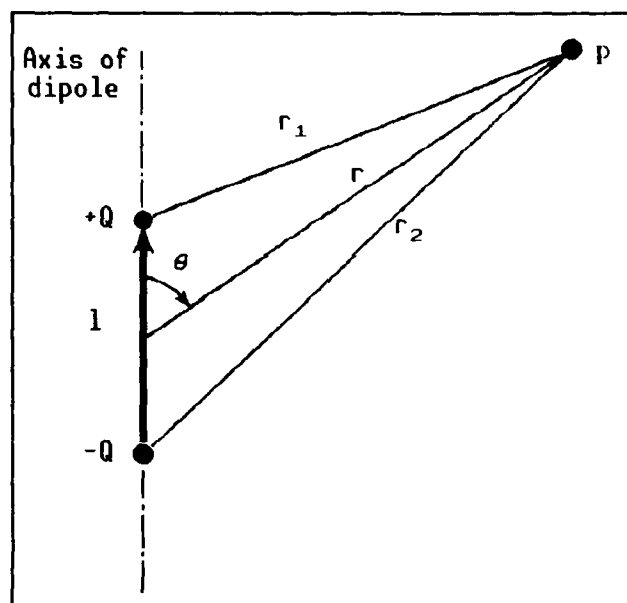
Figure 2-2. Simple Dipole (13).

If we place the dipole in Figure 2-2 an arbitrary distance from and orientation with respect to the origin point (p), the voltages at point p due to +Q and -Q are (assuming a free-space medium) (13:35):

$$V_1 = \frac{Q}{4\pi\epsilon_0 r_1} \qquad \text{(V) (2-1)}$$

$$V_2 = \frac{-Q}{4\pi\epsilon_0 r_2} \qquad \text{(V) (2-2)}$$

where Q is the fundamental unit of charge, and ϵ_0 is the dielectric constant of free-space.

Using the principle of linear superposition, the total voltage observed at point p is (13:35):

$$V_{TOT} = V_1 + V_2 = \frac{Q}{4\pi\epsilon_0}\left|\ \frac{1}{r_1} - \frac{1}{r_2}\ \right| \qquad \text{(V)}. \ (2\text{-}3)$$

For r much greater than the charge separation (l) (see Figure 2-2), the distances between p and each of the charges can be approximated by (13:36):

$$r_1 = r - \frac{l\cos(\theta)}{2} \qquad \text{(m)} \ (2\text{-}4)$$

$$r_2 = r + \frac{l\cos(\theta)}{2} \qquad \text{(m)}. \ (2\text{-}5)$$

The total voltage can then be re-written as:

$$V_{TOT} = \frac{Ql\cos(\theta)}{4\pi\epsilon_0[r^2 - (0.25)l^2\cos^2(\theta)]} \qquad \text{(V)}. \ (2\text{-}6)$$

Since r is much greater than l, the l^2 term in the denominator can be ignored. Thus (13:36):

$$V_{TOT} = \frac{Qlcos(\theta)}{4\pi\epsilon_0 r^2} \qquad (V). \ (2\text{-}7)$$

By definition, the electric field is the negative gradient of the voltage (13:35). Therefore, the electric field is (in polar coordinates) (13:36):

$$E = \hat{r} \frac{Qlcos(\theta)}{2\pi\epsilon_0 r^3} + \hat{\theta} \frac{Qlsin(\theta)}{4\pi\epsilon_0 r^3} \qquad (V/m). \ (2\text{-}8)$$

<u>Dipole Theory Applied to Crystals.</u> As an example, consider the crystal shown in Figure 2-3. In its equilibrium state (Figure 2-3a), there is no net electrical field. When the crystal is strained as shown in Figure 2-3b, however, the net electric field becomes:

$$E = \hat{\theta} \frac{Ql}{4\pi\epsilon_0 r^3} (-0.155) \qquad (V/m) \ (2\text{-}9)$$

where l is the distance between the central (negative) ion and any of the positive ions, and r is the distance to the point of observation.
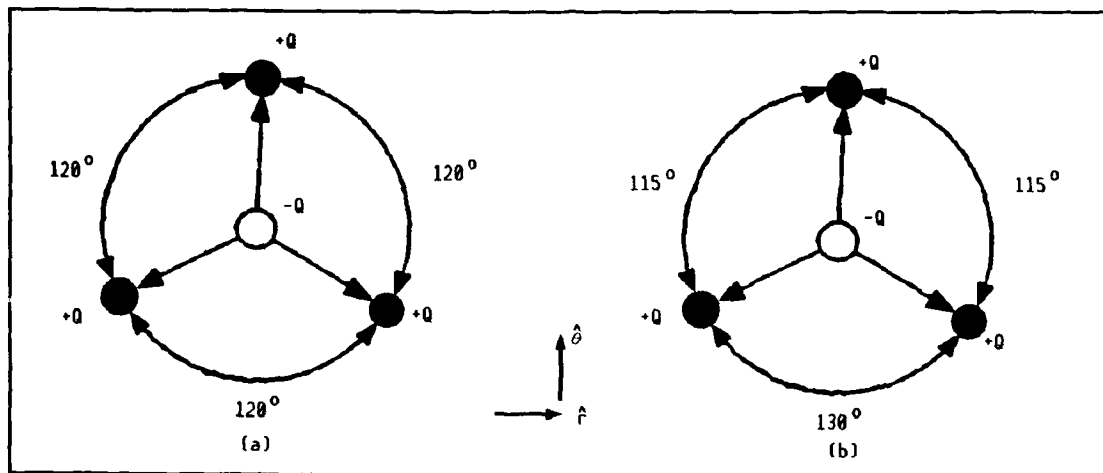
Figure 2-3. Example Crystal in Two States. (a) Equilibrium and (b) Strained (7:2.9).

This simple two-dimensional case illustrates how some of the early piezoelectric researchers were able to predict which of the 32 crystal classes would be piezoelectric.

Although the atomic view is a convenient way to understand the nature of piezoelectricity, it is difficult to predict a given crystal's exact behavior using atomic theory. The reason for this dilemma has been discussed by Cady in his book, *Piezoelectricity:*

> In spite of the fact that molecular or atomic theories of piezoelectricity began to appear very soon after the Curies' discovery, a satisfactory theoretical treatment of the phenomenon can hardly be said to have passed the initial stage. The resources of modern lattice dynamics are still unequal to the task of predicting anything better than a rough approach to the order of magnitude of the piezoelectric effect, even for the simplest structures [10:731].

Therefore a larger, macroscopic view was adopted to establish useful predictions about a piezoelectric crystal's behavior.

Macroscopic Analysis. The macroscopic nature of piezoelectricity and the piezoelectric coefficients are based on three fundamental physical properties of a crystal: stress, strain, and polarization (10:178).

Stress. The stress applied to a crystal's surface has the units of force per unit area, and has six degrees of freedom (three normal stresses and three shearing stresses) (9:21;10:47). Figure 2-4a is a normal stress, while Figure 2-4b depicts a shear stress. Stresses will be represented by the letter 'X' with a subscript spanning between one and six, that corresponds with each of the degrees of freedom (7:2.12):

$$X_x, Y_y, Z_z, Y_z, Z_x, X_y \ = \ X_1, X_2, X_3, X_4, X_5, X_6 \qquad (N/m^2). \ (2\text{-}10)$$

The upper-case letters on the left side of Eq (2-10) denote the direction of the force, and the subscript represents the normal to the surface to which the force is being applied (7:2.14;10:47).

Strain. Strain is the relative deformation of a crystal under an applied stress (7:2.14;10:47). It is similar to stress since it has six degrees of freedom; however, because it is a ratio, it is unitless. Strain will be represented by the letter 'S' with a subscript having a value between one and six (7:2.15):

$$x_x, y_y, z_z, y_z, z_x, x_y \ = \ S_1, S_2, S_3, S_4, S_5, S_6 \qquad (unitless). \ (2\text{-}11)$$

2-9

Like stress, the subscripted letters indicate the direction of the normal to the crystal's surface to which the force causing the strain is being applied. The other letters (x, y, and z) represent the direction of the applied force (10:47-52).
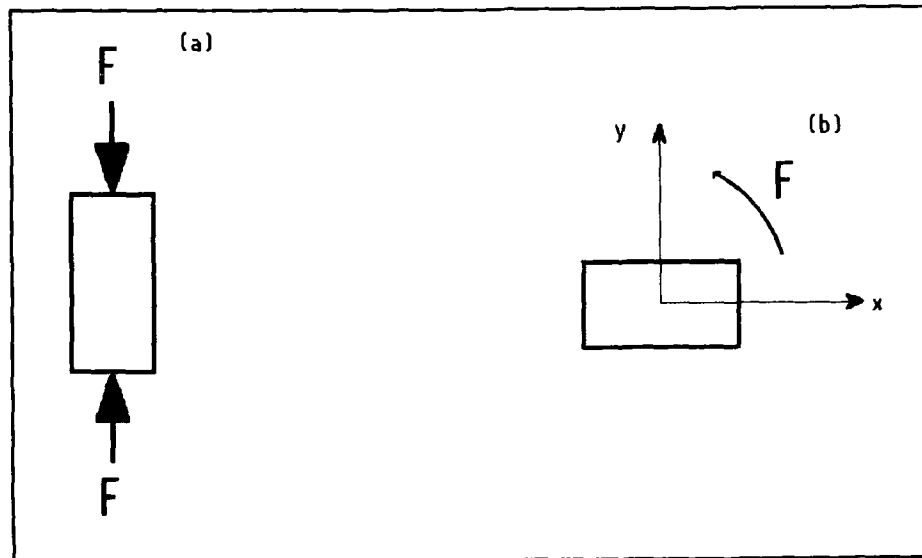
Figure 2-4. Stress Types. (a) Normal Stress and (b) Shear Stress (7:2.14).

Polarization. Polarization differs from stress and strain in that it only has three degrees of freedom (there is no such thing as a "shearing" polarization). It is represented using the letter 'P' with a subscript spanning between one and three (7:2.18).

P_1 = x-directed polarization

P_2 = y-directed polarization $\qquad$ (C/m^2). (2-12)

P_3 = z-directed polarization

2-10

General Elastic Crystal Equations. For a generic crystal (not piezoelectric), the stresses and strains are related by Hooke's Law (7:2.16;10:48):

$$S_i = \sum_i^6 \sum_k^6 s_{ik} X_k \qquad \text{(unitless)} \quad (2\text{-}13)$$

$$X_i = \sum_i^6 \sum_k^6 c_{ik} S_k \qquad (N/m^2) \quad (2\text{-}14)$$

where s_{ik} is the elastic compliance coefficient, and c_{ik} is the stiffness coefficient (7:2.17).

Furthermore, the polarization of a crystal is directly related to the applied electric field (7:2.18;14:511):

$$P_m = \sum_m^3 \sum_i^3 \epsilon_{im} E_i \qquad (C/m^2) \quad (2\text{-}15)$$

where ϵ_{im} is the dielectric constant, and E_i is the applied electric field.

These equations pertain only to non-piezoelectric materials since, if the crystal were piezoelectric, Eqs (2-13), (2-14), and (2-15) would take on extra terms.

Piezoelectric Crystal Equations. The additional terms in the piezoelectric equations stem from the fact that in a piezoelectric crystal, a mechanical strain generates a polarization (the direct effect). Similarly, for the converse effect, an electrical field generates a stress. The direct piezoelectric effect can thus be represented by (7:2.18;10:183):

2-11

$$P_m = \sum_i^6 d_{mi} X_i + \sum_k^3 \epsilon^X_{km} E_k \qquad m = 1,2,3 \qquad (C/m^2) \text{ (2-16)}$$

where d_{mi} is the piezoelectric strain constant, and the superscript X refers to a constant strain.

Furthermore, the converse effect can be represented by (7:2.18;10:183):

$$S_i = \sum_k^6 s^E_{ik} X_k + \sum_m^3 d_{mi} E_m \qquad i = 1,2...5,6 \qquad \text{(unitless) (2-17)}$$

where the superscript E in s^E_{ik} refers to a constant electric field.

The electro-mechanical coupling factor (k) indicates the energy conversion efficiency of a particular piezoelectric material. It is the ratio of the energy generated (mechanical or electrical) to the energy provided (electrical or mechanical) (15:10). Oftentimes, the coupling factor will be subscripted to indicate the direction of the applied energy and the location of the electrodes (11:18). A numbering convention of x=1, y=2, and z=3 is used for the subscripts (11:9). As an example, k_{13} means that the coupling factor was measured with electrodes perpendicular to the 1 (or x) direction, and the strain was induced in (or applied to) the 3 (or z) direction (this numbering convention is also used for the piezoelectric strain coefficient). Typical values of the electro-mechanical coupling factor range from zero (non-piezoelectric) to almost unity.

With an understanding of the origin of the piezoelectric coefficients and the definition of the electro-mechanical coupling factor, comparisons between various piezoelectric materials can be made.

Piezoelectric Materials

Early Materials. Two of the earliest materials used in piezoelectric devices were quartz and rochelle salt. This was probably due to their relative abundance (quartz occurs naturally, and rochelle salt was used for medicinal purposes) (9:114).

Rochelle Salt. Rochelle salt has a very high coupling factor (0.9). Unfortunately, it suffers from environmental restrictions because of its composition (which consists of a significant amount of water) (9:115). The chemical formula for rochelle salt is $NaKC_4H_4O_6 \cdot 4H_2O$, and the water molecules are an integral part of its structure (9:115). If the environment changes, the crystals' performance will be degraded. That is,

> . . . if the humidity of the surrounding atmosphere is below 35 per cent at 25°C, the water vapor pressure of the crystal is greater than the vapor pressure of water in the surrounding atmosphere and the crystal will lose water and dehydrate. . .Above 85 per cent humidity, the crystal will absorb water from the atmosphere on its surface and will slowly dissolve if kept in such an atmosphere [9:117].

Therefore, care must be taken when using rochelle salt in uncontrolled environments. One way to minimize the effects of the environment is to place the crystal (with its electrodes attached) into a hermetically sealed container along with both powdered and dehydrated rochelle salt (9:117). Consequently, the humidity stabilizes at the desired range for proper operation of the rochelle salt crystal.

The piezoelectric efficiency of Rochelle salt is also strongly temperature dependant (9:129). It only functions effectively in the temperature range of -18°C to 24°C (9:117). Because of these environmental constraints, rochelle salt was primarily used as a transducer at low-frequencies (9:114).

Quartz. Since quartz does not require water molecules in its crystal matrix, it has a major environmental advantage compared to rochelle salt. Unfortunately, its coupling factor is only on the order of 0.1 (15:10). In spite of its low coupling factor, it does make a very stable oscillator element, which explains its widespread use in watches and other time-dependent devices (9:78).

Ceramics. Piezoelectric ceramics would have seemed an impossibility to researchers prior to World War II since a ceramic is a conglomeration of random crystallites (see Figure 2-5) (15:1). However, in 1946, a method for transforming a polycrystalline material into a piezoelectric material was discovered:

> . . . the polarity needed to impart piezoelectric properties can be given to an originally isotropic polycrystalline ceramic, more or less permanently, by temporary application of a strong electric field. This process, called "poling", is analogous to the magnetizing of a permanent magnet [15:1].

Poling, then, refers to the application of an intense direct current electric field across the ceramic. This field tends to align the polarization axes of the crystallites in the ceramic, thus rendering it piezoelectric.

One of the first piezoelectric ceramics extensively investigated was barium titanate since it possessed a higher coupling factor compared to the other known piezoelectric materials (except for rochelle salt) (15:53). The basic cell of barium titanate (as well as most other piezoelectric ceramics) is the Perovskite structure shown in Figure 2-6 (15:53).
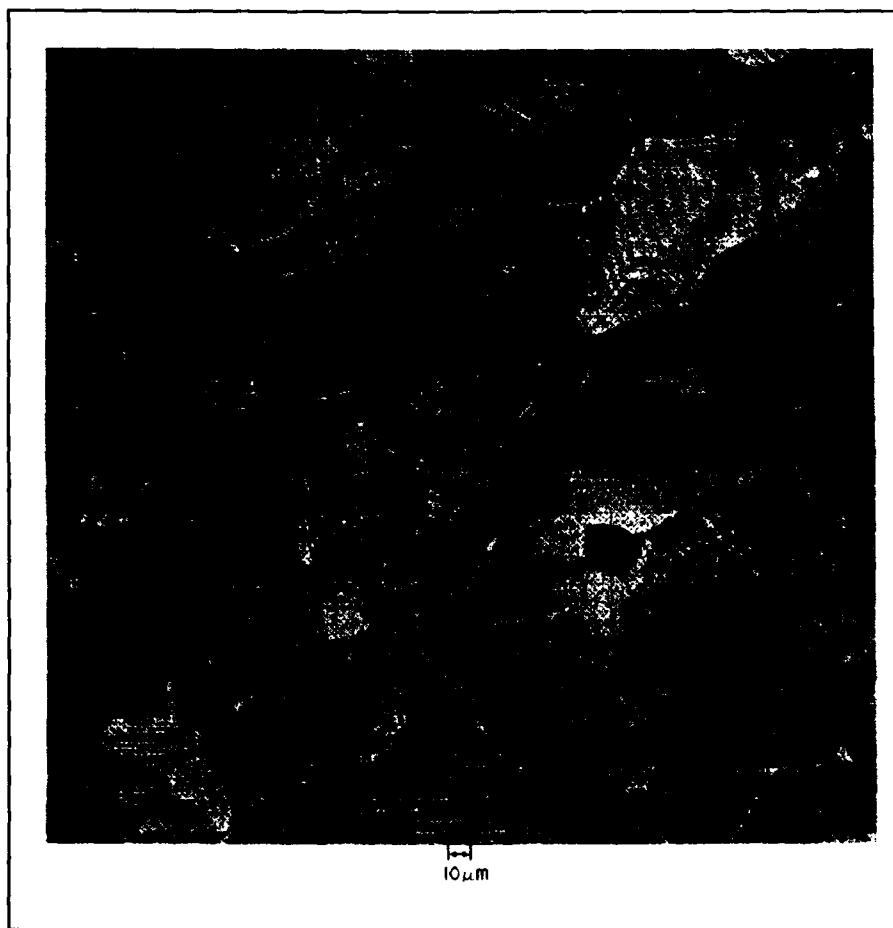

Figure 2-5. Barium Titanate Crystallites (15:65).

When the coupling factors of a pure crystal of barium titanate are compared with the ceramic version (see Table 2-1), there is a noticeable difference. This difference is attributable to the fact that "the anisotropy is much smaller for the poled ceramics than for a single crystal" (15:72).
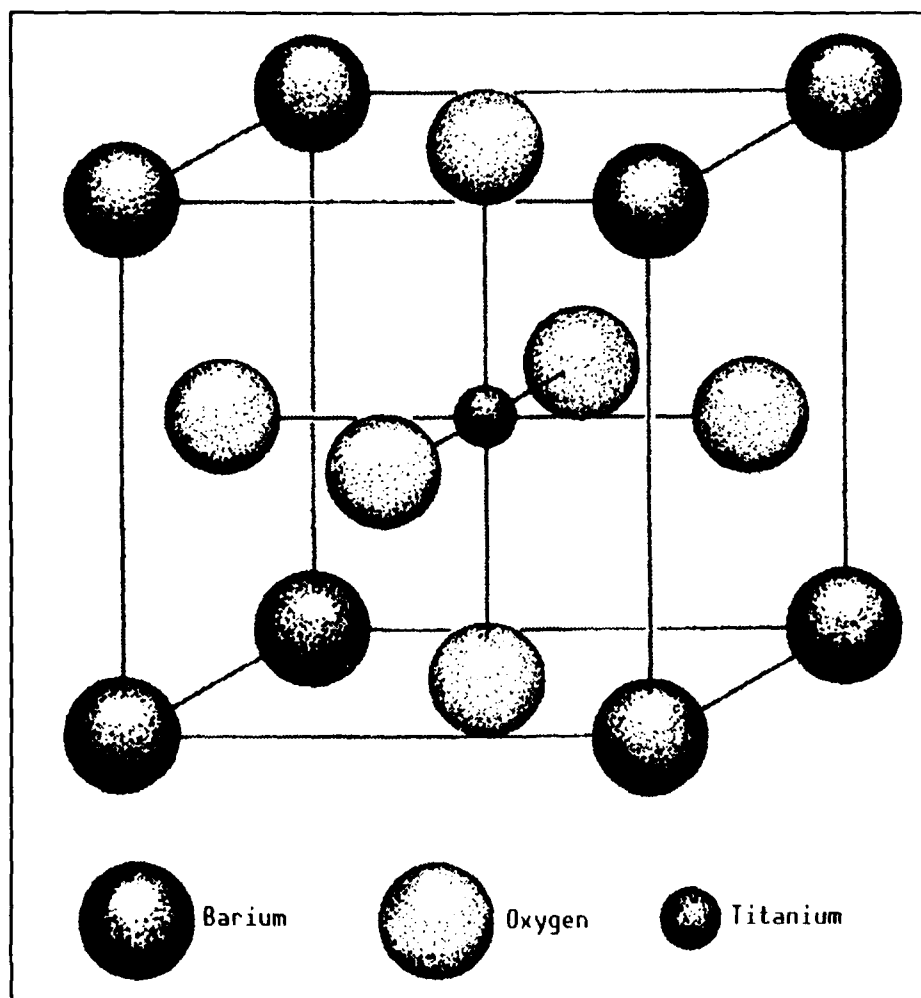
Figure 2-6. Perovskite Structure (15:49).

Table 2-1. Barium Titanate Coupling Factors (15:74).

Coupling Factor	Ceramic	Crystal
k_{15}	0.476	0.570
k_{31}	0.208	0.315
k_{33}	0.493	0.560

Organic Polymers. The poling process is also fundamental to piezoelectric organic polymers. Among them is the polymer polyvinylidene fluoride (PVDF). In 1969, Kawai determined that polarized PVDF "developed far greater piezo activity than any other synthetic or natural polymer" (16:975). PVDF can be polarized in a manner very similar to the process used to make ceramics piezoelectric (poling) (11:5).

Fabrication. In order to make poling effective, however, it is necessary to align as many of the polymer chains as possible. This result is accomplished by stretching the material into thin sheets. Because of this step, PVDF films cannot be made very thick. Typical thicknesses range between 9 and 800 microns (11:14). After stretching the PVDF film, it is necessary to pole it to turn it into a piezoelectric material.

The predominant phase in the stretched PVDF film is the non-polar α-phase (see Figure 2-7a) (12:26-27). Since the polarized (and hence, piezoelectric) β-phase is the preferred phase (see Figure 2-7b), the PVDF sheet must go through a poling step to convert as many of the α-phase crystallites into the β-phase (see Figure 2-8) (12:27).

Disadvantages. One of the major disadvantages of PVDF film is its sensitivity to extreme temperatures (80°C to 120°C). When the PVDF film

reaches these temperatures, mechanical relaxation in the material degrades its piezoelectric activity (12:51).

Other disadvantages of PVDF film compared to traditional piezoelectric materials include: a relatively low coupling coefficient (0.19), sensitivity to electromagnetic interference, and the relative thinness of the films (7:2.25-2.26). Despite these disadvantages, PVDF film has found its way into a myriad of applications because it possesses many other desirable characteristics.
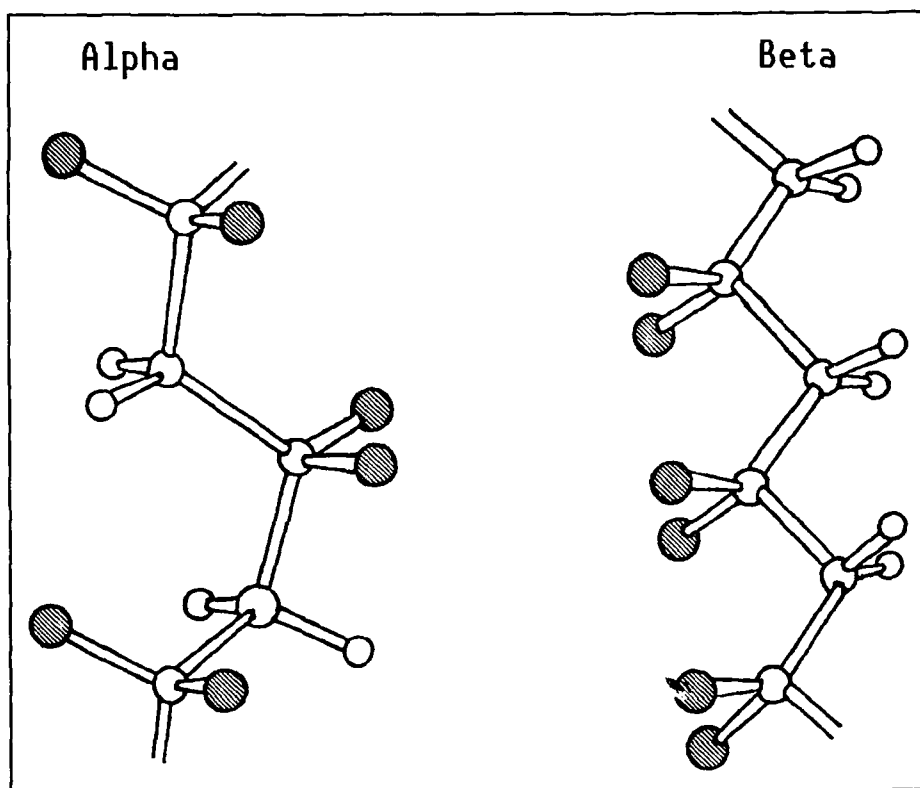

Figure 2-7. PVDF α-and β-Phases. The small white spheres represent hydrogen atoms, the larger white spheres represent carbon atoms, and the cross-hatched spheres represent fluorine atoms (12:27-28).

Advantages. The major advantages of PVDF film compared to conventional piezoelectric materials include (7:2.24-2.25):

1. The film can function over an extremely wide frequency range (DC to approximately 10MHz).

2. It has a low acoustic impedance. (This feature makes it a good impedance match for medical ultrasound and hydrophone applications.)

3. The film possesses a higher dielectric strength than piezoceramic material (30 V/micron versus 1.5 V/micron) and, therefore, can be exposed to higher electric fields.

4. The film has a relatively high electrical impedance. (This advantage allows the film to provide a complimentary match to high-impedance devices (for example, CMOS) and circuits.)

5. Since the film is thin and flexible, it can be laminated to a vibrating structure without significantly distorting the motion of the structure.

6. Because the film is a high molecular weight fluoropolymer, it is mechanically strong and resistant to extreme environmental conditions (most solvents, acids, oxidants, and ultraviolet radiation).

7. The film can be cut and formed into complex shapes or prepared as a large transducer area.

8. The material and fabrication costs of the film are generally lower than those of other piezoelectric materials.

These attractive properties make the disadvantages of PVDF film tolerable, and thus, it is an ideal candidate for a wide range of piezoelectric devices.

PVDF Film Tactile Sensors

One of the recent applications of PVDF film has been in the arena of tactile sensors (11:37). PVDF film is an appropriate piezoelectric material to use in this application since its advantages strongly correlate with the basic requirements and considerations of an ideal tactile sensor.
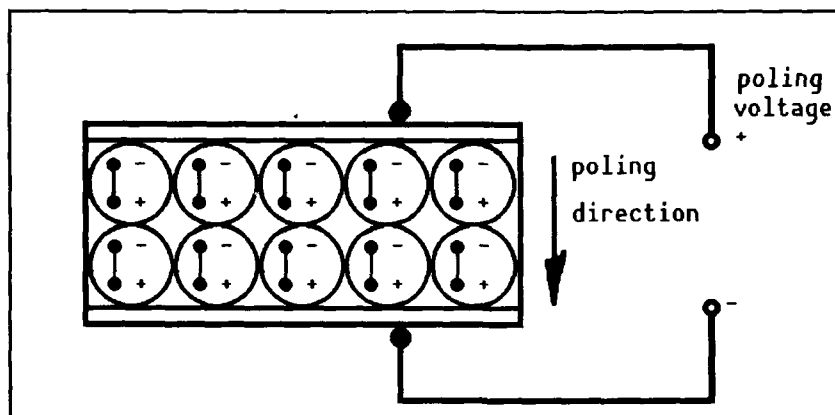
Figure 2-8. PVDF Poling (12:29).

Considerations. Several of these considerations include (but are not limited
to) the following factors. First, in order to function in a human environment,
a tactile sensor should possess the spatial resolution of the human fingertip
(4:46;6:200-201). Secondly, since the initial application of these sensors will
probably be in industry (where robots are used in hazardous environments),
the sensor material should be relatively inert. Thirdly, it should have a
bandwidth of at least DC to 100 Hz (for the control loop requirement) (4:46).
Finally, it would be desirable to have the sensor perform low level integration
of the inputs in order to minimize the information traffic to the central
processor (17:82).

All of these objectives can be realized with a PVDF film tactile sensor. The
spatial resolution of a human fingertip (see Figure 2-9) can be achieved simply
by patterning an array of electrodes on the surface of the film. The stability
of PVDF film in hazardous environments has been discussed along with its

frequency limitations. Finally, since PVDF film is available in thin sheets, the material can be applied directly to either a printed circuit board or a silicon substrate where sensing, amplification and signal processing can be accomplished (4:51).
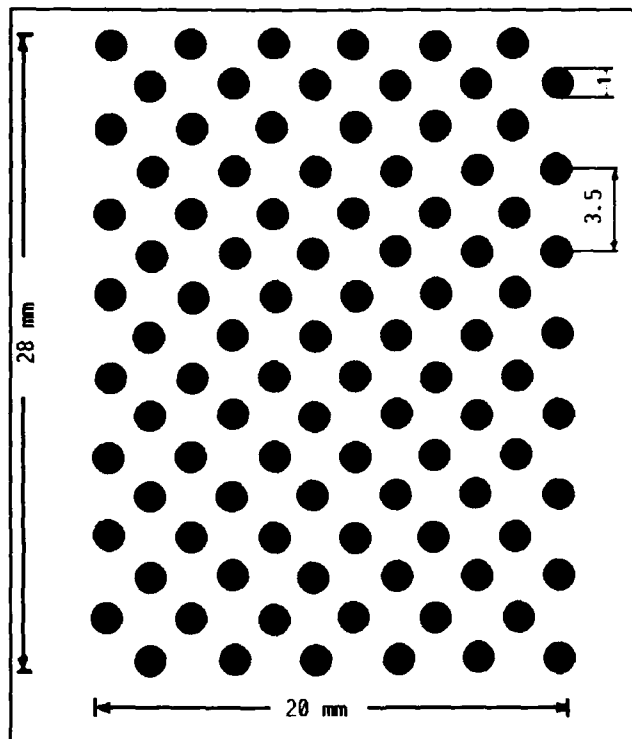
Figure 2-9. Equivalent Spatial Resolution of the Human Fingertip (6:205).

<u>Tactile Sensor Concept.</u> Figure 2-10 depicts a tactile sensor constructed with two levels of PVDF film (to model the human dermis and epidermis layers). The upper layer of electrodes is protected with a thin mylar film, and the two PVDF film layers are separated by two layers: a resistive layer (used for thermal sensing purposes) and a flexible layer (4:52).

2-21

The flexible layer between the two piezoelectric layers serves to make the outer layer more sensitive by flexing, thereby creating more strain in the epidermal PVDF film layer (4:52). The electrodes can be realized using a metallization technique, a conductive epoxy, or a conductive metallic adhesive tape. Finally, in addition to providing a support structure for the sensor, the backing can serve to locate the sensing, amplification, and integration circuitry.

Conclusion

Piezoelectricity, the conversion between mechanical energy and electrical energy, has a fascinating history. From the discovery of tourmaline to the development of piezoelectric polymers, scientists have explored the fundamental properties of piezoelectricity, and attempted to explain them in various ways.

The physical theory of piezoelectricity (in the atomic view) is based on the relatively simple dipole theory, while the macroscopic (and more pragmatic) analysis establishes the piezoelectric constants and the coupling factor in terms of stress, strain, polarization, and Hooke's Law.

With an understanding of piezoelectric theory, various piezoelectric materials can be discussed and compared. Ranging from the early materials (quartz and rochelle salt) to the more recent materials (ceramics and polymers), all of the piezoelectric materials have advantages and disadvantages. The advantages of the PVDF polymer can be used as the basis of a robotic tactile sensor. A PVDF film tactile sensor can be configured to possess the spatial resolution of the human fingertip; and the sensor can be coupled to

either a PC board or an integrated circuit which incorporates sensing, amplification and signal processing circuitry.
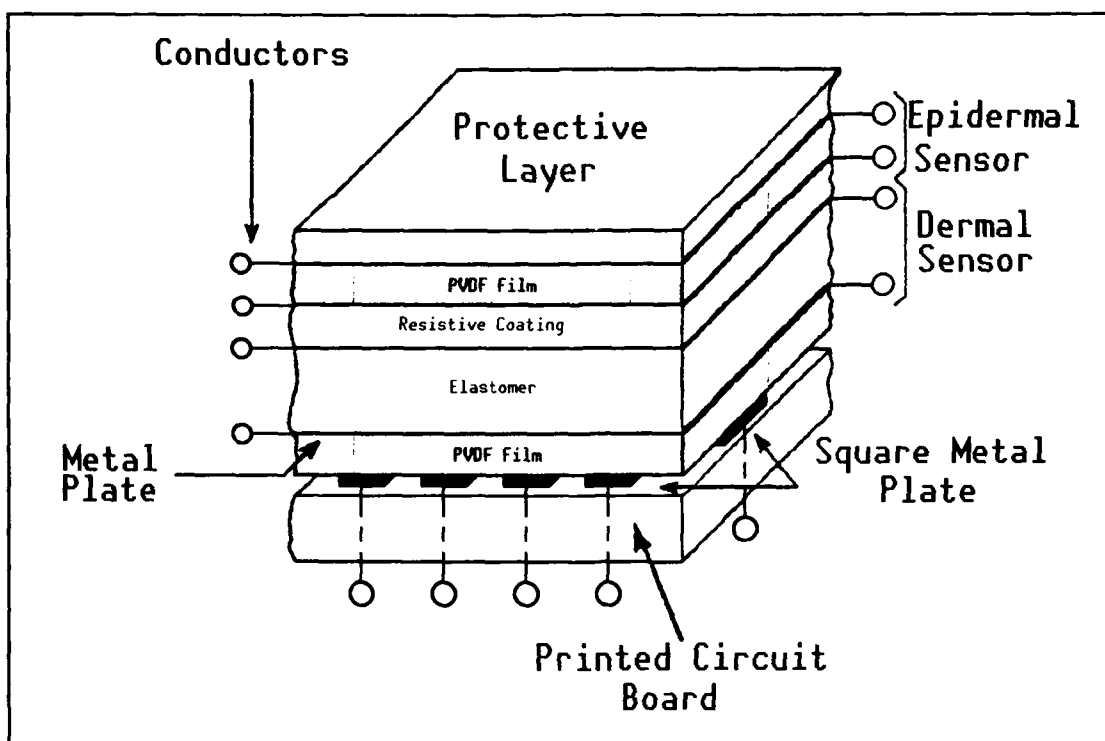
Figure 2-10. Sample Tactile Sensor (4:52;7:2.53).

III. Experimental Procedures

Introduction

In order to accomplish the goal of realizing a tactile sensor, a number of items must be designed and fabricated (the integrated circuit, a loading test probe, and a test board). In addition to the design of the sensor's hardware, of parallel importance is the development of a method for testing the tactile sensor and its subcomponents. The design and fabrication of the hardware and the basic test plan is presented in a chronological order, starting with the design of the integrated circuit and ending with a completed test plan.

Integrated Circuit

The design of the integrated circuit was influenced by a number of factors which included the design of the electrodes, investigation of signal propagation delays, and the design of the sensor amplifiers. In order to design and fabricate an integrated circuit in a reasonable period of time (less than three months), it was decided that MOSIS would fabricate the ICs from a design accomplished with AFIT's CAD tools and submitted electronically. To further increase the probability that the returned circuits would be operative (since there was no way of controlling any of the processing steps), and to reduce the cost of the sensor (since submicron geometry features were not required), the 3 micron MOSIS technology was selected (the largest feature size and most inexpensive MOSIS technology).

<u>Electrode Size.</u> The size of the IC sensor element electrodes was based on
two important factors, the spatial resolution of a human fingertip (the
minimum distance between two points before they become indistinguishable
from a single point) and the amount of real-estate available on a MOSIS
fabricated integrated circuit. Since the largest feasible IC size was limited to
an area of $7900\mu m \times 9200\mu m$, and a portion of the area had to be reserved for
the amplification circuitry, the area available for the electrodes was limited to
a $6000\mu m \times 6000\mu m$ square centered on the IC (see Figure 3-1).
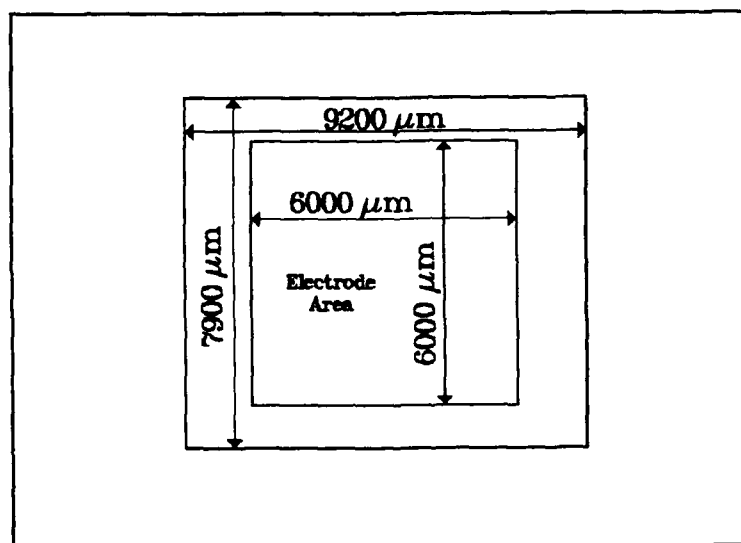
Figure 3-1. Integrated Circuit Partitioning.

Furthermore, in order to minimize the degree of electrical and mechanical
coupling between discrete sensor elements, a 5×5 sensor array was utilized,
whereby individual electrodes were separated from their nearest neighbors by
a distance equal to the edge length of a square electrode array element.
Twenty-five electrodes ($600\mu m \times 600\mu m$ each) in a $6000\mu m \times 6000\mu m$ square

corresponds to a spatial resolution that is approximately four times greater than that of the human fingertip (6:205).

This choice of electrode size affected the voltage generated by the PVDF film since voltage is related to area by $V = (qt)/(\epsilon A)$ where q is the charge generated by the PVDF film, t is the thickness of the PVDF film, ϵ is the permittivity of the PVDF film ($\epsilon = \epsilon_0 \epsilon_r$), and A is the area of the sensor electrode (13:70). The worst case would be the voltage generated by the thinnest (25μm thick) film with an applied weight of 1g (an applied force of 0.01N). This force distributed over an area of 600μm×600μm should generate approximately 0.1V (from Appendix C, $d_{33} = 16$pC/N so q=0.16pC, and $\epsilon_r = 11$).

The maximum voltage would be generated by the thickest (110μm thick) film with an applied weight of 100g (an applied force of 1N). This configuration will produce a voltage at the sensor electrode of approximately 50V (this assumes that there are no charge saturation effects; that is, an unlimited supply of charge carriers).

Line Length Considerations. When connecting the electrodes to the amplifiers, two interconnect strategies were evaluated. The first used a direct route to the amplifiers, and the second was devised to insure that the electrical length of each electrode/amplifier interconnect was identical. Obviously the simplest approach is to use the direct route. However, if the difference in signal propagation delays between the electrodes becomes significant, the second method is preferable. In order to make the determination of which method to use, a simple calculation was accomplished based on the typical

interconnect resistance and capacitance parameters characteristic of 3μm feature size integrated circuits.

Assuming an interconnect length of 4000μm (a maximum value in the IC design), a conductor width of 6μm, a capacitance between the metal layer and the substrate of 1×10^{-4} pF/μm^2, and a sheet resistance (for aluminum) of 0.05Ω/square, the resistance of the line would be approximately 33Ω, and the capacitance would be about 2.4pF (18:121,135). This results in an RC time constant of roughly 80 pico-seconds. This time constant was considered insignificant, so the direct wiring route was adopted.

Amplifier Design. In order to achieve a gain greater than unity for the in situ amplifiers, two inverting amplifiers were used. Although a single stage, non-inverting amplifier was desired (as the PVDF film response increases, the output of the amplifier should increase), a single-stage non-inverting amplifier would only have a maximum gain of unity. Therefore, two inverting amplifiers were placed in series. The preliminary design is shown in Figure 3-2.

This amplifier was modelled in Spice using the default three micron feature size MOSIS models to determine appropriate resistor values (19). Since process parameters could vary between the default Spice model and the actual fabricated amplifier, the amplifier was designed so that its linear region would be centered on 5 volts (for a 10V V_{dd}). The approximate minimum voltage generated by the PVDF film was calculated to be 0.1V (see page 3-3), so the output voltage with a gain of 5 in the linear region (see Figure 3-3) would be 0.5V (which should be detectable by external measurement devices). The linear amplification region is approximately 2V wide (see Figure 3-3). N-type

MOSFETs were used because electrons possess a higher mobility and this feature manifests itself in a larger gain per transistor area (18:40-41). The MOSFET geometry used incorporated a 3µm gate length and a 12µm gate width.
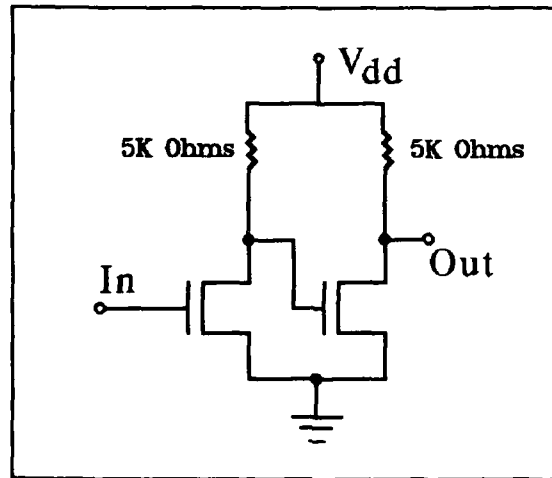
Figure 3-2. Schematic of the Discrete Sensor Element Amplifier Design.

The resistors were designed using an n-diffusion so that they could be placed in the same well as the transistors. A sheet resistance of 25Ω/square was assumed for the n-diffusion (18:121). In order to create a 5KΩ resistor (from the Spice analysis), 200 squares were required. Consequently, a resistor was created that was 4.5 µm wide and 900 µm long (see Figure 3-4).

To minimize the line resistance and capacitance, the amplifier should be as close to the sensor electrode as possible. However, since the electrodes will be beneath a layer of PVDF film, it would make testing difficult (since there would be no direct access to the electrode signal, or to the amplifier).

Therefore, a compromise was attained, and the amplifiers were placed on the periphery of the integrated circuit (see Figure 3-5).
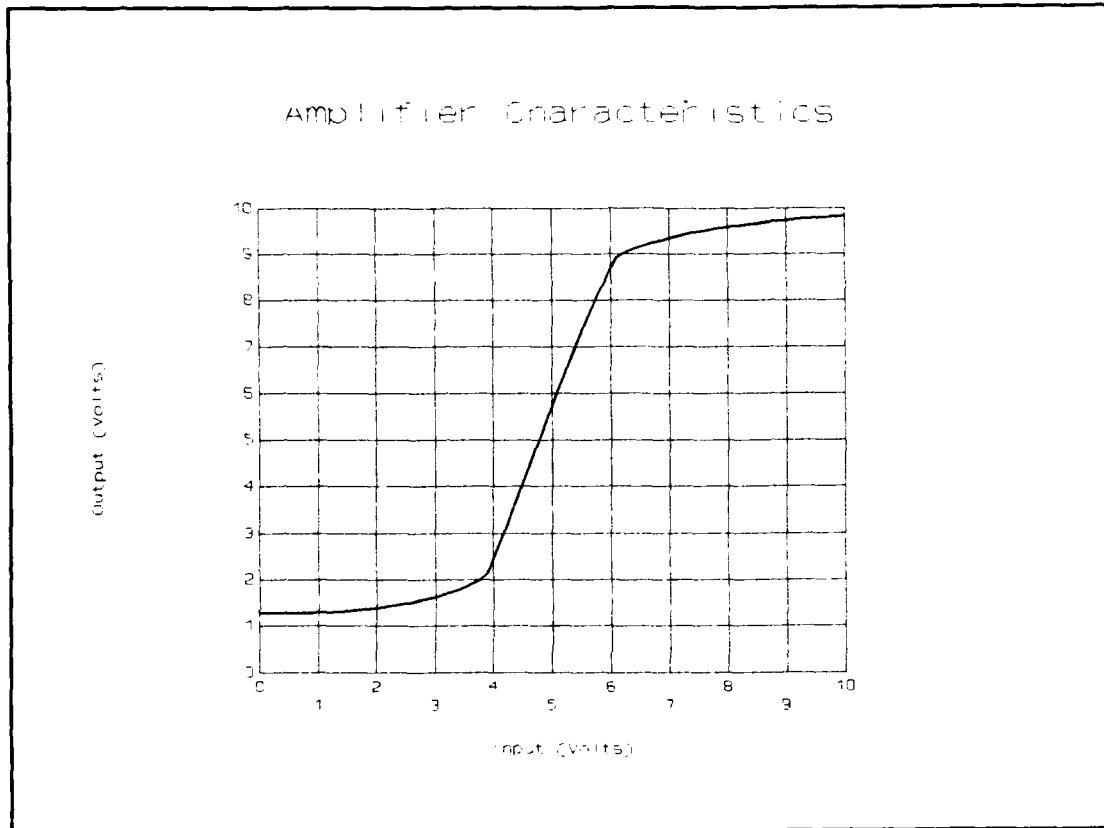
Figure 3-3. Spice Plot of Amplifier Characteristics.

For subsequent testing and verification of the amplifier characteristics, it was important to place sufficient pads to permit separate testing of each component (two MOSFETs and two resistors per amplifier). With the three pads shown in Figure 3-4 (and the V_{dd} and ground pads shown in Figure 3-5), it is possible to test each resistor and transistor.

```
cifplot* Window: -3675# 252## -1215# 4155#  ---  Scale: 1 micron is .015 inches (381x)
```

Test Pad

Input Test Pad

MOSFET

Resistor

Output Bonding Pad

Figure 3-4.   Caltech Intermediate Form (CIF) Plot of the Tactile Sensor's Amplifier.

Bias Voltage Considerations. Since the minimum signal generated by the PVDF film should be near 0.1V (see page 3-3), a bias voltage is required to bring the signals into the linear region of the amplifier. The easiest way to

accomplish this objective is to provide a resistor network on the input of the amplifier (20:397-400). The disadvantage with using this method, however, is that placing a relatively low resistance (compared with the high gate-to-substrate resistance of the MOSFET) between the electrode (which is the signal source) and ground would defeat the objective of using a MOSFET as a high input impedance amplifier, and would further attenuate an already small amplitude signal.

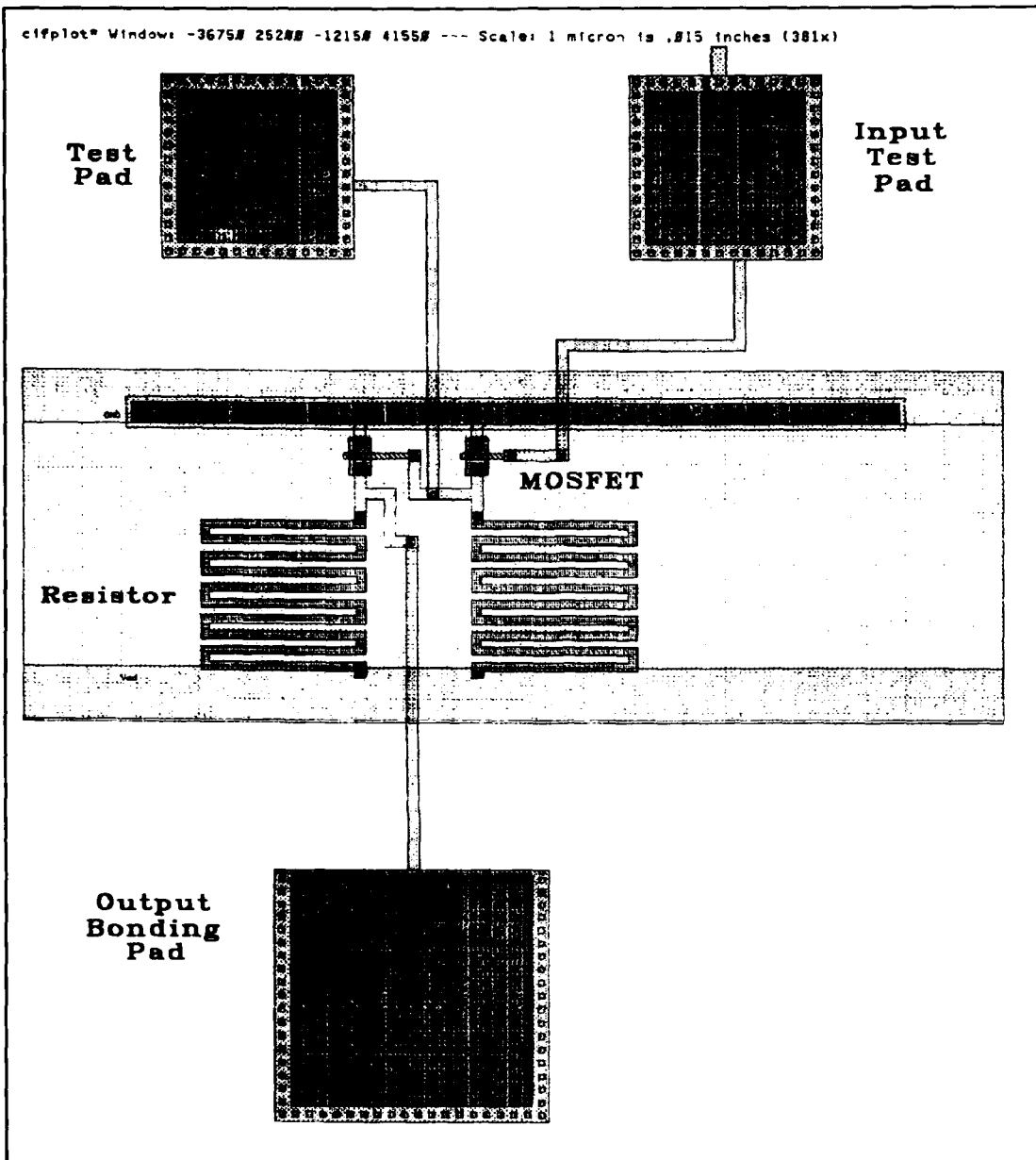An alternative scheme was devised to provide a biasing voltage for the top surface of the PVDF film. Since PVDF is a polar dielectric, the biasing voltage will be transferred to the electrode on the bottom of the film through the PVDF dipole moment after the system has equilibrated (13:35-37).

MOSIS CIF Submission. The complete layout for the integrated circuit is shown in Figure 3-5. The two vertical amplifier strips on either side of the circuit are electrically isolated, so the second strip can be used if one strip gets damaged. Located at each of the four corners are large pads which can be used to bias the top layer of the PVDF film. The entire electrode array is surrounded by alignment marks to facilitate locating particular elements after the array is covered with the PVDF film (that is, for proper placement of the loading test probe). The pads on the extreme left (16 pads) and right (17 pads) are the bonding pads. Should the IC behave as anticipated, these pads will permit testing of the IC without any probes. Also, the two sides without bonding wires will permit mounting the PVDF film and minimize damaging the delicate wire bonds. This layout was created using the Magic VLSI circuit

editor and converted to a CIF file which was then sent to MOSIS (8). The Magic file is listed in Appendix D.
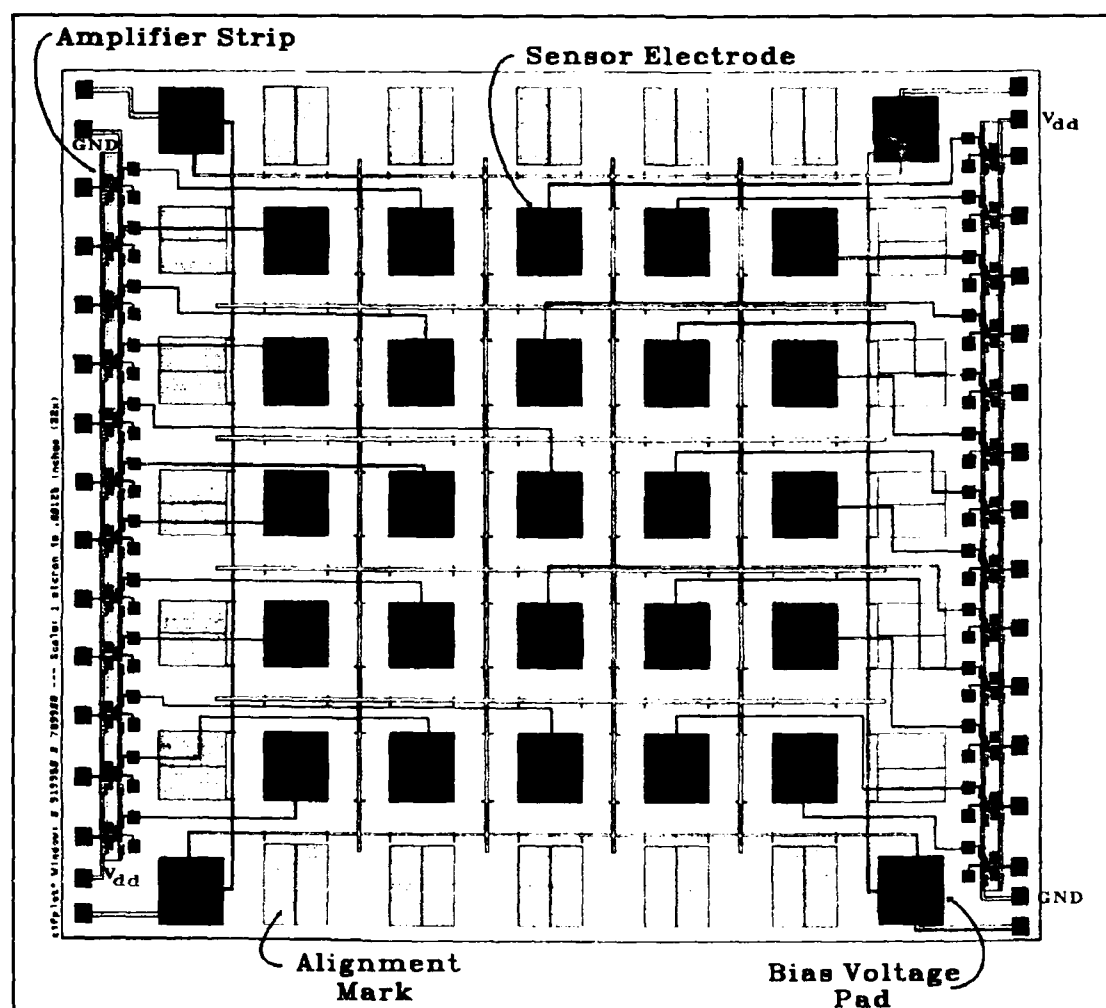

Figure 3-5. Caltech Intermediate Form (CIF) Plot of the Integrated Circuit.

Test Probe

Minimum and Maximum Loading Forces. The minimum and maximum test probe loading forces were derived from a suggested minimum force of 10^{-2}N applied over an area of 1×10^{-6} m^2, and a suggested maximum force of

3-9

10N applied over the same area (6:201). These parameters equate to a minimum weight of 3.7g applied over a discrete electrode area ($600\mu m \times 600\mu m$), and a maximum weight of 3.7Kg applied over the same area (assuming a gravitational acceleration of $9.8m/sec^2$).

The maximum weight seemed a bit unrealistic (it is similar to administering a 3Kg weight via a pencil point to the human fingertip) and would also be difficult to keep aligned over the small geometries of the tactile sensor. The maximum weight was therefore reduced to 100g (and the minimum weight was reduced to 1g).

<u>Alignment Considerations.</u> It was also necessary to determine, within the width of one electrode ($600\mu m$), where the loading probe would make contact, so a means of aligning the probe with respect to the tactile sensor's surface was devised. Rather than designing a relatively complex alignment mechanism, an existing instrument was identified; that is, a micromanipulator was used with an IC microprobe station. A loading probe sub-assembly, which was compatible with the micromanipulator arm, was then designed.

<u>Microprobe Sub-Assembly.</u> A diagram of the microprobe sub-assembly is shown in Figure 3-6 along with a loading weight (50g when made out of lead). Since the loading probe was fabricated from aluminum, it should weigh approximately 2g (based upon the volumetric density of aluminum).

<u>Actual Minimum and Maximum Weights (Calibration).</u> The loading probe and three weights were fabricated in the AFIT Model Shop. When they were returned, the entire system (micromanipulator and loading test probe with zero, one, two and three weights) was calibrated.
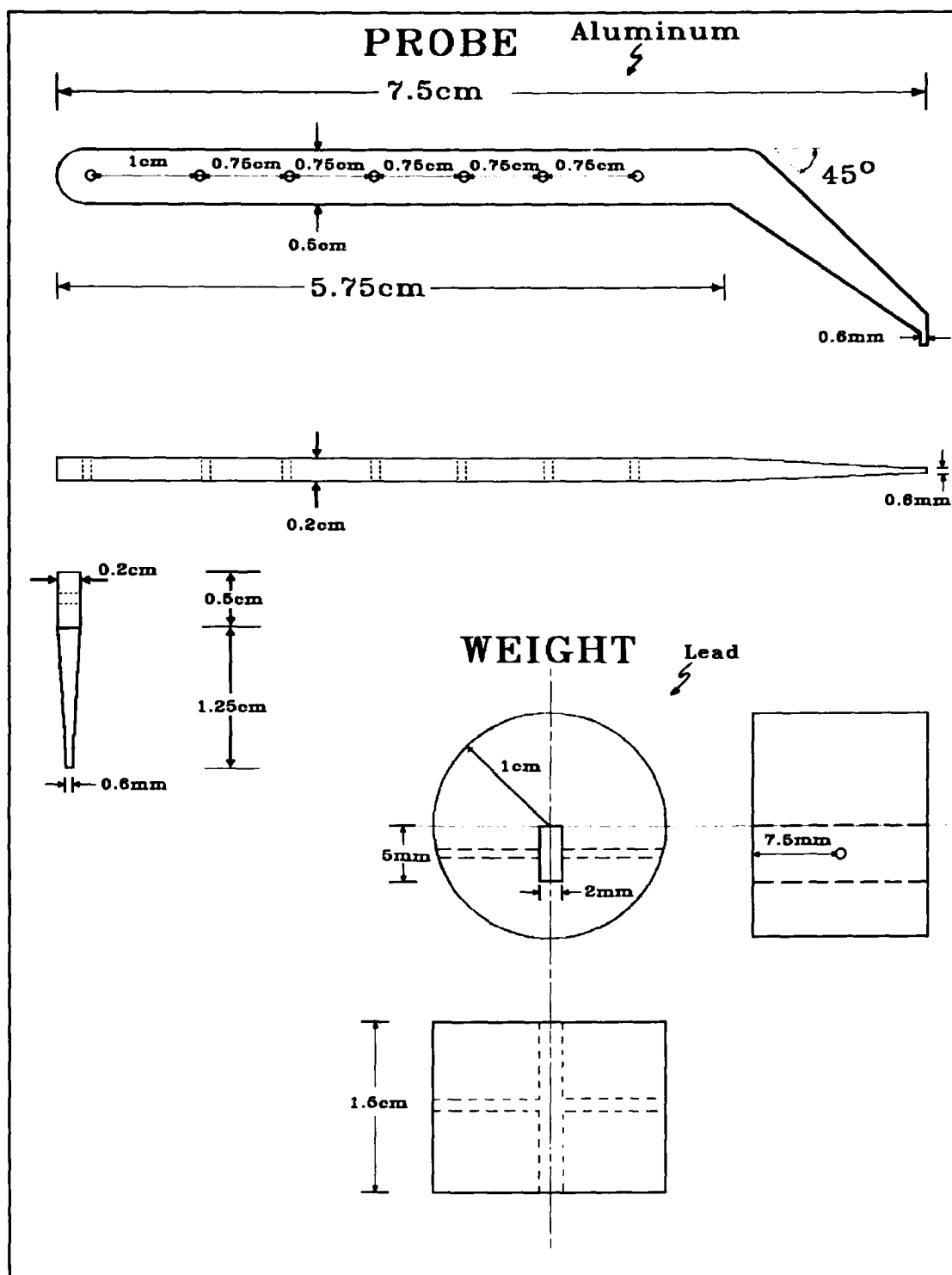
3-10

Figure 3-6. Microprobe Sub-Assembly.

With no weights, the loading probe presented a weight of 0.8g to a balance located in the same relative position as that of the tactile sensor during the test phase. With all three weights, the probe presented 76g to the balance. These weights were slightly lower than predicted, but still sufficient for investigating a range of weights (forces) spanning two orders of magnitude.

Test Protoboard

A protoboard was configured to provide the proper signals to the tactile sensor IC for testing. These signals included ground (pins 9 and 42), V_{dd} (pins 23 and 55), and V_{bias} (pins 4, 8, 24, 41, and 56). The protoboard also permitted easy access to the output signals.

LED Test Grid

In order to facilitate examining the response of the entire tactile sensor array, and to provide a means of obtaining a qualitative feel for the operation of the sensor, a second test board was designed and fabricated. This board consisted of an array of LEDs connected to the output of each of the 25 amplifiers. The schematic of a single LED indicator is shown in Figure 3-7.

This board produced a visual picture of the state of the entire sensor array without having to probe each of the outputs. This tool was invaluable during the initial biasing phase of each test, since the LEDs displayed the same relative brightness when the sensor elements were in a similar bias state.

PVDF Film Etching/Cutting Process

A process for etching and cutting the bulk PVDF film for subsequent tests was also created. The vendor procured films are available in sheets roughly 8 by 11 inches with aluminum metallization on both surfaces. Since the

required PVDF film samples had to be cut into squares the size of the electrode array (6mm×6mm), and since they could have metal on only one side, the following process was implemented to realize the desired PVDF material configuration (the required materials and equipment are listed in Appendix A):
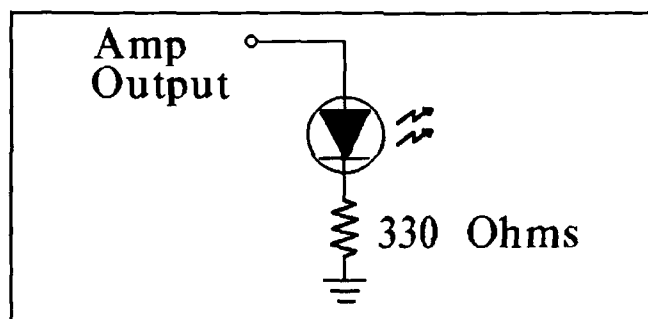
Figure 3-7.   Schematic of a Single LED Indicator Element.

1) A grid of 6mm by 6mm squares was created on a sheet of plain white paper.

2) A glass-slide was placed beneath the bulk PVDF film and a section of PVDF film was cut (using a #11 scalpel) so that it would fit within the borders of the glass-slide. A drop of isopropyl alcohol was placed on the glass-slide *prior to the placement of the PVDF* film to keep the film in place. The top surface was marked with an indelible marker by placing a dot in one corner (this action facilitated subsequent determination of the polarity of the PVDF film sample).

3) The exposed metallized surface of the film was etched with a cotton swab wetted with dilute ferric chloride (1 part ferric chloride to 10 parts

de-ionized water). The etchant was kept away from the PVDF film boundaries since it could diffuse beneath the film. Etching through the thin aluminum film occurred in approximately 1 to 5 minutes, and it was marked by a distinct darkening of the etched area.

4) The PVDF film was then cleaned by rinsing it thoroughly in de-ionized water for 2 minutes. This rinse was accomplished by removing the PVDF film from the glass-slide. When the rinsing operation was completed, a fresh glass-slide was used to hold the PVDF film (the PVDF film was oriented so that the orientation dot was on the top surface). Excess moisture was removed from the PVDF film/glass-slide assembly with a paper towel.

5) The glass-slide was placed over the 6mm paper grid. Using the gridlines as a guide, the PVDF film was cut into 6mm squares. A sharp scalpel was essential, and the cuts were made as smoothly and as quickly possible. The PVDF film squares were cut from the center (etched area) of the film so that there was no possibility of leaving metal on both sides of the film. The orientation dot was then transferred to each square with an indelible marker.

6) The squares were stored dry in folded lens tissue (after insuring that the squares were separate and had no chance of scratching each other).

Tactile Sensor Fabrication

The procedure for creating tactile sensors was developed and refined after attempting several experimental procedures. Unanticipated problems with

charge storage on both the floating gates and the PVDF film squares damaged some of the integrated circuits. To minimize this failure mechanism, the following procedures were implemented to fabricate the tactile sensors from the integrated circuits and the cut PVDF film samples (the required materials and equipment are listed in Appendix A):

1) Since charges can be stored on the floating gate and on the PVDF film squares, it is essential that these charges be neutralized immediately before contacting the IC and the PVDF film squares. To neutralize these charges, the IC was dipped into grounded water (200ml of de-ionized water and 1 drop of concentrated HCl in a beaker with an electrical connection to earth ground) for 1 minute. The same procedure was accomplished for the PVDF film square. The IC was dried with nitrogen gas carefully aimed so as not to break any of the delicate wire bonds. The PVDF film square was dried with lens tissue.

2) A drop of the adhesive (Shipley Miroposit 1400-17 Photoresist) was deposited on a clean glass-slide. A small amount of photoresist was then drawn up into a 1mm glass pipette. Enough photoresist was transferred to the IC to thinly cover the central 9 electrodes (a dissecting microscope proved useful). The PVDF film square was carefully placed (metal side up--verified with an ohm-meter) on the IC so that it covered all 25 electrodes. Some photoresist escaped near the PVDF film edges.

3) A compression block (made from a glass-slide cut into approximately 7mm×7mm squares with a diamond scribe, was coated with a thin layer silicone oil. The compression block was gently placed on the PVDF film

(silicone oil between the compression block and the PVDF film) using tweezers. Once the compression block was in place, a binder clip was positioned so that it compressed the IC/photoresist/PVDF film/compression-block sandwich (see Figure 3-8). The whole assembly was placed into a 70°C oven for 20 minutes. After baking, any stored charge was removed by dipping the whole assembly in grounded water.
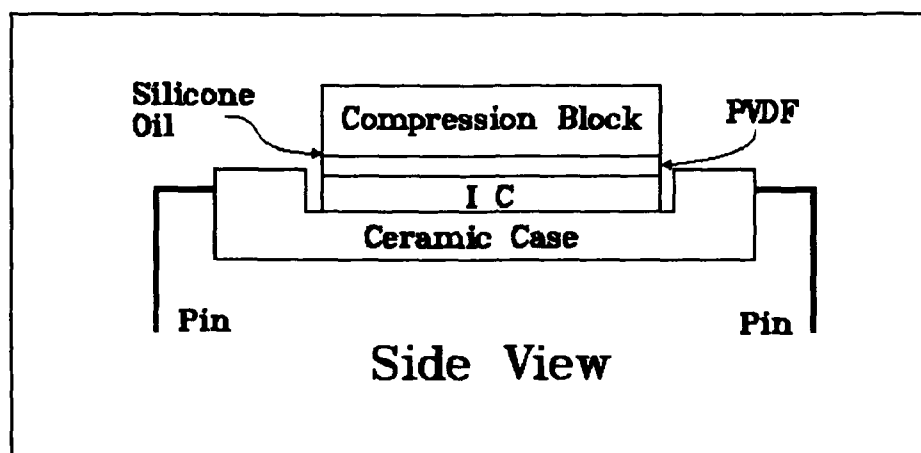
Figure 3-8. IC/Photoresist/PVDF/Compression-Block Sandwich.

4) The top (metallized) surface of the PVDF film was connected to an external pin with a 1 mil wire and silver paint. Originally, the metallized surface would have been connected to the bias voltage pads by placing silver paint on one or more corners of the PVDF film and drawing the paint over the edge so that it contacted the bias voltage pad. However, the silver paint residue is difficult to remove from the surface of the IC. Thus, in order to conserve ICs (so that a single IC could be used for multiple tests), a 1 mil wire provided the connection

between the metallized surface of the PVDF film and to external pin 4 (see Figure 3-9). Good electrical contact was verified by placing one lead of a continuity checker on top of the PVDF film and another lead on pin 4 of the IC.

Figure 3-9. Fabricated Tactile Sensor.
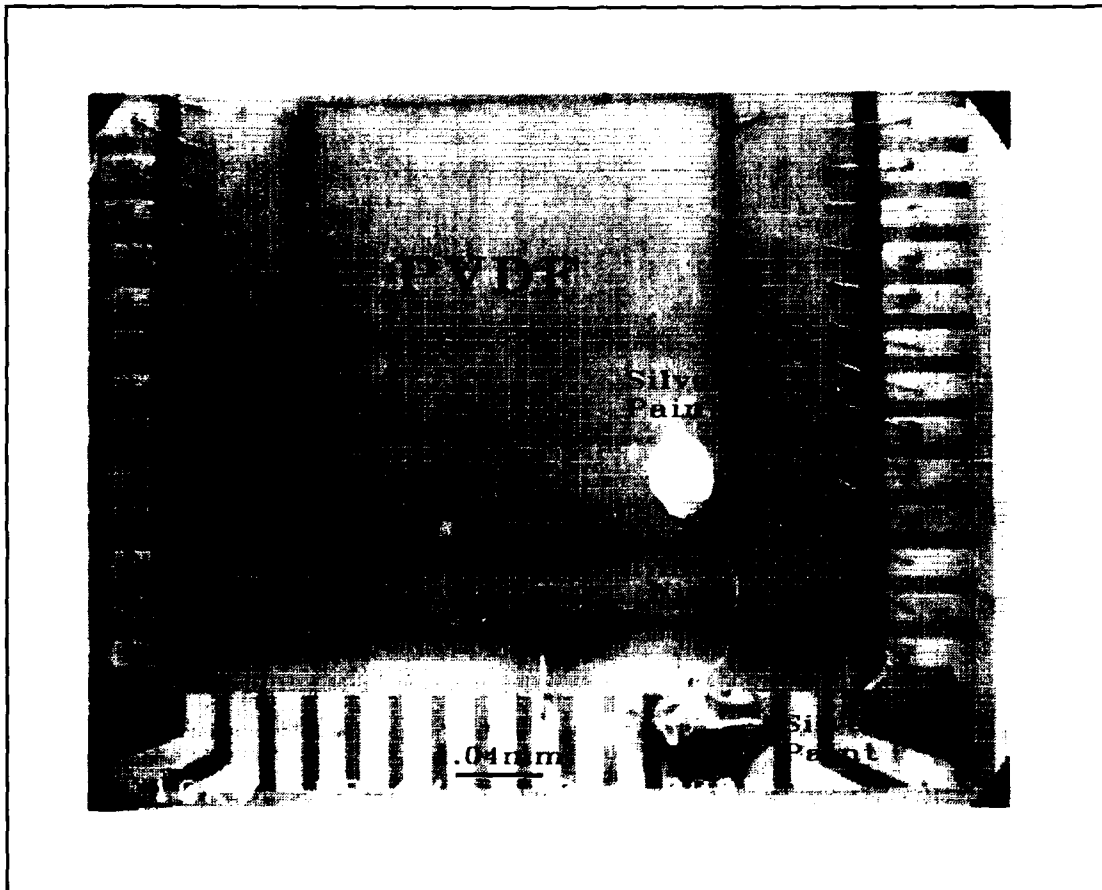
Test and Evaluation

The final area of design was the development of a test plan which was broken down into logically arranged sub-tests which contributed to the

knowledge concerning the performance of the components of the tactile sensor before actually fabricating and testing the completed tactile sensor. These sub-tests consisted of an integrated circuit test, a PVDF film sample test, and a complete tactile sensor test (the materials and equipment used in these tests are listed in Appendix A).

Integrated Circuit Testing. The purpose of this test was to verify proper operation of the fabricated ICs (insuring that the vendor did not make any fabrication errors) and to validate the design by amplifying controlled test signals. This test was compartmented into 4 major areas: MOSFET tests, resistor tests, amplifier tests and sensor element interconnection tests.

MOSFET Characteristics. The MOSFETs were tested by randomly selecting several MOSFETs from various ICs and connecting the gate, source, and drain (using the probe pads and the microprobe station) to a semiconductor parameter analyzer (Hewlett Packard Model HP 4145). After the discrete transistor curves were obtained, amplifier testing was initiated. If malfunctions were noted, further tests would be conducted to determine if the fault was a MOSIS fabrication problem, or a design flaw. The test protocol included the following critical steps:

1) The selected IC was placed on a blank protoboard (to protect the IC pins) and this assembly was placed on the stage of the microprobe station (Micromanipulator Model 6200).

2) Three microprobes (Micromanipulator Model 450) were connected to the gate, source and drain connections of the semiconductor parameter analyzer. The three microprobe tips were then carefully guided to rest

on their respective pads (see Figure 3-4).

3) The MOSFET test for a V_{ds} range of 0 to 10V and a V_g range of 0 to 10V was initiated (this is a built in test for the HP 4145).

4) The data was plotted on an attached plotter.

5) The test was repeated on several different transistors and ICs.

Resistor Value Measurement. This measurement determined the actual value of the amplifier resistors (which were designed to be 5KΩ). Since the amplifier was designed with potential fabrication variations in mind, the actual resistor values would have to be considerably different from the predicted values (approximately less than 1KΩ or greater than 10KΩ) before the amplifier performance would have been adversely affected. This measurement was composed of the following steps:

1) The selected IC was placed on a blank protoboard (to protect the pins), and this assembly was placed on the stage of the microprobe station.

2) Two microprobes were connected to the two inputs of an ohm-meter (see Figure 3-10).

3) One microprobe was gently placed on the V_{dd} pad (see Figure 3-5), and the other microprobe was gently placed on a pad connected to a resistor (see Figure 3-4). The resistance value was taken from the ohm-meter (Fluke Model 77/AN).

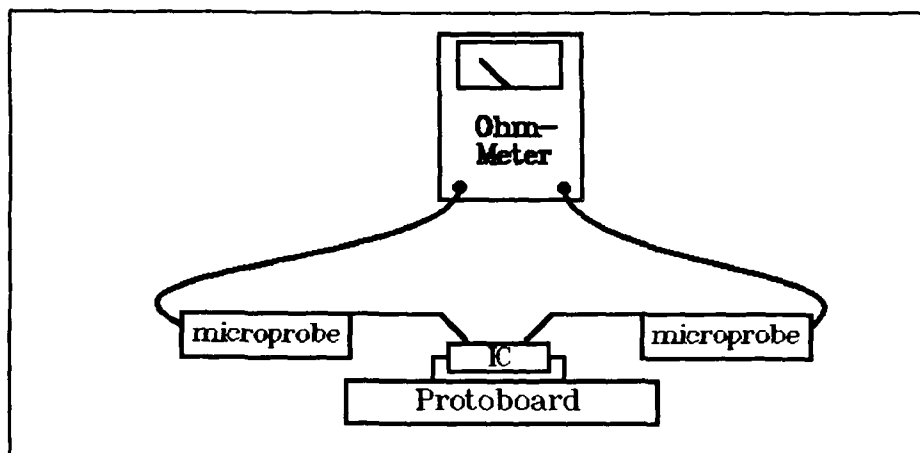4) Step 3 was repeated on several different ICs.

Figure 3-10. Instrumentation Configuration for the Resistor Measurement and Interconnection Tests.

Amplifier Characteristics. For a random selection of amplifiers, a known signal was applied to their inputs, and the outputs were compared with the predicted Spice values (see Figure 3-3). If the results were within the margin of error associated with the fabrication process, the next test was accomplished. Otherwise, as before, further tests would be conducted in order to determine if the fault was a MOSIS fabrication problem, or a design flaw. The program provided in Appendix E was used to automate the routine. The following procedure was followed when conducting this test:

1) The selected IC was positioned on a wired protoboard with appropriate ground and V_{dd} connections (see page 3-12), and this assembly was placed on the stage of the microprobe station.

2) A microprobe was connected to the V_{source} output of the electrometer (Keithley Model 617). The microprobe tip was gently placed on the input pad of the amplifier (see Figure 3-4). The input of the

3-20

electrometer was connected to the output pin of the amplifier (see Figure 3-11).

3) A 10V V_{dd} was applied to the IC through the protoboard connections.

4) The V_{source} of the electrometer was set to 0V, and the V_{source} output was enabled. The electrometer was set to measure volts and the data collection computer (Zenith Model 248) was connected to the GPIB port of the electrometer.

5) The program listed in Appendix E was run.

6) The test was repeated for several amplifiers.
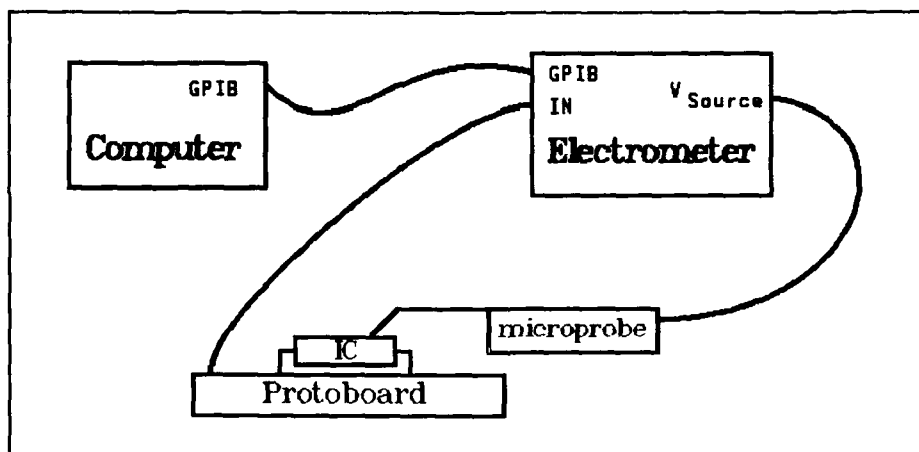

Figure 3-11. Instrumentation Configuration for the Amplifier Test.

Interconnect Verification. The final IC test was implemented to verify the proper interconnection between the electrode array elements and their respective amplifiers. If there was a good electrical connection between the electrodes and their amplifiers, and the previous tests proved successful, the

3-21

ICs were fabricated (in all probability) without any characteristic flaws. This test was accomplished using the microprobe station to probe the electrode (which will eventually lie beneath the PVDF film) and the input pad of the amplifier (which was used to inject a signal in the previous test) to verify that there were no open circuits (with a ohm-meter). This test was composed of the following steps:

1) The selected IC was placed on a blank protoboard (to protect the pins), and this assembly was placed on the stage of the microprobe station.

2) Two microprobes were connected to the two inputs of an ohm-meter (see Figure 3-10).

3) One microprobe was gently placed on the selected electrode, and the other microprobe was gently placed on the input to the respective amplifier (see Figure 3-4). A good connection resulted in a low ($<10\Omega$) reading.

4) Step 3 was repeated for the entire electrode array.

PVDF Film Test. The next test dealt with the properties of the PVDF film and was implemented to insure that the film possessed the required piezoelectric properties (in addition to determining the film polarization). A sample of PVDF film was connected to an IC amplifier through the microprobe station to insure that the signals generated by the strained PVDF film could be amplified by the IC amplifier. Also, the signal change between the strained state and the relaxed state (either positive or negative) was used to determine the polarity of the sample. Since each sample had a marking dot indicating the

top surface of the bulk sheet, the polarity of the sample was used to determine the polarity of the sheet. The polarity property was used to decide which surface to etch for subsequent tactile sensor preparation. This test was composed of the following critical steps:

1) The PVDF film sample (with copper tape attached to both sides) was placed between the glass-slides and one surface of the sample was connected to the V_{source} output of the electrometer, and the other surface was connected to a microprobe (see Figure 3-12).

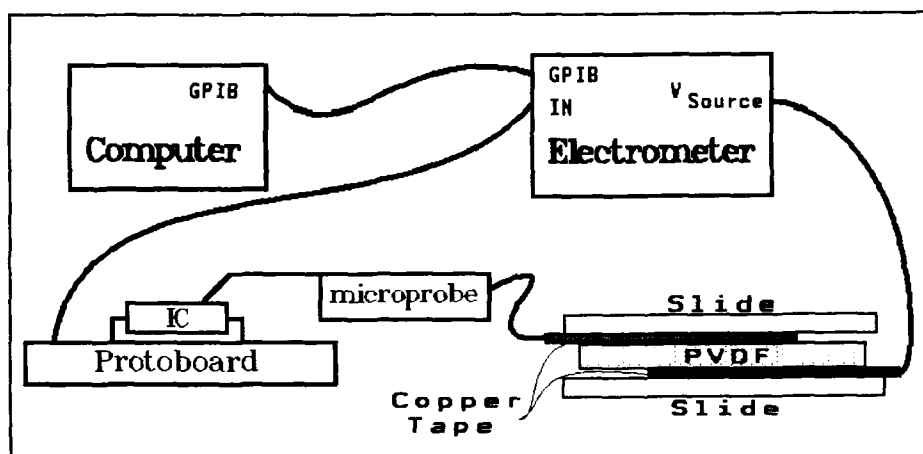Figure 3-12. Isolated PVDF Film and Amplifier Instrumentation Configuration.

2) An IC was selected and placed in a protoboard with appropriate ground and V_{dd} connections (see page 3-12). This assembly was then placed on the stage of the microprobe station.

3) The input of the Keithley 617 electrometer was connected to the output of the amplifier (see Figure 3-12). The V_{source} of the electrometer was

set to 4V and enabled. The GPIB port of the electrometer was connected to the data collection computer. The microprobe tip was gently placed on the input pad of an amplifier (see Figure 3-4).

4) The program listed in Appendix E was run.

5) Ten seconds into the program, a weight (100g-500g) was gently lowered on the glass-slide.

6) Thirty seconds into the program, the weight was removed.

7) The test was repeated for a number of weights and PVDF film orientation.

Tactile Sensor Testing. After the tactile sensors were fabricated, their performance characteristics were measured. The first phase of tactile sensor tests concentrated on the performance of individual sensor elements. The second phase focused on determining the degree of coupling between nearest neighbor sensor elements. Phase three compared the response of the various sensor configurations to a fixed bias voltage. The fourth and final phase demonstrated the response of the sensor to an applied load with a distinctive shape.

Individual Sensor Response. This test characterized the response of an individual element with respect to a series of test loads. Six measurements were accomplished for each sensor configuration for six different loads (resulting in 36 tests for each sensor configuration). Simultaneously, measurements were accomplished with respect to a sensor element's nearest

neighbors to facilitate the next phase of tests. The following procedure was used to perform this test:

1) A tactile sensor was prepared and placed in a protoboard with appropriate ground and V_{dd} connections (see page 3-12). This assembly was then placed on a flat and level surface.

2) The output pin of the tactile sensor element under test was connected to channel 1 of digitizing oscilloscope (Hewlett Packard Model HP 54100) as shown in Figure 3-13. The output pin of the nearest neighbor of the element under test was connected to channel 2 of the oscilloscope (see Figure 3-13). The GPIB port of the oscilloscope was connected to the data collection computer. The oscilloscope was set to trigger on a 3V signal on channel 1.
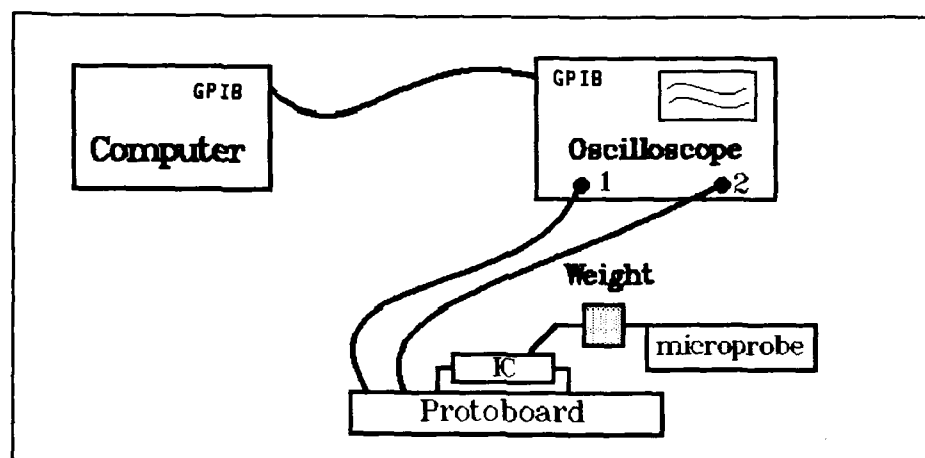

Figure 3-13. Instrumentation Configuration for the Tactile Sensor Test.

3) The loading test probe (with an appropriate load) was positioned next to the mounted tactile sensor.

4) The applied bias voltage was adjusted such that there was a constant 2V output on channel 1 (the output of the sensor element under test).

5) The loading test probe was gently lowered onto the sensor element.

6) The data displayed on the oscilloscope was both printed and saved to a disk (using the programs listed in Appendix E).

7) Steps 4 through 6 were repeated for the next load to be evaluated.

8) Steps 1 through 7 were repeated for all tactile sensor configurations.

Nearest Neighbor Response. The purpose of this test was to determine the degree of coupling between a strained element and its nearest neighbors. If the nearest neighbor (from the individual sensor response test) shows a high degree of coupling, the "individual sensor response" test was repeated for the next nearest neighbor and so on until there was no detectable coupling. This information is critical for establishing the minimum separation between sensor elements in order to minimize undesirable coupling.

Bias Voltage Response. This test determined the effect of a fixed bias voltage applied to the various sensor configurations for a fixed amount of time. The no-load output voltage of the amplifier at the end of the time period yielded a relative idea as to how quickly the various PVDF film thicknesses responded to bias voltages. This provided the information necessary to determine the optimal sensor configuration. The following steps were used to implement this test:

1) A tactile sensor was selected and placed in a protoboard with appropriate ground and V_{dd} connections (see page 3-12).

2) The amplifier output of the central electrode was connected to the electrometer's input. The GPIB port of the electrometer was connected to the data collection computer.

3) A V_{dd} of 10V was applied.

4) A 10V bias voltage was applied and periodic electrometer measurements were made using the program listed in Appendix E.

5) The program was stopped after 10 minutes.

6) The test was repeated for the other tactile sensor configurations.

Group Response. This test demonstrated the operation of the entire sensor array with an applied load with a distinctive shape. The load consisted of a plastic ring with an outside diameter of 5mm and an inside diameter of 2.5mm mounted on a 300g weight (see Figure 3-14).

Initial experiments indicated that without an elastomeric membrane between the load and the tactile sensor, only a few sensors would be activated (since both the load and the tactile sensor had minor surface variations and perfect alignment was difficult). Therefore, prior to this test, the entire tactile sensor surface was coated with Dow Corning 3140 RTV silicone sealer (so that the level of silicone was even with the height of the package--it was smoothed with a glass-slide) and allowed to cure for 48 hours in a 50°C oven. This coating provided an elastomeric membrane to minimize any surface variations between the tactile sensor and the object.
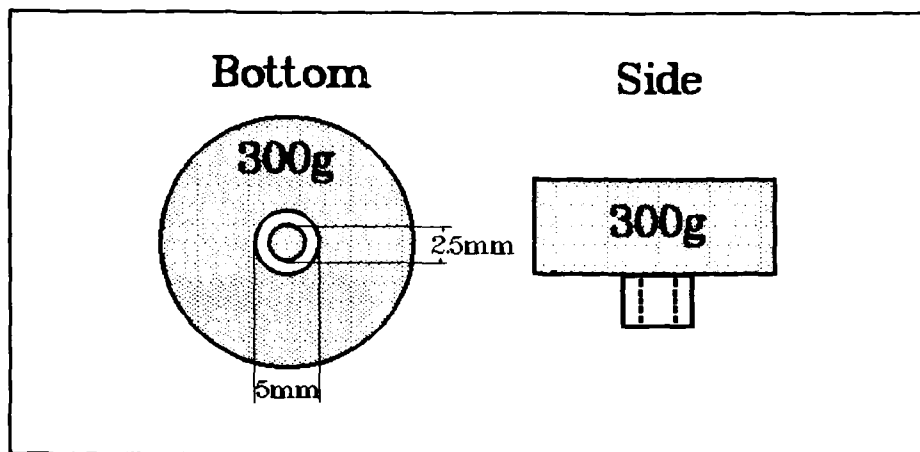
Figure 3-14. The Group Response Test Load.

Since this was the last test, the tactile sensor configuration used was the optimal configuration that was determined from the results of the previous tests. The following test procedure was used:

1) The tactile sensor was placed in a protoboard with appropriate ground and V_{dd} connections (see page 3-12). This assembly was placed on a flat and level surface.

2) The bias voltage was adjusted so that there was a constant 2V output on the sensors. The input of the electrometer was connected to a probe (to aid in quickly scanning the values on the 25 amplifiers). The GPIB port of the electrometer was connected to the data collection computer.

3) Prior to the load application, the values of the entire electrode array were scanned using the program listed in Appendix E.

4) The load was gently lowered onto the surface of the tactile sensor.

5) The values of the entire electrode array were scanned using the program listed in Appendix E.

Conclusion

This chapter discussed the considerations that influenced the design of the major hardware components required to implement and evaluate an IC-based PVDF film tactile sensor. Also described were the critical steps required to fabricate tactile sensors from the basic subcomponents. Finally, a detailed test plan was presented which integrates the results from tests associated with the individual subcomponents of the sensor before tests were conducted on a fabricated tactile sensor. This feature eliminated many unknowns that would have undoubtedly appeared if only a completed tactile sensor were tested. The results of these tests and all the pertinent data collected are discussed in the next chapter.

IV. Experimental Data and Analysis

Introduction

The data collected from the performance tests described in Chapter III is presented in this chapter along with an analysis of the results. The order of presentation is identical to the order of the performance tests discussed in Chapter III, as are the major areas of investigation: the integrated circuit, the PVDF film, and the tactile sensor.

Integrated Circuit Testing

The integrated circuit tests were composed of the MOSFET test, the resistor test, the amplifier test and the interconnect test. Since the MOSFETs were the components most susceptible to fabrication variations, they were tested first.

MOSFET Characteristics. The MOSFET electrical performance test was conducted in accordance with the procedure discussed in Chapter III. The theoretical (Spice) MOSFET curves are compared with the experimental values in Figure 4-1. The experimental values were collected with a Hewlett Packard semiconductor parameter analyzer (model HP 4145) and were very close to the values predicted by Spice (19). Since the transistors were the components most sensitive to fabrication variations, the results from this test indicated that there were probably no significant fabrication errors introduced by the vendor, so the next test was initiated.
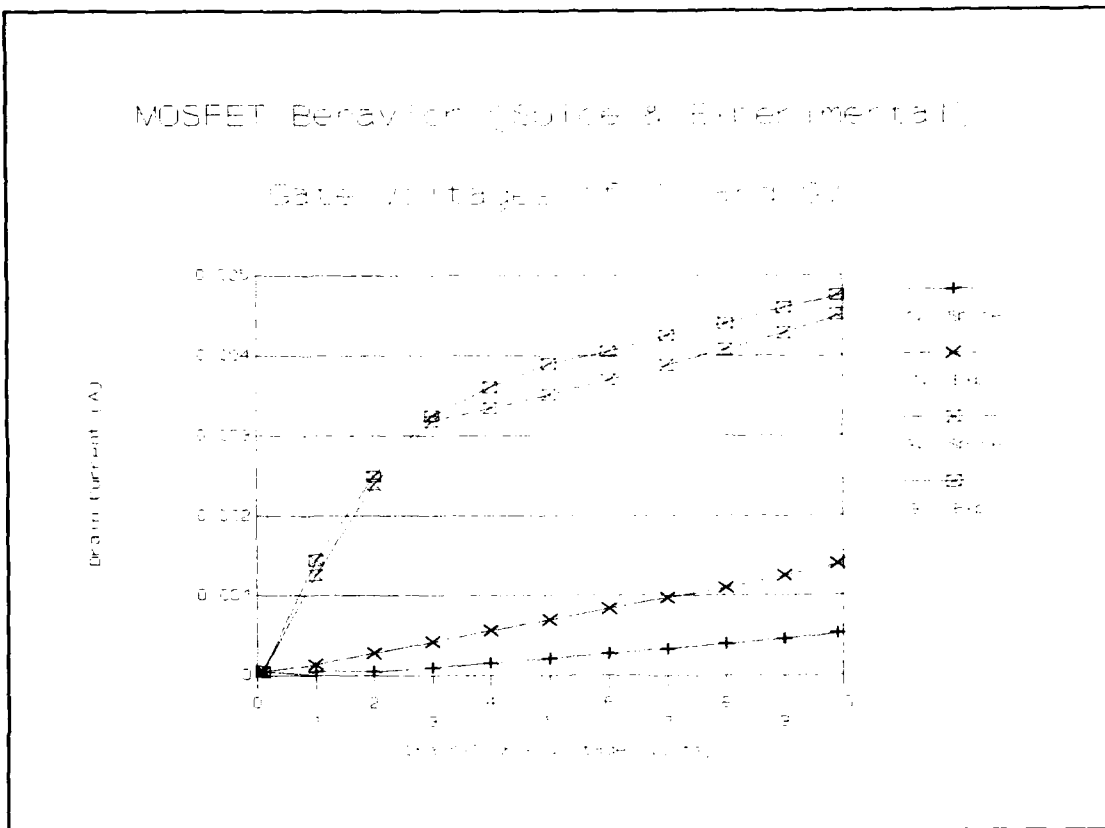
Figure 4-1. Typical Electrical Performance Curves for the MOSIS Fabricated MOSFETs.

Resistor Value Measurement. The resistor measurement test described in Chapter III yielded an average value for the resistors of 6.4KΩ. The designed value was 5KΩ (see Chapter III) with an assumed sheet resistance for the n-doped silicon of 25Ω/square. The actual sheet resistance (based on 6.4KΩ over 200 squares) was 32Ω/square, and the vendor reported value for this IC run was 29.5Ω/square. These values are all well within the margin of error associated with the amplifier design (which could tolerate a resistor value as high as 10KΩ). However, because of the larger resistance, the linear region

4-2

of the amplifier was expected to shift away from the 5V operating point. The next test confirmed this observation.

Amplifier Characteristics. The amplifier test described in Chapter III was used to test six amplifiers from different ICs. A plot of the average result (and the corresponding standard deviation) is shown in Figure 4-2. The center of the linear region shifted from the designed value of 5V to approximately 4V. This shift can be attributed to the increased value of the amplifier resistors. The full linear region of the amplifier was still available, so the only change in subsequent performance testing would be a reduction of the bias voltage. Since the amplifier performed as expected, the only barrier to a fully functional IC would be a flaw in the interconnections between the amplifiers and the sensor electrodes.

Interconnect Verification. The final IC test revealed one small error. Specifically, the amplifier connected to bonding pad 10 had a missing connection to its corresponding sensor electrode. The interconnect stopped short of the intended sensor electrode by 3μm (see Figure 4-3). This was not a fabrication problem because a subsequent check of the submitted design also showed a missing connection. The error was introduced into the original design when the zoom-out mode in the VLSI CAD tool, Magic, was used. When in the zoom-out mode, a 3μm error is indistinguishable from a valid connection. The missing connection to amplifier 10 (numbered after the corresponding bonding pad location) was turned into an advantage because it was subsequently used as a control amplifier after the PVDF film was applied. The remaining 24 sensor electrodes had good connections; so, with the exception of

the single bad connection, the IC performed as expected. The next test determined if the IC would amplify actual PVDF signals.
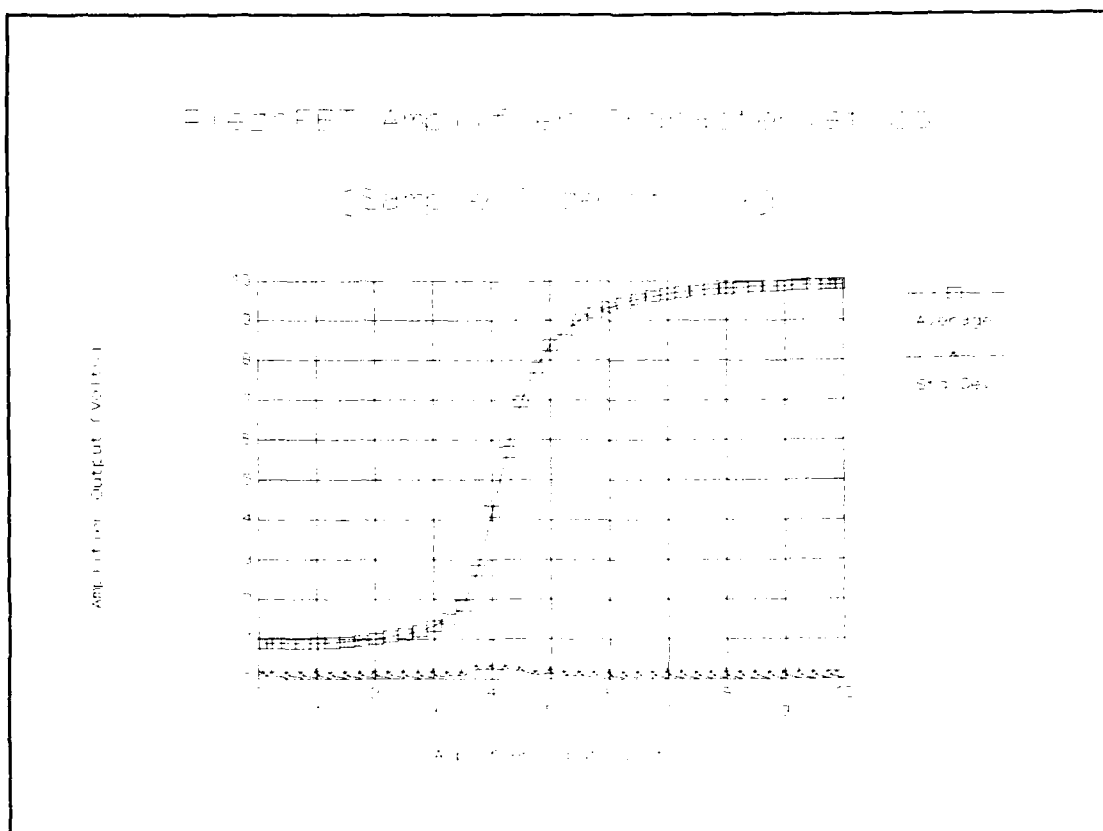

Figure 4-2. Actual Amplifier Performance Characteristics (Average of Six Different Amplifiers).

PVDF Film Test

The PVDF film test was performed as described in Chapter III. Shown in Figure 4-4 is the average of three test trials associated with the Solef 40μm thick film. There is very little change between the peak amplitudes of the various loads due to the saturation effect of the amplifier. The PVDF film was biased so that the amplifier produced approximately a 4V output signal in the no-load

state (which required a bias voltage of approximately 4V). However, from Figure 4-2, the amplifier begins to saturate with an input voltage of approximately 5V. Since there is only a 1V linear region (in the increasing positive voltage sense), the amplifier saturated for the loads used in this test.
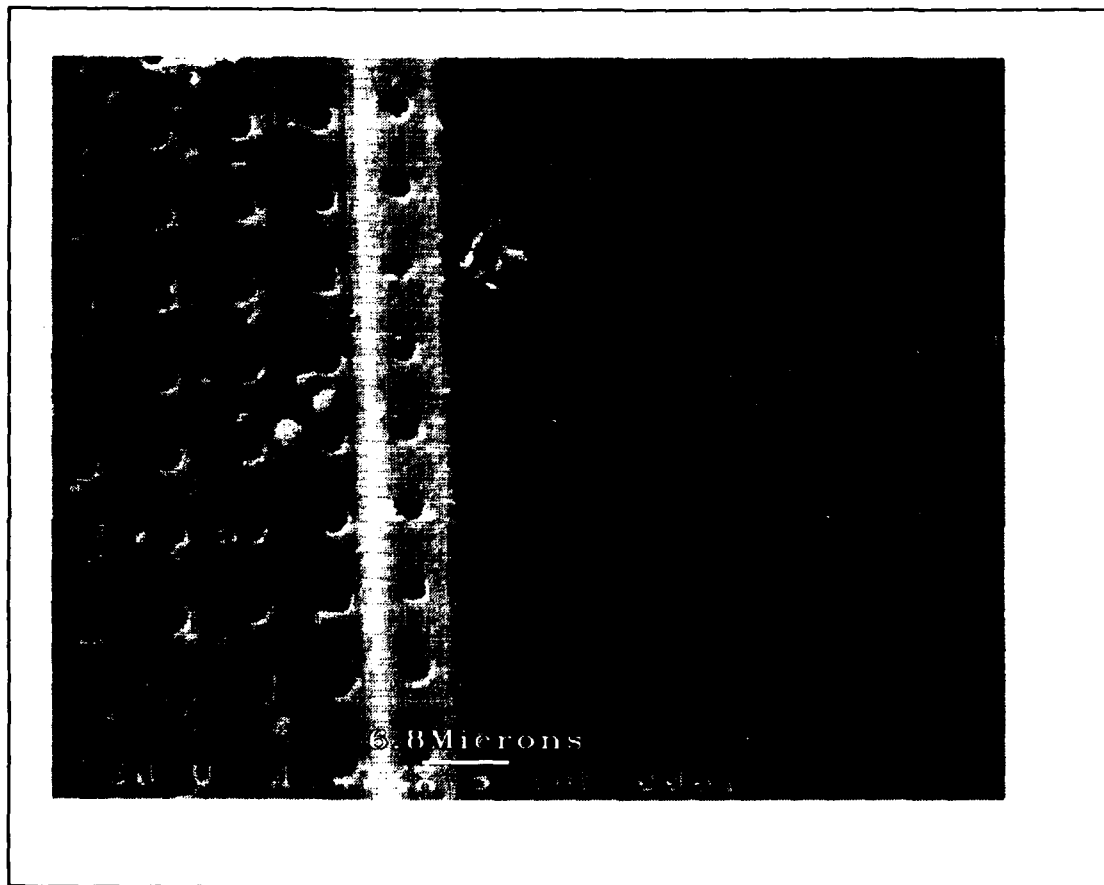

Figure 4-3. Missing Interconnection (Magnified 1,470 Times).

The different rates of decay during the time that the film was loaded are the only obvious manifestations of the magnitude of the loads. The rate of decay is based on the time it takes the charge generated in the PVDF film to

equilibrate through the fixed resistances associated with the test instrumentation arrangement (in this case, the input impedance of the microprobe). As the load increases, the amount of charge generated increases (see Chapter II). Therefore, the larger the load, the slower the rate of decay (since there is more charge to equilibrate). This behavior is evident in Figure 4-4 since the slowest rate of decay is caused by the 500g load, while the fastest decay rate is caused by the 100g load.
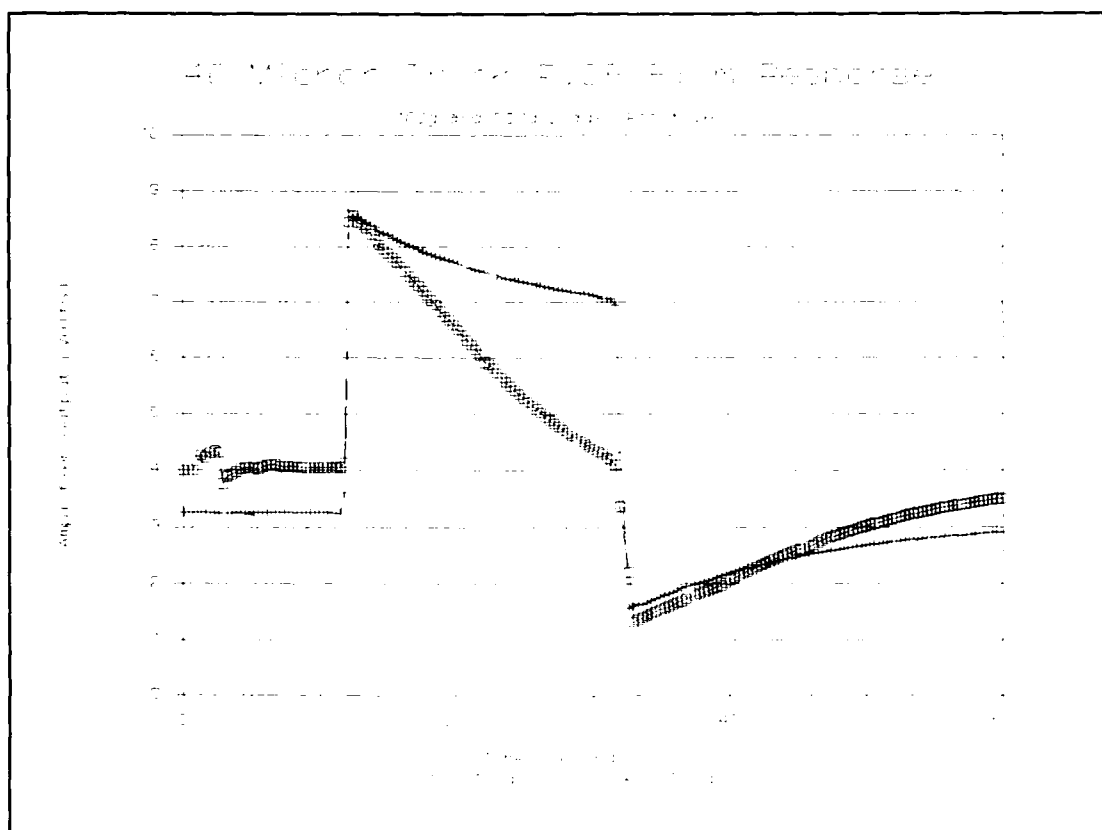

Figure 4-4. Response of the Solef 40μm Thick Film for 100g and 500g Loads The Film was Orientated so that a Load Application Produced a Positive Voltage Change.

Another key piece of information revealed by this test was the polarity of the film. When the same sample of PVDF film used in Figure 4-4 was turned over, and the test repeated, Figure 4-5 depicts the result. Reversing the orientation of the film reversed the direction of the voltage change when a load was applied. Using this simple test, the polarity of each of the bulk PVDF film sheets was determined. The surface which was subsequently etched was the surface which had to be facing down (that is, contacting the gate electrodes) in order to create a positive change in the output voltage when a load was applied (as in Figure 4-4).

Tactile Sensor Performance Test

The tactile sensor performance tests were composed of the individual sensor response test, the nearest neighbor response test, the bias voltage response test, and the group (multiple sensor element) response test. The individual sensor response test was accomplished first to facilitate determining the optimal sensor configuration for the group response test.

Individual Sensor Response. The individual sensor response test was performed on film thicknesses of 25μm, 40μm, 52μm, and 110μm. The 110μm thick film was chosen as the upper bound since it was too thick to uniformly conform to the surface features of the IC. The 25μm thick film was chosen as the lower bound because the thinnest film available (9μm thick), was much to thin too work with (it tended to buckle and wrinkle).

A sample of the results of a load application during this test is shown in Figure 4-6. The full set of data collected during this series of tests is presented in Appendix F. A summary of the average readings for each of the four tactile

4-7

sensor configurations is shown in Figure 4-7. Biased with a no-load output of 2V, the 110μm thick film was operating close to the saturation point of the amplifiers. Therefore the 110μm thick film test was repeated, but with a no-load output of 1.5V for the amplifiers. The results are also shown in Figure 4-7.
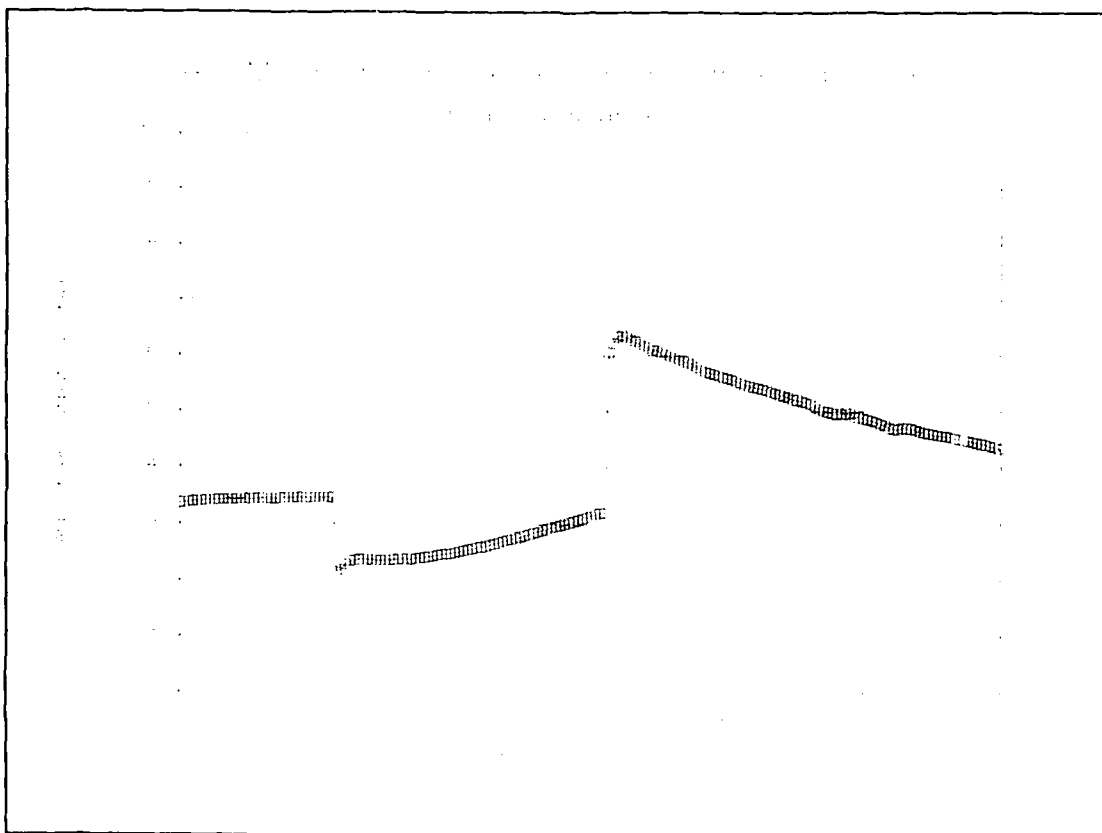

Figure 4-5. Response of the Solef 40μm Thick Film to a 500g Load. The Film was Oriented so that a Load Application Produced a Negative Voltage Change.

For the conditions of this test (2V no-load output), the film thickness which performed the best was the 25μm thick film. It exhibited an essentially linea· response for loads between 0.8g and 76g. The other films could also exhibit

4-8

this linear response if the bias voltage were decreased (as was the case for the 110μm film with a 1.5V no-load output), but the purpose of this test was to compare the individual element responses for the various sensor configurations under identical conditions. The issue of coupling between neighboring elements for the four sensor configurations was addressed in the next test.
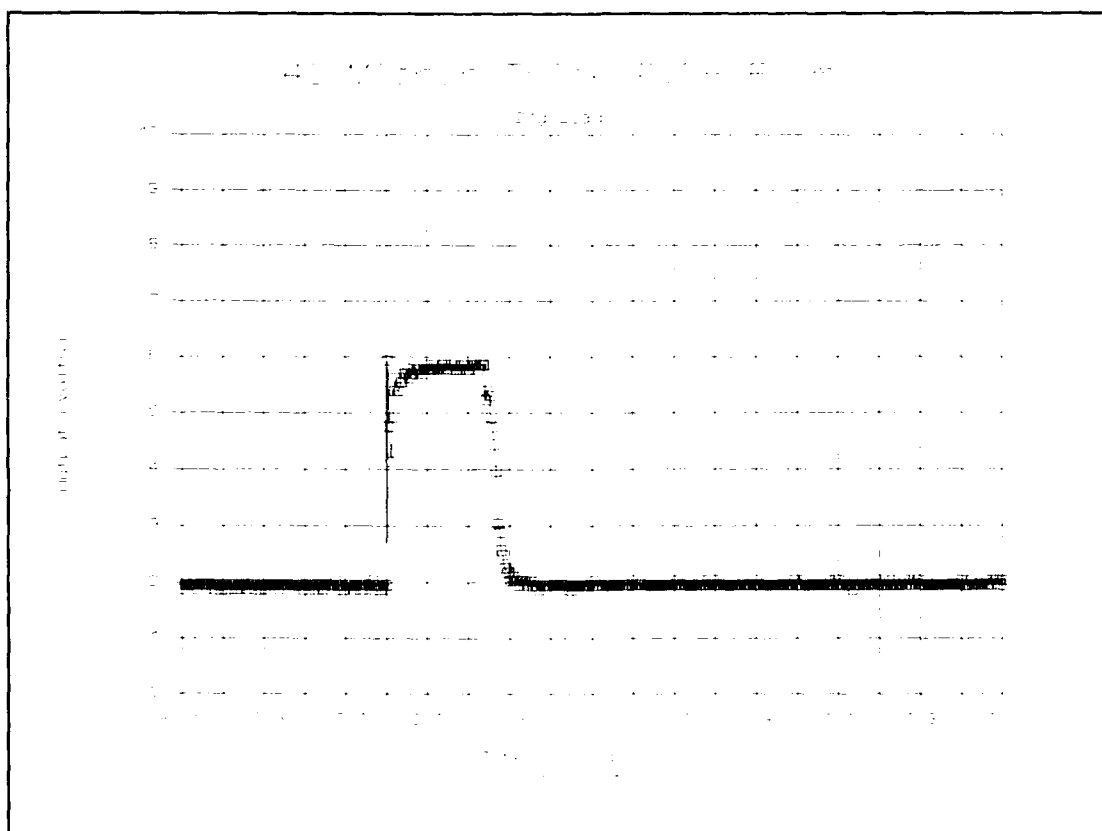

Figure 4-6. Individual Sensor Response to a 21g Load Placed on a Tactile Sensor Fabricated from the Solef 40μm Thick PVDF Film.

Nearest Neighbor Response. The nearest neighbor response shown in Figure 4-8 is representative of all of the tactile sensor configurations. There was essentially no detectable response in the nearest neighbor for any

4-9

combination of load or film thickness. This means that the sensor elements can be placed much closer together than they were in this research. Assuming that the individual element sizes will remain the same, and additional electrodes will be placed in the gaps between the existing electrodes, the density of the sensor array would be sixteen times greater than the spatial resolution of a human fingertip (6:205).
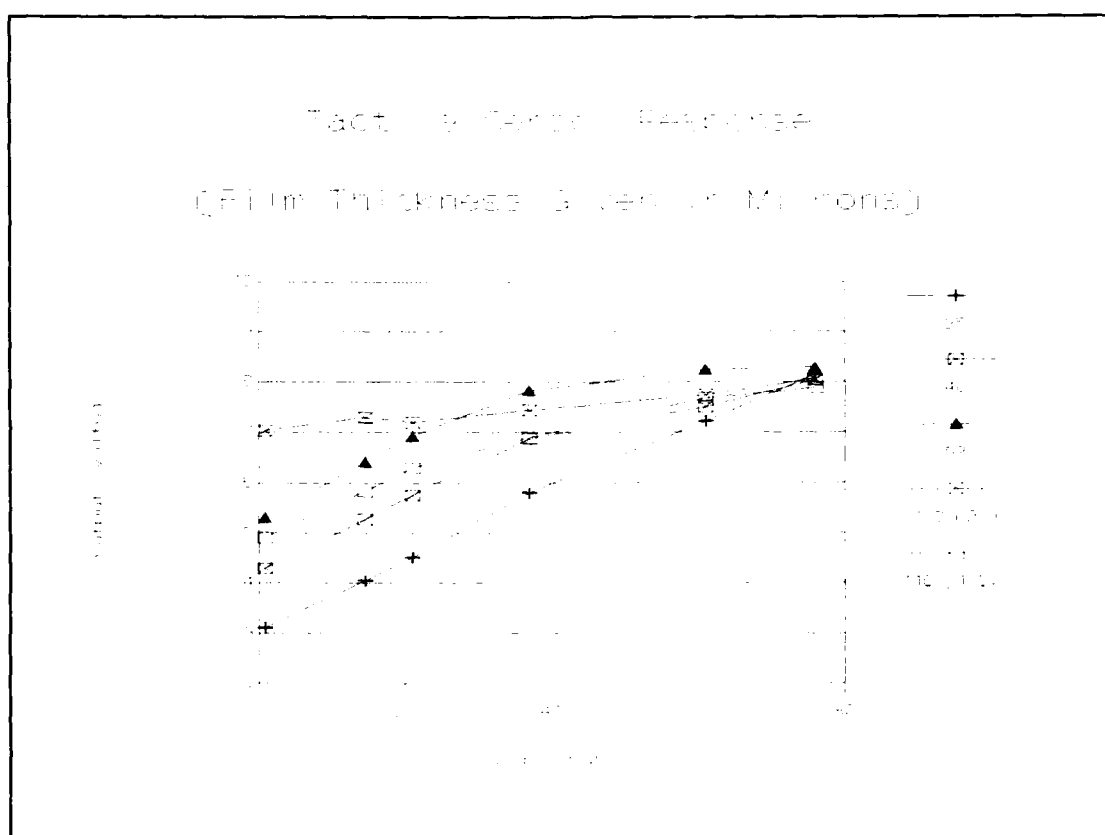

Figure 4-7. Average Response for Each of the Tactile Sensor Configurations.
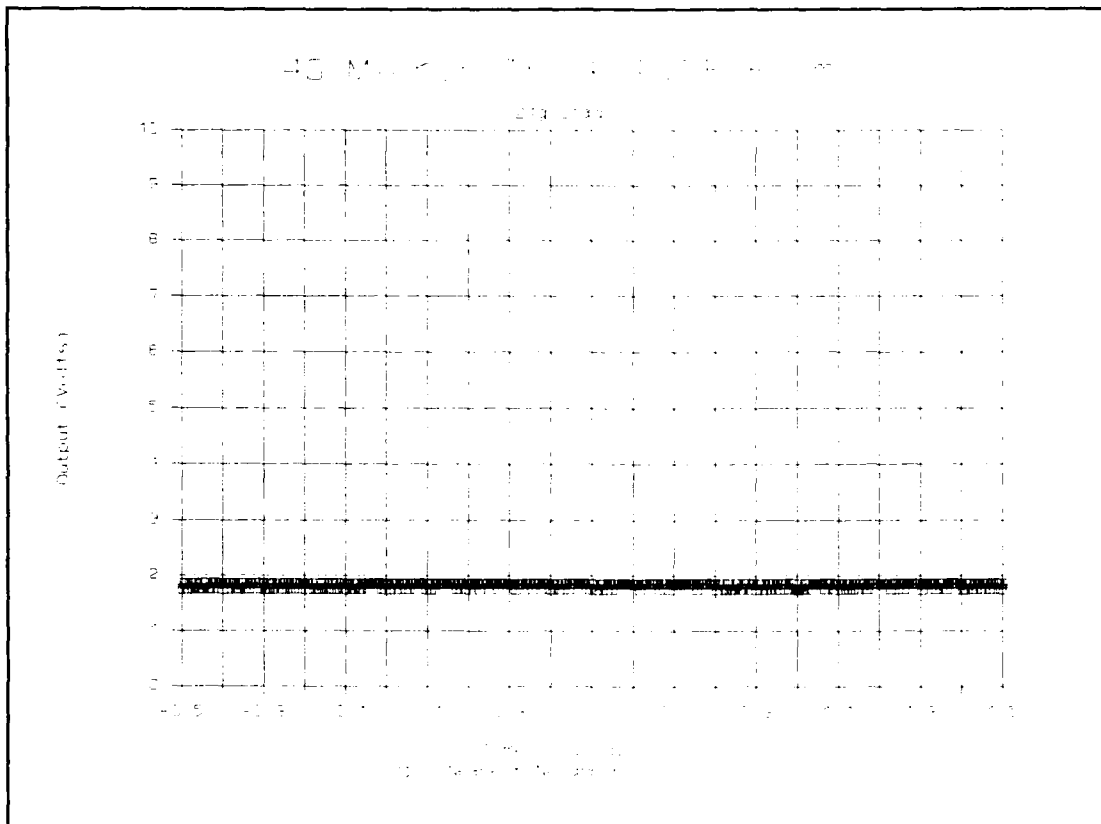
Figure 4-8. Nearest Neighbor Response to a 21g Load Placed on a Tactile Sensor Fabricated from the Solef 40μm Thick PVDF Film.

<u>Bias Voltage Response.</u> The various sensor configurations seemed to perform equally well (assuming appropriate biasing conditions), however, the time required to bias each film thickness varied considerably (see Figure 4-9). The 25μm thick film attained equilibrium bias conditions the fastest. This was expected for two reasons. First, as the film thickness decreases, the amount of material that must be reoriented (through the dipole moment) is reduced. Second, the thinner the film, the larger the magnitude of the electric field for a fixed applied voltage. Consequently, the 25μm thick film represented the

4-11

optimum thickness because it had a linear response for the loading test, and it biased the fastest in the bias voltage response test.
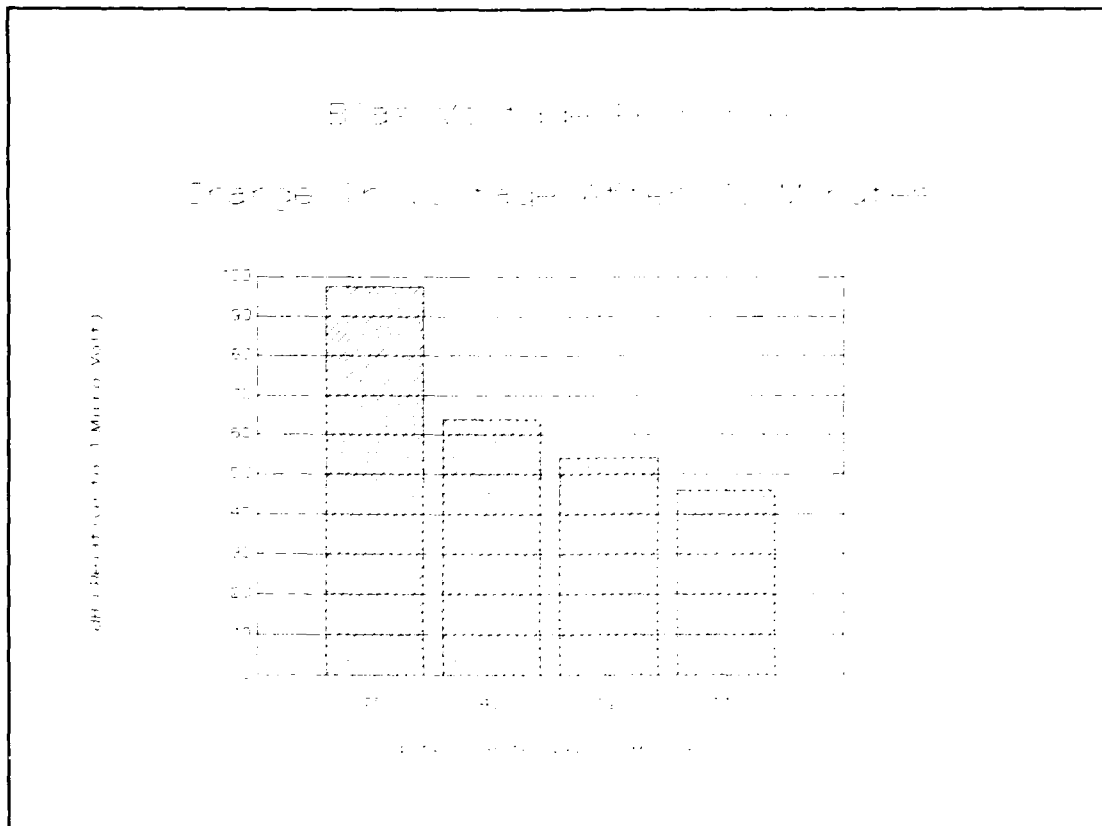
Figure 4-9. Amplifier Output After 10 Minutes With a 10V Bias for the Various Sensor Configurations.

Group Response. The final test used the optimal sensor configuration (the 25μm thick film) and the load described in Chapter III to determine the response of the sensor to a load which was larger than a single element. The major problem encountered in performing this test was obtaining a relatively consistent no-load output voltage across the entire electrode array. Even if all of the electrodes had an identical charge state at the beginning of the test

(that is, immediately after tactile sensor fabrication), the first time a load was placed on the sensor, each of the sensor electrodes was driven into a different charge state. This problem was somewhat overcome by scanning the array twice. Once immediately prior to loading the sensor, and again immediately after loading the sensor. The difference between the two readings was then plotted.

Figure 4-10 shows the difference between the loaded and unloaded states. This plot is oriented so that element (1,1) is the sensor connected to pin 10. Since element (1,1) had the unconnected sensor electrode, its value (for the purposes of Figure 4-10) was assumed to be the same as an element which was in an equivalent spatial position with respect to the load (in this case, element (4,1) was used).

A topographical slice through the 0.3V level (chosen after the data was collected) reveals a recognizable representation of the load shape described in Chapter III (see Figure 4-11). The distance between the centers of neighboring sensor elements is 1.2mm, so Figure 4-11 shows an approximate inner diameter of two elements (or 2.4mm) and an approximate thickness of one element (or 1.2mm). The actual inner diameter was approximately 2.5mm and the actual thickness was approximately 1.25mm. Although the amplitude of the output of the loaded sensor contained information about the mass of the load, the inconsistent no-load bias state prevented drawing any conclusions concerning *the mass seen by the sensor*.
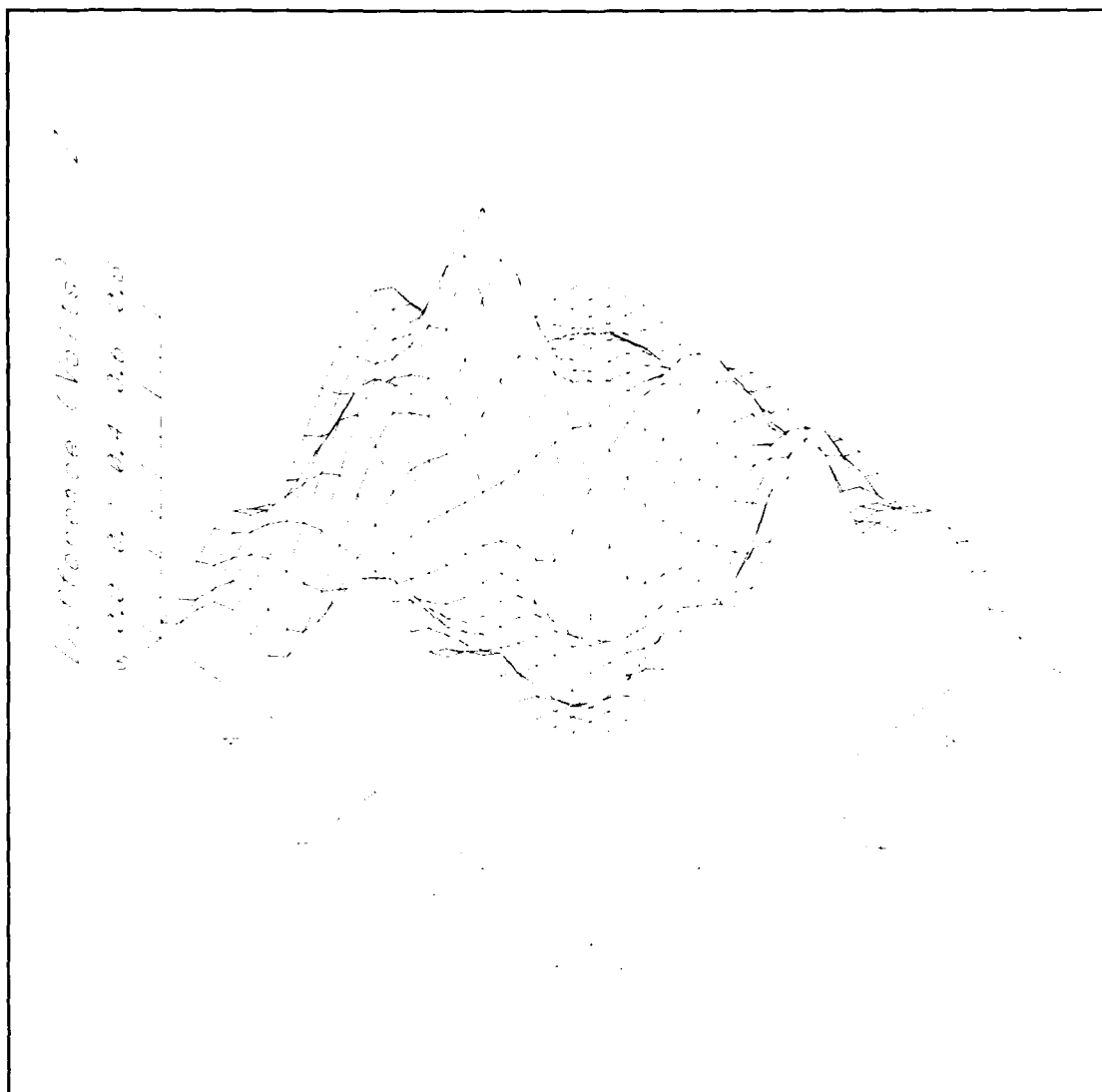
Figure 4-10. Three-Dimensional Graph of the Group Response Test. The Z-Axis Value is the Difference Between the Loaded and Unloaded States of the Sensor. The Numbers on the X and Y Axes Refer to the Center of a Sensor.

Conclusion

The performance tests discussed in this chapter included the IC tests, the

PVDF film test, and the tactile sensor tests. With the exception of a single

missing connection between an amplifier and a sensor electrode pad, the IC

4-14

passed all of its tests. The PVDF film test demonstrated the ability of the IC
to amplify PVDF film signals without sacrificing any ICs. Finally, the complete
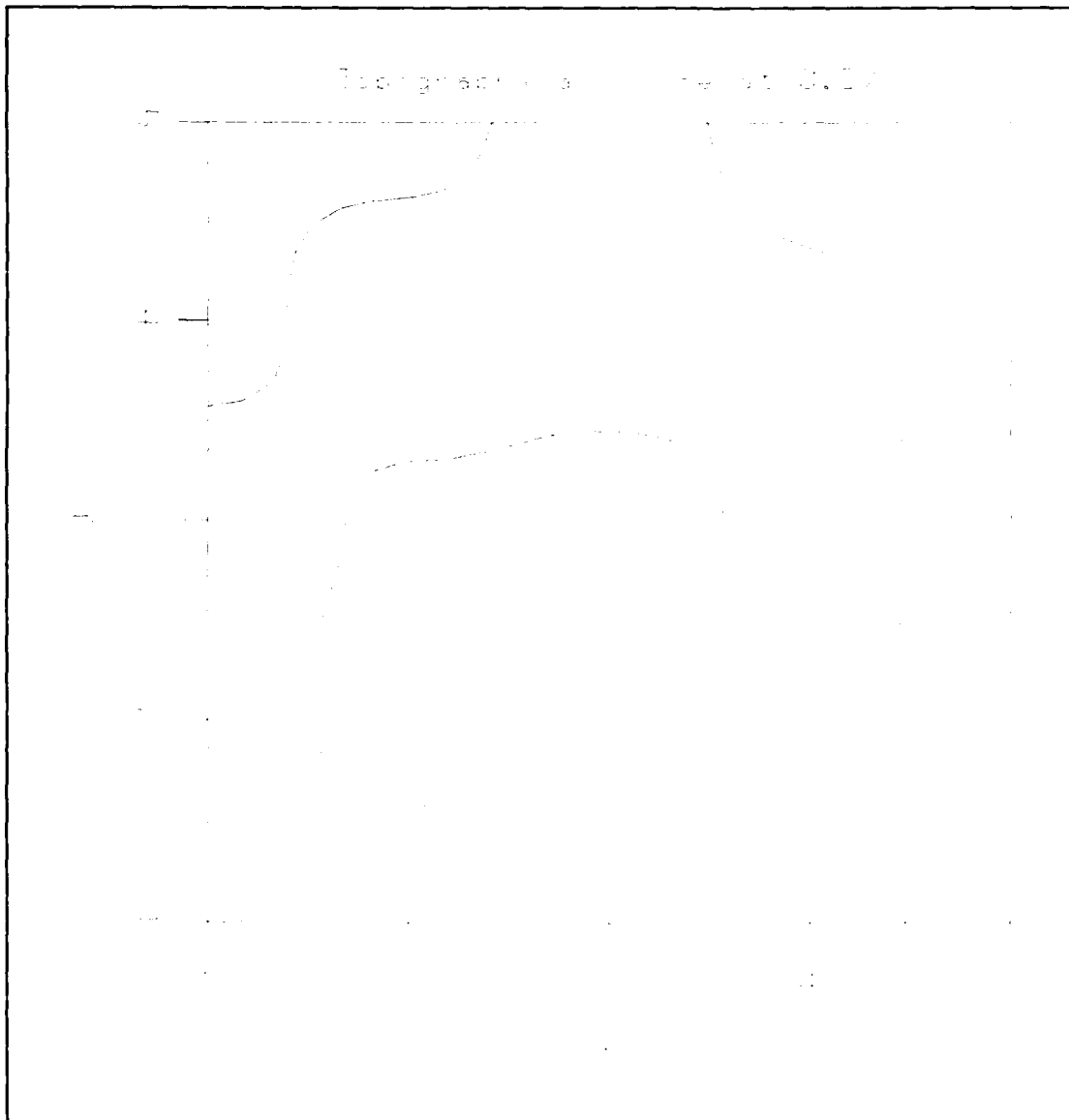tactile sensor performed better than expected in the tactile sensor tests.

Figure 4-11. Topographical Slice of the Group Response at a 0.3V Level. The
Numbers on the X and Y Axes Refer to the Center of a Sensor.

The tactile sensors were sensitive to extremely small loads (0.8g) and exhibited essentially no coupling between nearest neighbor elements. Although problems in attaining a consistent no-load output voltage for the entire array prevented a demonstration of the sensors ideal performance for a large load, the information provided by the sensor array was still adequate to "recognize" the circular shape of the load. These tests also revealed a number of possible improvements to the tactile sensor design. These improvements will be discussed in the next chapter along with some general conclusions.

V. Conclusions and Recommendations

Conclusions

The goal of this research was to design and fabricate a tactile sensor by intimately coupling a sample of PVDF film to an integrated circuit containing a high input impedance amplifier circuit. In order to accomplish this objective, hardware and a test methodology was devised. The hardware consisted of an integrated circuit (containing 25 sensor electrodes and 25 associated MOSFET amplifiers), and a loading test probe (capable of applying loads between 0.8g and 76g). The test methodology was developed such that any problems with the IC or the PVDF film would be discovered prior to the fabrication of a tactile sensor.

This research effort was successful in designing, fabricating and characterizing the performance of a robotic tactile sensor fabricated from PVDF film. The response of the optimal sensor configuration (fabricated from 25μm thick PVDF film) was linear across the load range investigated (0.8g to 76g), there was no detectable coupling between nearest neighbors, and the group response test demonstrated the potential of using this tactile sensor in future robotics applications to recognize contacted shapes. There remains room for improvement, particularly with respect to the area of obtaining a consistent bias voltage across the entire sensor array.

Recommendations

In order to improve the performance of the tactile sensors designed in this research, the following recommendations are presented:

Gate-Electrode Switch. In order to initialize the charge state on each of the sensor electrodes to the same value, an additional MOSFET for every electrode can be introduced as a gate-electrode switch. The drain of this new MOSFET would be attached to the interconnect between the sensor electrode and the amplifier (see Figure 5-1). The source of all of the gate-electrode switches would be connected together to an external pad, and their gates would be connected and routed to another external pad. Placing a high voltage on the gates of these switches would force the charges on all of the sensor electrodes to the value provided on the external pad, and the entire electrode array would be driven to a consistent biased state. A sensor reading would then be accompanied by a prior initialization, and the problems with inhomogeneous charge distribution would be eliminated.

PVDF Film Adhesive. Although the photoresist adhesive was adequate for the purposes of short term testing, and proved useful in recycling ICs for multiple tests (the photoresist was easily removed with acetone), the photoresist tended to fracture after approximately two days. Since the fundamental design has been validated, subsequent research will require sensors for long term use. Therefore, a more robust adhesive should be used. The conformal coatings used for PC boards are possible candidates for rugged adhesives. They are available in a variety of formulations (silicone, urethane, and acrylic), they are thin enough to spread evenly across the surface of an IC,

and they have the necessary electrical insulating properties to prevent shorts on the IC.
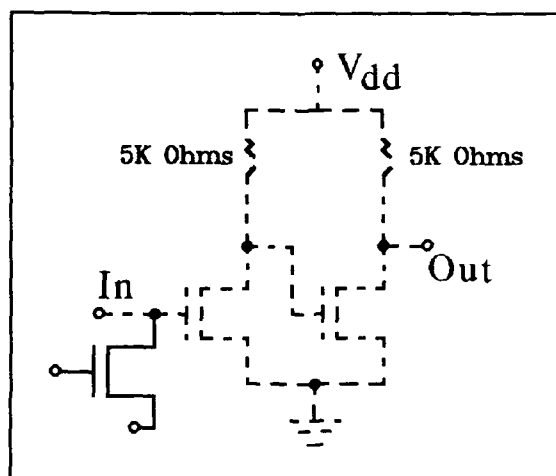

Figure 5-1. Gate-Electrode Switch Connected to the Input of the Sensor Amplifier. The Amplifier is Shown With Dotted Lines.

Array Glass Cut. Instead of cutting through the overglass directly around each electrode, an overglass cut should be performed over the entire electrode area. This feature will facilitate a more intimate contact between the sensor's electrode and the PVDF film.

Increased Electrode Density. Since it was determined that there was no detectable coupling between nearest neighbor elements, the density of the sensor array can be quadrupled by placing sensor elements between existing elements. The spatial resolution will then be approximately sixteen times greater than that of a human fingertip. Also, since the response of the optimal sensor configuration to a load of 0.8g was a voltage change in excess of 1V, the

size of the individual sensor elements could be reduced, further increasing the spatial resolution of the sensor.

Resident Analog Multiplexer. Finally, a resident analog multiplexer would permit scanning the entire electrode array without mechanically moving the data collection probe. This analog multiplexer could be implemented with either an internal clock to send each sensor element's response in succession (after a trigger pulse), or an external digital signal to select a particular sensor element. This word would only have to be $\log_2 N$ bits wide where N is the number of array elements (that is, 32 elements would require 5 bits).

Appendix A: Materials and Equipment

Table A-1. Materials and Equipment.

Materials

Solef PVDF film (25μm, and 40μm), Solvay & Cie Company, Brussels, Belgium

Kynar PVDF film (52μm, and 110μm), Pennwalt Corporation, King of Prussia PA

Shipley Photoposit 1400-17 Photoresist, Shipley Company, Inc., Whitehall PA

Dow Corning 3140 RTV Silicone Coating, Dow Corning Corporation, Midland MI

Ferric Chloride

Silver Paint

MOSIS Circuits

Cotton Swabs

1 mil Bonding Wire

Binder Clips

De-Ionized Water

Concentrated (37%) HCl

Glass Slides

Isopropyl Alcohol

Equipment

Hewlett Packard HP 54100 Digitizing Oscilloscope, Hewlett Packard, Colorado Springs, CO

Hewlett Packard HP 4145 Parameter Analyzer, Hewlett Packard, Colorado Springs, CO

Fluke 77/AN Multimeter, John Fluke Manufacturing Company, Everett WA

Keithley 617 Electrometer, Keithley Instruments, Inc., Cleveland OH

Zenith 248 Data Collection Computer (With IEEE-488 Interface), Zenith Data Systems, Glenview IL

ISI WB-6 Scanning Electron Microscope, International Scientific Instruments, Inc., Milpitas CA

Micromanipulator Model 6200 Test Station, The Micromanipulator Company, Inc., Escondido CA

Micromanipulator Model 450/360VM Manipulators (3), The Micromanipulator Company, Inc., Escondido CA

Dissecting Microscope

Loading Test Probe

Weights (3)

Group Test Load

Protoboard

Scalpel (#11)

Appendix B: MOSIS Spice Parameters

*** MOSIS PMOS MOSFET MODEL FOR 3 MICRON CMOS PVDFET 20 JUL 88 ***

.MODEL P PMOS LEVEL=2.00000 LD=0.325645U TOX=418.000E-10

+NSUB=7E+15 VTO=-0.822049 KP=1.73164E-05 GAMMA=0.583513

+PHI=0.600000 UO=209.614 UEXP=0.214077 UCRIT=72408.3

+DELTA=0.734324 VMAX=100000. XJ=.4U LAMBDA=.0374271

+NFS=1.34086E+12 NEFF=1.001000 NSS=1E+12 TPG=-1.00000

+RSH=112.300010 CGSO=2.69008E-10 CGDO=2.69008E-10 CGBO=7.43469E-10

+CJ=2.376E-4 MJ=0.475 CJSW=3.652E-10 MJSW=0.2747 PB=0.72

*** MOSIS N-CHANNEL MOSFET MODEL FOR 3 MICRON CMOS 20 JUL 88 ***

.MODEL N NMOS LEVEL=2.00000 LD=0.4U TOX=418.000E-10

+NSUB=2.97056E+16 VTO=0.881794 KP=5.49941E-05 GAMMA=1.20205

+PHI=0.600000 UO=665.699 UEXP=0.240761 UCRIT=73478.7

+DELTA=0.001 VMAX=64117.6 XJ=0.4U LAMBDA=2.92501E-02

+NFS=2.896196E+12 NEFF=1.001 NSS=1E+12 TPG=1.00000

+RSH=29.370003 CGSO=3.30431E-10 CGDO=3.30431E-10 CGBO=2.47823E-10

+CJ=0.0003789 MJ=0.5283 CJSW=4.15E-10 MJSW=0.32 PB=0.84

Appendix C: PVDF Film Specifications

Table C-1. PVDF Film Electrical and Mechanical Parameters.

	Solef 25μm (21)	Solef 40μm (21)	Kynar 52μm (22)	Kynar 110μm (22)
d_{33}	16pC/N	16pC/N	20-22pC/N	20-22pC/N
ϵ_r (at 1KHz)	11	11	11-13	11-13
k_{33}	10-15%	10-15%	19%	19%
Tensile Strength	180MPa	180MPa	160-330MPa	160-330MPa

Table C-2. PVDF Film Chemical Resistance (23).

Chemical	Maximum Temperature for Exposure
Acetone	Not Recommended
Acetone (10% in Water)	125°F
Butyl Acetate	80°F
Ferric Chloride	275°F
Hydrochloric Acid (Concentrated)	275°F
Isopropyl Alcohol	140°F
Methyl Ethyl Ketone	Not Recommended
Silicone Oil	250°F
Xylene	200°F

Appendix D: IC Magic Listing

<u>Top Cell: IC</u>

magic
tech scmos
timestamp 579294502
<< metal1 >>
rect 0 5263 6133 5266
rect 0 3 3 5263
rect 1159 5218 1177 5222
rect 1159 5211 1163 5218
rect 1173 5211 1177 5218
rect 1159 5207 1177 5211
rect 1182 5218 1197 5222
rect 1204 5218 1219 5222
rect 1225 5218 1243 5222
rect 1248 5218 1265 5222
rect 1182 5211 1186 5218
rect 1204 5211 1208 5218
rect 1182 5207 1193 5211
rect 1204 5207 1219 5211
rect 1159 5195 1163 5207
rect 1169 5195 1173 5207
rect 1182 5199 1186 5207
rect 1215 5199 1219 5207
rect 1182 5195 1197 5199
rect 1204 5195 1219 5199
rect 1232 5195 1236 5218
rect 1248 5199 1252 5218
rect 1261 5199 1265 5218
rect 1248 5195 1265 5199
rect 1270 5218 1281 5222
rect 1270 5195 1274 5218
rect 1277 5199 1281 5218
rect 1284 5199 1288 5222
rect 1277 5195 1288 5199
rect 192 5132 445 5158
rect 419 5009 445 5132
rect 419 4983 612 5009
rect 185 4883 375 4903
rect 355 4759 375 4883
rect 5873 4956 5953 4976
rect 5873 4954 5880 4956
rect 5576 4850 5637 4855
rect 499 4659 733 4664
rect 728 4548 733 4659
rect 5576 4581 5581 4850
rect 3060 4576 5581 4581
rect 728 4543 2266 4548
rect 2261 4409 2266 4543
rect 3060 4406 3065 4576
rect 3871 4492 5638 4497
rect 3871 4404 3876 4492
rect 499 4301 1110 4306

rect 1105 4236 1110 4301
rect 1105 4231 1277 4236
rect 4852 4222 4948 4227
rect 4943 4139 4948 4222
rect 4943 4134 5641 4139
rect 499 3943 733 3948
rect 728 3788 733 3943
rect 3035 3860 5459 3865
rect 728 3783 2295 3788
rect 2290 3612 2295 3783
rect 3035 3604 3040 3860
rect 5454 3781 5459 3860
rect 5454 3776 5639 3781
rect 3873 3735 5344 3740
rect 3873 3619 3878 3735
rect 494 3585 1135 3590
rect 1130 3434 1135 3585
rect 1130 3429 1282 3434
rect 5339 3423 5344 3735
rect 5339 3418 5639 3423
rect 4865 3413 5217 3418
rect 499 3227 579 3232
rect 574 3101 579 3227
rect 574 3096 3078 3101
rect 499 2869 2282 2874
rect 2277 2816 2282 2869
rect 3073 2809 3078 3096
rect 5212 3065 5217 3413
rect 5212 3060 5639 3065
rect 3855 2958 5457 2963
rect 3855 2824 3860 2958
rect 5452 2707 5457 2958
rect 5452 2702 5643 2707
rect 1140 2630 1284 2635
rect 1140 2516 1145 2630
rect 4841 2617 5211 2622
rect 496 2511 1145 2516
rect 5206 2349 5211 2617
rect 5206 2344 5643 2349
rect 3053 2255 5495 2260
rect 499 2153 2267 2158
rect 2262 1998 2267 2153
rect 3053 2017 3058 2255
rect 3855 2172 5377 2177
rect 3855 2023 3860 2172
rect 1136 1826 1272 1831
rect 1136 1800 1141 1826
rect 4809 1816 5208 1821
rect 495 1795 1141 1800
rect 495 1437 640 1442
rect 635 1391 640 1437
rect 635 1386 3077 1391
rect 865 1318 2306 1323

rect 865 1084 870 1318
rect 2301 1189 2306 1318
rect 3072 1223 3077 1386
rect 3864 1341 5030 1346
rect 3864 1201 3869 1341
rect 496 1079 870 1084
rect 5025 917 5030 1341
rect 5203 1275 5208 1816
rect 5372 1633 5377 2172
rect 5490 1991 5495 2255
rect 5490 1986 5639 1991
rect 5372 1628 5639 1633
rect 5203 1270 5637 1275
rect 5025 912 5643 917
rect 1461 726 1466 863
rect 4655 745 4660 828
rect 4655 740 5477 745
rect 499 721 1466 726
rect 5472 559 5477 740
rect 5472 554 5637 559
rect 243 379 263 472
rect 186 359 263 379
rect 188 134 613 160
rect 5761 262 5781 302
rect 5761 242 5956 262
rect 2651 3 2681 4
rect 3451 3 3481 4
rect 4651 3 4681 4
rect 5051 3 5081 4
rect 6130 3 6133 5263
rect 0 0 6133 3
<< metal2 >>
rect 1266 4696 1464 5169
rect 1468 4696 1666 5169
rect 2066 4696 2264 5169
rect 2268 4696 2466 5169
rect 2866 4696 3064 5169
rect 3068 4696 3266 5169
rect 3666 4696 3864 5169
rect 3868 4696 4066 5169
rect 4466 4696 4664 5169
rect 4668 4696 4866 5169
rect 5257 5131 5949 5157
rect 5257 5112 5283 5131
rect 609 4235 1031 4433
rect 5119 4235 5541 4433
rect 609 4033 1031 4231
rect 5119 4033 5541 4231
rect 609 3435 1031 3633
rect 5119 3435 5541 3633
rect 609 3233 1031 3431
rect 5119 3233 5541 3431
rect 609 2635 1031 2833

rect 5119 2635 5541 2833
rect 609 2433 1031 2631
rect 5119 2433 5541 2631
rect 609 1835 1031 2033
rect 5119 1835 5541 2033
rect 609 1633 1031 1831
rect 5119 1633 5541 1831
rect 609 1035 1031 1233
rect 5119 1035 5541 1233
rect 609 833 1031 1031
rect 5119 833 5541 1031
rect 1266 96 1464 569
rect 1468 96 1666 569
rect 2066 96 2264 569
rect 2268 96 2466 569
rect 2866 96 3064 569
rect 3068 96 3266 569
rect 3666 96 3864 569
rect 3868 96 4066 569
rect 4466 96 4664 569
rect 4668 96 4866 569
rect 5344 95 5370 106
rect 5344 69 5959 95
<< nwell >>
rect 92 5097 192 5197
rect 85 4858 185 4958
rect 612 4762 1012 5162
rect 5949 5118 6049 5218
rect 5095 4712 5495 5112
rect 5953 4920 6053 5020
rect 86 312 186 412
rect 88 101 188 201
rect 613 90 1013 490
rect 5124 106 5524 506
rect 5956 213 6056 313
rect 5959 35 6059 135
<< m2contact >>
rect 92 5097 192 5197
rect 85 4858 185 4958
rect 612 4762 1012 5162
rect 5949 5118 6049 5218
rect 5095 4712 5495 5112
rect 5953 4920 6053 5020
rect 86 312 186 412
rect 88 101 188 201
rect 613 90 1013 490
rect 5124 106 5524 506
rect 5956 213 6056 313
rect 5959 35 6059 135
<< glass >>
rect 98 5103 186 5191
rect 91 4864 179 4952
rect 618 4768 1006 5156
rect 5955 5124 6043 5212
rect 5101 4718 5489 5106
rect 5959 4926 6047 5014
rect 92 318 180 406
rect 94 107 182 195

rect 619 96 1007 484
rect 5130 112 5518 500
rect 5962 219 6050 307
rect 5965 41 6053 129
use amp2 amp2_1
array 0 0 -578 0 11 358
timestamp 579044557
transform -1 0 254 0 1 550
box -245 -81 168 277
use elec2 elec2_0
array 0 4 800 0 4 800
timestamp 579290076
transform 1 0 1066 0 1 633
box -100 -100 900 900
use amp2 amp2_0
array 0 0 454 0 12 358
timestamp 579044557
transform 1 0 5882 0 1 383
box -245 -81 168 277
<< end >>

Amplifier Cell: AMP2

magic
tech scmos
timestamp 579044557
<< polysilicon >>
rect -90 91 -88 95
rect -90 48 -88 60
<< metal1 >>
rect -121 239 -101 277
rect -245 171 -234 176
rect -121 -41 -109 239
rect -91 99 -87 114
rect -101 83 -96 87
rect -82 83 -68 87
rect -77 71 -73 83
rect -77 64 -73 67
rect -87 60 -73 64
rect -59 55 -55 59
rect -77 51 -55 55
rect -77 44 -73 51
rect -101 40 -96 44
rect -86 40 -64 44
rect -121 -81 -101 -41
rect -9 -81 11 277
<< metal2 >>
rect -164 179 -129 183
rect -133 118 -129 179
rect -133 114 -91 118
rect -194 67 -77 71
rect -194 40 -190 67
rect -55 59 68 63
<< pwell >>
rect -121 -81 12 277
<< nwell >>
rect -234 141 -164 211

rect -234 -30 -164 40
rect 68 10 168 110
<< polycontact >>
rect -91 95 -87 99
rect -91 60 -87 64
<< m2contact >>
rect -234 141 -164 211
rect -234 -30 -164 40
rect -91 114 -87 118
rect -77 67 -73 71
rect -59 59 -55 63
rect 68 10 168 110
<< psubstratepcontact >>
rect -109 -41 -101 239
<< glass >>
rect -228 147 -170 205
rect -228 -24 -170 34
rect 74 16 162 104
use pfet2 pfet2_1
timestamp 578945382
transform 0 1 -94 -1 0 91
box 0 -2 12 12
use res5k res5k_1
timestamp 578945382
transform -1 0 -27 0 1 91
box -22 -8 41 52
use pfet2 pfet2_0
timestamp 578945382
transform 0 1 -94 -1 0 48
box 0 -2 12 12
use res5k res5k_0
timestamp 578945382
transform -1 0 -27 0 -1 36
box -22 -8 41 52
<< labels >>
rlabel pwell -105 -51 -105
-51 1 GND
rlabel pwell -6 -45 -6 -45 1
Vdd
<< end >>

Electrode Cell: ELEC2

magic
tech scmos
timestamp 579290076
<< metal2 >>
rect 0 800 10 900
rect -100 790 10 800
rect 200 800 205 821
rect 398 800 402 806
rect 595 800 600 821
rect 200 790 600 800
rect 790 800 800 900
rect 790 790 900 800
rect 200 780 205 790
rect 398 789 402 790

rect 595 780 600 790
rect -31 595 20 600
rect 0 402 10 595
rect -6 398 11 402
rect 0 205 10 398
rect -31 200 20 205
rect 780 595 843 600
rect 790 402 800 595
rect 789 398 806 402
rect 790 205 800 398
rect 780 200 843 205
rect 0 198 10 200
rect 200 10 205 20
rect 398 10 402 11
rect 595 10 600 20
rect -100 0 10 10
rect 0 -100 10 0
rect 200 0 600 10
rect 200 -36 205 0
rect 398 -6 402 0
rect 595 -36 600 0
rect 790 0 900 10
rect 790 -100 800 0
<< nwell >>
rect 200 200 600 600
<< m2contact >>
rect 200 200 600 600
<< glass >>
rect 206 206 594 594
<< end >>

FET Cell: PFET2

magic
tech scmos
timestamp 578945382
<< polysilicon >>
rect 0 4 2 6
rect 10 4 12 6
<< ndiffusion >>
rect 2 8 4 12
rect 8 8 10 12
rect 2 6 10 8
rect 2 2 10 4
rect 2 -2 4 2
rect 8 -2 10 2
<< ndcontact >>
rect 4 8 8 12
rect 4 -2 8 2
<< ntransistor >>
rect 2 4 10 6
<< end >>

Resistor Cell: RES5K

magic
tech scmos
timestamp 578945382
<< ndiffusion >>
rect -19 49 -10 52
rect -19 -4 -16 49
rect -18 -8 -16 -4
rect -13 -5 -10 49
rect -7 49 2 52
rect -7 -5 -4 49
rect -13 -8 -4 -5
rect -1 -5 2 49
rect 5 49 14 52
rect 5 -5 8 49
rect -1 -8 8 -5
rect 11 -5 14 49
rect 17 49 26 52
rect 17 -5 20 49
rect 11 -8 20 -5
rect 23 -5 26 49
rect 29 49 38 52
rect 29 -5 32 49
rect 23 -8 32 -5
rect 35 -4 38 49
rect 35 -8 37 -4
<< ndcontact >>
rect -22 -8 -18 -4
rect 37 -8 41 -4
<< end >>

Amplifier Test Program

```
100 DEF SEG=&HC400                          ' ADDRESS OF GP-IB INTERFACE
110 INIT%=0                                 ' OFFSET OF INITIALIZE ROUTINE
120 TRANSMIT%=3                             ' OFFSET OF TRANSMIT ROUTINE
140 SEND%=9                                  ' OFFSET OF SEND ROUTINE
160 ENTER%=21                                ' OFFSET OF ENTER ROUTINE
200                                    ' GP-IB ADDRESSES OF INSTRUMENTS
220 PRINTER%=1: MY.ADDR%=21: K617%=27
250 SYSCON%=0                                'PC488 ACTS AS CONTROLLER
260 '
270 CALL INIT%(MY.ADDR%,SYSCON%)
290 S$="REN SDC 27"
300 CALL TRANSMIT%(S$,STATUS%)
340                            'SET-UP ELECTROMETER FOR MEASUREMENT
360 S$="F0X"                                'SET TO MEASURE VOLTS
370 CALL SEND%(K617%,S$,STATUS%)
410 INPUT "NAME OF DATA FILE?", DFILE$
420 OPEN "O",#1,DFILE$
430 INPUT "ZEROING ELECTROMETER, HIT RETURN WHEN READY", NULL$
440 S$="C1XZ1XC0X"
450 CALL SEND%(K617%,S$,STATUS%)
460 INPUT "HIT RETURN TO BEGIN TEST RUN", NULL$
470 S$="Q7X"
480 CALL SEND%(K617%,S$,STATUS%)
490 S$="G1X"
500 CALL SEND%(K617%,S$,STATUS%)
510 FOR VS = 0 TO 10.1 STEP .05
520        VS$="V"+RIGHT$(STR$(VS),LEN(STR$(VS))-1)
530        S$="D1X"+VS$+"XO1X"
540        CALL SEND%(K617%,S$,STATUS%)
550        VSR$=SPACE$(12)
560        S$="B4X"
570        CALL SEND%(K617%,S$,STATUS%)
580        CALL ENTER%(VSR$,LENG%,K617%,STATUS%)
581        VSR=VAL(VSR$)
590        FOR Q=1 TO 800:NEXT Q           'PAUSE FOR READING TO STABILIZE
600        S$="D0XB0X"
610        CALL SEND%(K617%,S$,STATUS%)
620        VRD$=SPACE$(12)
630        CALL ENTER%(VRD$,LENG%,K617%,STATUS%)
631        VRD=VAL(VRD$)
640        FOR Q=1 TO 800:NEXT Q           'PAUSE FOR READING TO STABILIZE
660        PRINT VSR,VRD
670        WRITE #1,VSR,VRD
680 NEXT VS
690 CLOSE #1
```

PVDF Film Test Program

```
100 DEF SEG=&HC400                          ' ADDRESS OF GP-IB INTERFACE
110 INIT%=0                                  ' OFFSET OF INITIALIZE ROUTINE
120 TRANSMIT%=3                              ' OFFSET OF TRANSMIT ROUTINE
130 SEND%=9                                   ' OFFSET OF SEND ROUTINE
150 ENTER%=21                                 ' OFFSET OF ENTER ROUTINE
180 '
190 ' GP-IB ADDRESSES OF INSTRUMENTS
200 '
210 PRINTER%=1: MY.ADDR%=21: K617%=27
240 SYSCON%=0                                'PC488 ACTS AS CONTROLLER
250 '
260 CALL INIT%(MY.ADDR%,SYSCON%)
280 S$="REN SDC 27"
290 CALL TRANSMIT%(S$,STATUS%)
330                             'SET-UP ELECTROMETER FOR MEASUREMENT
350 S$="F0X"                                 'SET TO MEASURE VOLTS
360 CALL SEND%(K617%,S$,STATUS%)
400 INPUT "NAME OF DATA FILE?", DFILE$
410 OPEN "O",#1,DFILE$
420 INPUT "ZEROING ELECTROMETER, HIT RETURN WHEN READY", NULL$
430 S$="C1XZ1XC0X"
440 CALL SEND%(K617%,S$,STATUS%)
450 INPUT "HIT RETURN TO BEGIN TEST RUN", NULL$
460 S$="Q7X"
470 CALL SEND%(K617%,S$,STATUS%)
480 S$="G1X"
490 CALL SEND%(K617%,S$,STATUS%)
500 TI=TIMER
520 VRD$=SPACE$(12)
530 CALL ENTER%(VRD$,LENG%,K617%,STATUS%)
535       T=TIMER-TI
540       VRD=VAL(VRD$)
550       SC=INT(8*VRD)
560       PRINT T;TAB(SC);"*"
570       WRITE #1,T,VRD
590 IF T<61 THEN 530
600 CLOSE #1
```

Tactile Sensor Test Program (Channel 1)

```
10 DEF SEG=&HC400              ' ADDRESS OF GP-IB INTERFACE
20 INIT%=0                     ' OFFSET OF INITIALIZE ROUTINE
30 TRANSMIT%=3                 ' OFFSET OF TRANSMIT ROUTINE
40 RECEIVE%=6                  ' OFFSET OF RECIEVE ROUTINE
50 SEND%=9                     ' OFFSET OF SEND ROUTINE
60 ENTER%=21                   ' OFFSET OF ENTER ROUTINE
100 '
110 ' GP-IB ADDRESSES OF INSTRUMENTS
120 '
130 PRINTER%=1: MY.ADDR%=21: K617%=27: HPOS%=15
140 SYSCON%=0                            'PC488 ACTS AS CONTROLLER
150 '
160 CALL INIT%(MY.ADDR%,SYSCON%)
180 S$="REN SDC 15"
190 CALL TRANSMIT%(S$,STATUS%)
200 '
220 S$= "HEADER OFF"
250 CALL SEND%(HPOS%,S$,STATUS%)
260 S$="STORE CHANNEL1,MEMORY1"
270 CALL SEND%(HPOS%,S$,STATUS%)
280 INPUT "FILENAME FOR CHANNEL 1";DF$
290 OPEN "O",#1,DF$
300 S$="WAVEFORM SOURCE MEMORY1 TYPE NORMAL FORMAT ASCII"
310 CALL SEND%(HPOS%,S$,STATUS%)
320 R$=SPACE$(15)
330 S$="POINTS?"
340 CALL SEND%(HPOS%,S$,STATUS%)
350 CALL ENTER%(R$,LENGTH%,HPOS%,STATUS%)
360 PNTS=VAL(R$)
370 S$="YREF?"
380 CALL SEND%(HPOS%,S$,STATUS%)
390 CALL ENTER%(R$,LENGTH%,HPOS%,STATUS%)
400 YREF=VAL(R$)
410 S$="YINC?"
420 CALL SEND%(HPOS%,S$,STATUS%)
430 CALL ENTER%(R$,LENGTH%,HPOS%,STATUS%)
440 YINC=VAL(R$)
450 S$="YOR?"
460 CALL SEND%(HPOS%,S$,STATUS%)
470 CALL ENTER%(R$,LENGTH%,HPOS%,STATUS%)
480 YORG=VAL(R$)
490 S$="XINC?"
500 CALL SEND%(HPOS%,S$,STATUS%)
510 CALL ENTER%(R$,LENGTH%,HPOS%,STATUS%)
520 XINC=VAL(R$)
530 S$="XOR?"
540 CALL SEND%(HPOS%,S$,STATUS%)
550 CALL ENTER%(R$,LENGTH%,HPOS%,STATUS%)
560 XORG=VAL(R$)
570 S$="XREF?"
580 CALL SEND%(HPOS%,S$,STATUS%)
590 CALL ENTER%(R$,LENGTH%,HPOS%,STATUS%)
600 XREF=VAL(R$)
```

```
610 S$="DATA?"
620 CALL SEND%(HPOS%,S$,STATUS%)
630 S$="MLA TALK 15"
640 CALL TRANSMIT%(S$,STATUS%)
650 X$=SPACE$(15)
660 Y$=SPACE$(15)
670 FOR I=1 TO PNTS
680        CALL RECEIVE%(Y$,LENGTH%,STATUS%)
690        X=(I*XINC)+XORG
700        Y=((VAL(Y$)-YREF)*YINC)+YORG
710        WRITE #1,X,Y
720 NEXT I
730 CLOSE #1
740 S$="LISTEN 15 MTA"
750 CALL TRANSMIT%(S$,STATUS%)
760 S$="LOCAL"
770 CALL SEND%(HPOS%,S$,STATUS%)
780 SYSTEM
```

Tactile Sensor Test Program (Channel 2)

```
10 DEF SEG=&HC400                                      ' ADDRESS OF GP-IB INTERFACE
20 INIT%=0                                             ' OFFSET OF INITIALIZE ROUTINE
30 TRANSMIT%=3                                         ' OFFSET OF TRANSMIT ROUTINE
40 RECEIVE%=6                                          ' OFFSET OF RECIEVE ROUTINE
50 SEND%=9                                             ' OFFSET OF SEND ROUTINE
60 ENTER%=21                                           ' OFFSET OF ENTER ROUTINE
100 '
110 ' GP-IB ADDRESSES OF INSTRUMENTS
120 '
130 PRINTER%=1: MY.ADDR%=21: K617%=27: HPOS%=15
140 SYSCON%=0                                          'PC488 ACTS AS CONTROLLER
150 '
160 CALL INIT%(MY.ADDR%,SYSCON%)
180 S$="REN SDC 15"
190 CALL TRANSMIT%(S$,STATUS%)
200 '
220 S$="HEADER OFF"
250 CALL SEND%(HPOS%,S$,STATUS%)
260 S$="STORE CHANNEL2,MEMORY2"
270 CALL SEND%(HPOS%,S$,STATUS%)
280 INPUT "FILENAME FOR CHANNEL 2";DF$
290 OPEN "O",#1,DF$
300 S$="WAVEFORM SOURCE MEMORY2 TYPE NORMAL FORMAT ASCII"
310 CALL SEND%(HPOS%,S$,STATUS%)
320 R$=SPACE$(15)
330 S$="POINTS?"
340 CALL SEND%(HPOS%,S$,STATUS%)
350 CALL ENTER%(R$,LENGTH%,HPOS%,STATUS%)
360 PNTS=VAL(R$)
370 S$="YREF?"
380 CALL SEND%(HPOS%,S$,STATUS%)
390 CALL ENTER%(R$,LENGTH%,HPOS%,STATUS%)
400 YREF=VAL(R$)
410 S$="YINC?"
420 CALL SEND%(HPOS%,S$,STATUS%)
430 CALL ENTER%(R$,LENGTH%,HPOS%,STATUS%)
440 YINC=VAL(R$)
450 S$="YOR?"
460 CALL SEND%(HPOS%,S$,STATUS%)
470 CALL ENTER%(R$,LENGTH%,HPOS%,STATUS%)
480 YORG=VAL(R$)
490 S$="XINC?"
500 CALL SEND%(HPOS%,S$,STATUS%)
510 CALL ENTER%(R$,LENGTH%,HPOS%,STATUS%)
520 XINC=VAL(R$)
530 S$="XOR?"
540 CALL SEND%(HPOS%,S$,STATUS%)
550 CALL ENTER%(R$,LENGTH%,HPOS%,STATUS%)
560 XORG=VAL(R$)
570 S$="XREF?"
580 CALL SEND%(HPOS%,S$,STATUS%)
590 CALL ENTER%(R$,LENGTH%,HPOS%,STATUS%)
600 XREF=VAL(R$)
```

```
610 S$ = "DATA?"
620 CALL SEND%(HPOS%,S$,STATUS%)
630 S$ = "MLA TALK 15"
640 CALL TRANSMIT%(S$,STATUS%)
650 X$ = SPACE$(15)
660 Y$ = SPACE$(15)
670 FOR I=1 TO PNTS
680        CALL RECEIVE%(Y$,LENGTH%,STATUS%)
690        X=(I*XINC)+XORG
700        Y=((VAL(Y$)-YREF)*YINC)+YORG
710        WRITE #1,X,Y
720 NEXT I
730 CLOSE #1
740 S$ = "LISTEN 15 MTA"
750 CALL TRANSMIT%(S$,STATUS%)
760 S$ = "LOCAL"
770 CALL SEND%(HPOS%,S$,STATUS%)
780 SYSTEM
```

Bias Voltage Response Program

```
10 DEF SEG=&HC400
20 INIT%=0:TRANSMIT%=3:RECEIVE%=6
30 SEND%=9:SPOLL%=12:ENTER%=21
40 MY.ADDR%=21:K617%=27:SYSCON%=0                    'Instrument Addresses
60 CALL INIT%(MY.ADDR%,SYSCON%)
70 S$="REN SDC 27"
80 CALL TRANSMIT%(S$,STATUS%)
90 '****SET-UP ELECTROMETER FOR MEASUREMENT
100 VSET$="0"
110 S$="F0X"                                         'SET TO MEASURE VOLTS
120 CALL SEND%(K617%,S$,STATUS%)
130 S$="D0X"
140 CALL SEND%(K617%,S$,STATUS%)
150 REM INPUT "NAME OF DATA FILE?", DFILE$
160 DFILE$="rlbvlt.dat"
170 OPEN "O",#1,DFILE$
180 FLAG=0
190 REM INPUT "ZEROING ELECTROMETER, HIT RETURN WHEN READY", NULL$
200 S$="C1XZ1XC0X"
210 CALL SEND%(K617%,S$,STATUS%)
220 REM INPUT "HIT RETURN TO BEGIN TEST RUN", NULL$
230 S$="O1Q7X"
240 CALL SEND%(K617%,S$,STATUS%)
250 S$="G1X"
260 CALL SEND%(K617%,S$,STATUS%)
270 RT=0
280 VRD$=SPACE$(12)
290 '
300 'BEGIN DATA LOOP
310    T=0
320      TMR2=TIMER
330      WHILE ABS(TIMER-TMR2)<25:WEND
340      CALL ENTER%(VRD$,LENG%,K617%,STATUS%)
350      T=T+25
360      RT=RT+25
370      VRD=VAL(VRD$)
380      PRINT RT,VRD
390      WRITE #1,RT,VRD
400    CLOSE #1
410    OPEN DFILE$ FOR APPEND AS #1
420 '
430 GOTO 310
440 '
450 CLOSE #1
460 SYSTEM
```

Group Test Program

```
10 DEF SEG=&HC400                                    ' ADDRESS OF GP-IB INTERFACE
20 INIT%=0                                           ' OFFSET OF INITIALIZE ROUTINE
30 TRANSMIT%=3                                       ' OFFSET OF TRANSMIT ROUTINE
40 RECEIVE%=6                                         ' OFFSET OF RECIEVE ROUTINE
50 SEND%=9                                             ' OFFSET OF SEND ROUTINE
60 SPOLL%=12                                    ' OFFSET OF SERIAL POLL ROUTINE
70 ENTER%=21                                          ' OFFSET OF ENTER ROUTINE
100                                        ' GP-IB ADDRESSES OF INSTRUMENTS
110 PRINTER%=1: MY.ADDR%=21: K617%=27
120 BK2032%=6
130 '
140 SYSCON%=0                                   'PC488 ACTS AS CONTROLLER
150 '
160 CALL INIT%(MY.ADDR%,SYSCON%)
180 S$="REN SDC 27"
190 CALL TRANSMIT%(S$,STATUS%)
200                                 'SET-UP ELECTROMETER FOR MEASUREMENT
220 S$="F0X"                                     'SET TO MEASURE VOLTS
230 CALL SEND%(K617%,S$,STATUS%)
270 INPUT "NAME OF DATA FILE?", DFILE$
280 OPEN "O",#1,DFILE$
290 INPUT "ZEROING ELECTROMETER, HIT RETURN WHEN READY", NULL$
300 S$="C1XZ1XC0X"
310 CALL SEND%(K617%,S$,STATUS%)
320 INPUT "HIT RETURN TO BEGIN TEST RUN", NULL$
330 S$="Q7X"
340 CALL SEND%(K617%,S$,STATUS%)
350 S$="G1X"
360 CALL SEND%(K617%,S$,STATUS%)
370 VRD$=SPACE$(12)
380 FOR ELC = 1 TO 25
390         READ PN
400         PRINT"HIT RETURN TO READ PIN";PN
410         INPUT NULL$
420         CALL ENTER%(VRD$,LENG%,K617%,STATUS%)
430         VRD=VAL(VRD$)
440         READ XV,YV
450         PRINT XV,YV,VRD
460         WRITE #1,XV,YV,VRD
470 NEXT ELC
480 CLOSE #1
490 DATA 10,1,1,11,1,2,12,2,1,13,2,2,14,2,3,15,3,1
500 DATA 16,3,2,17,4,1,18,4,2,19,4,3,20,5,1,21,5,2,22,5,3
510 DATA 43,5,4,44,5,5,45,4,4,46,4,5,47,3,3,48,3,4,49,3,5
520 DATA 50,2,4,51,2,5,52,1,3,53,1,4,54,1,5
```
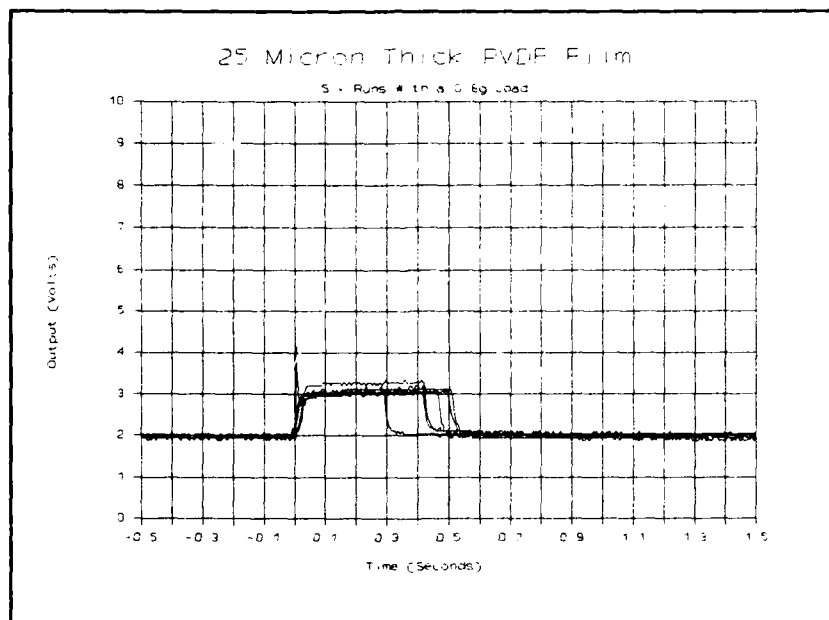
Figure F-1. 25μm Thick PVDF Film With a 0.8g Load.
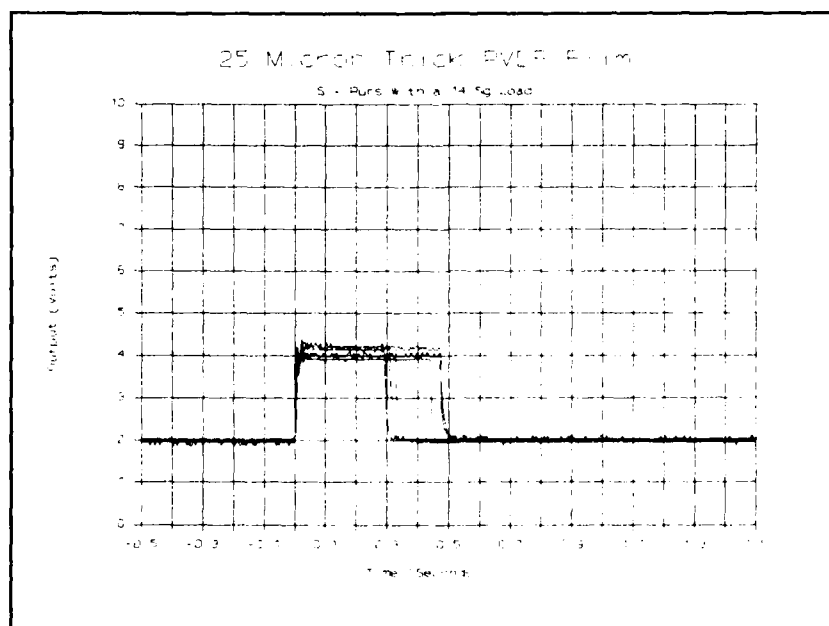
Figure F-2. 25μm Thick PVDF Film With a 14.5g Load.
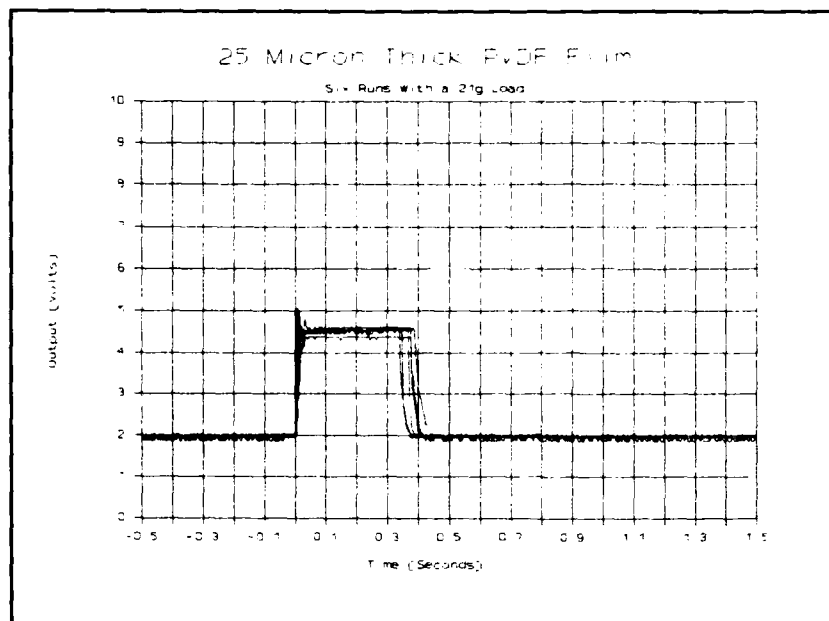
Figure F-3. 25μm Thick PVDF Film With a 21g Load.
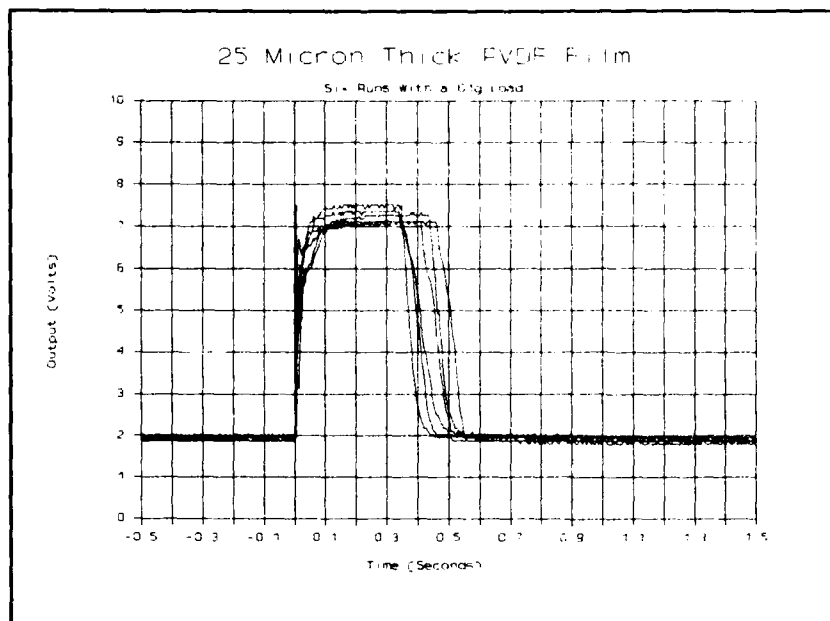

Figure F-4. 25μm Thick PVDF Film With a 37g Load.

F-2
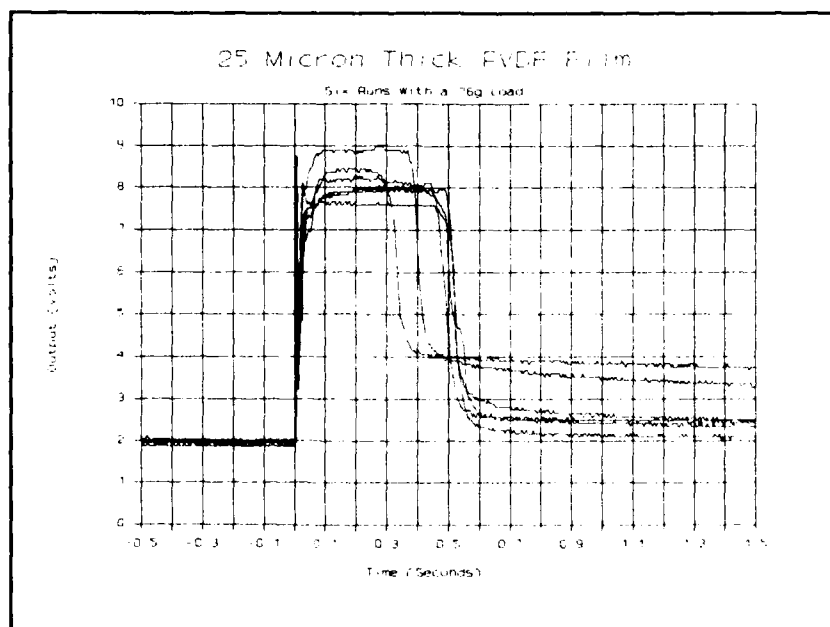
Figure F-5. 25μm Thick PVDF Film With a 61g Load.
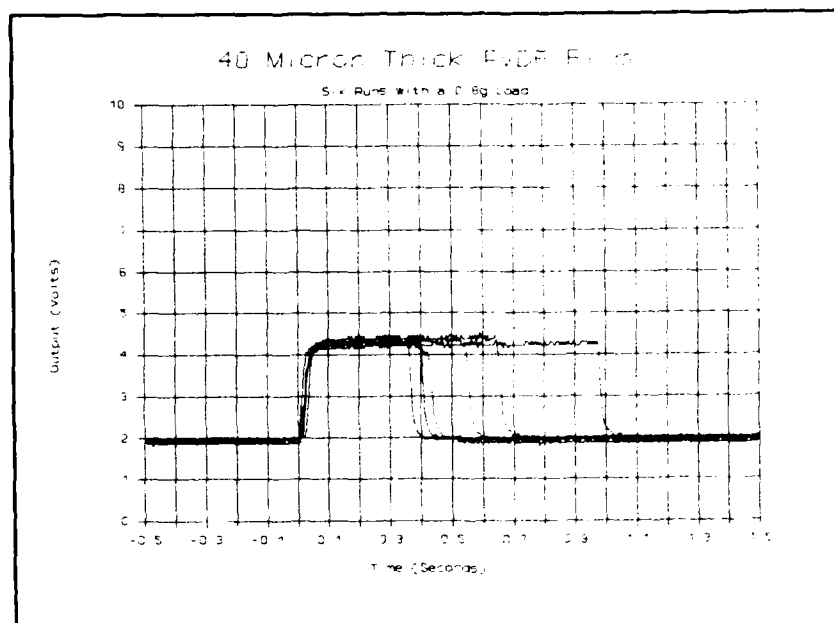

Figure F-6. 25μm Thick PVDF Film With a 76g Load.
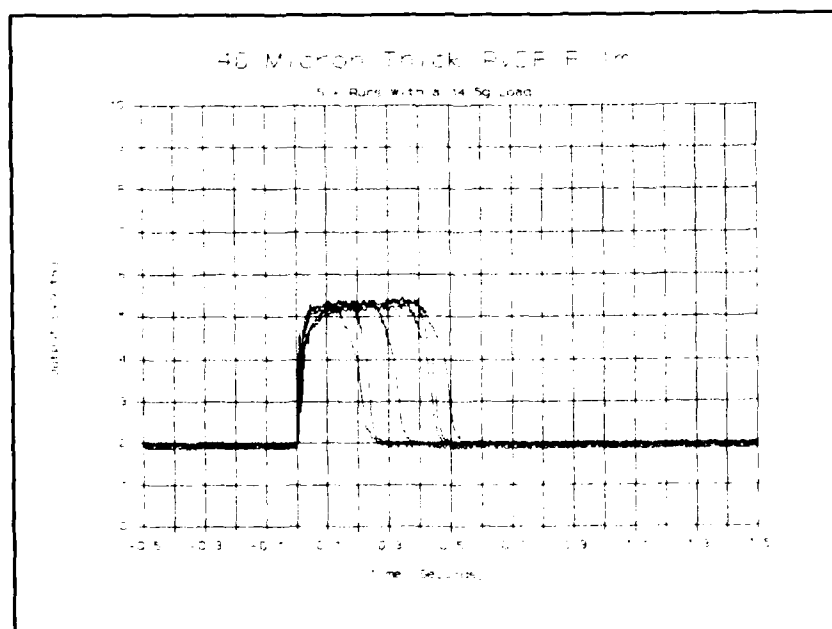
F-3

Figure F-7. 40μm Thick PVDF Film With a 0.8g Load.
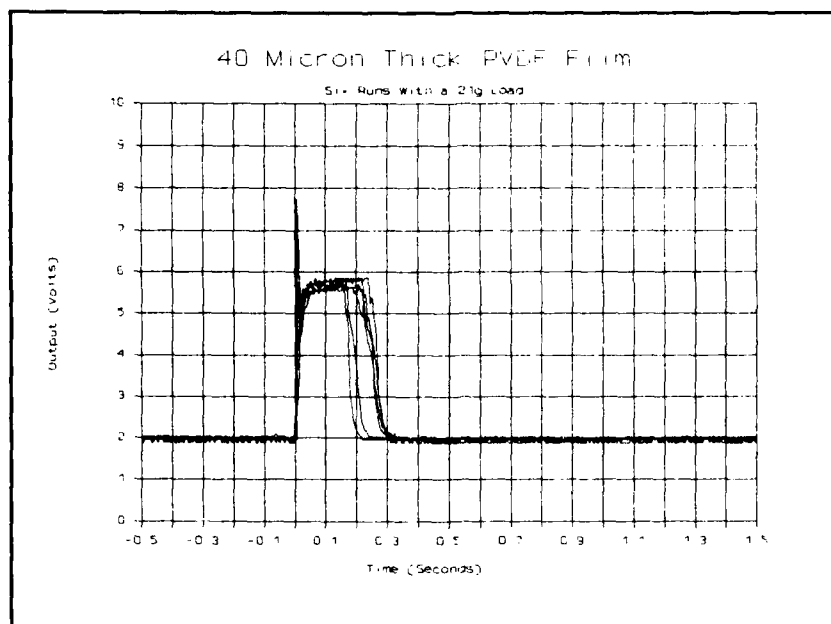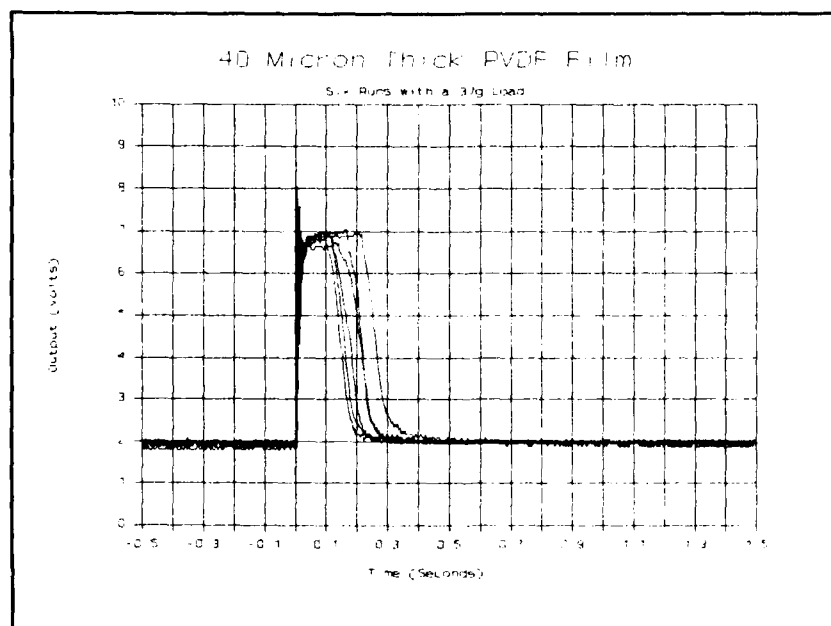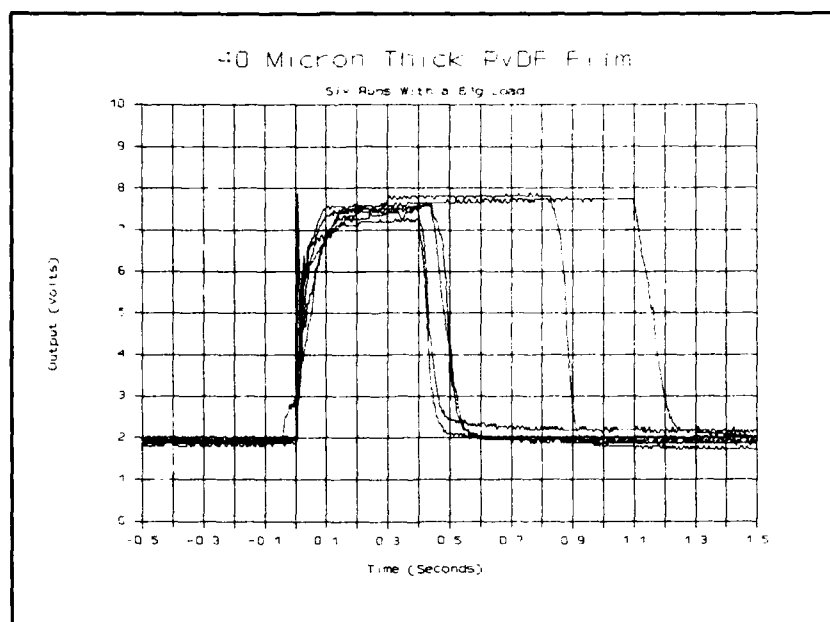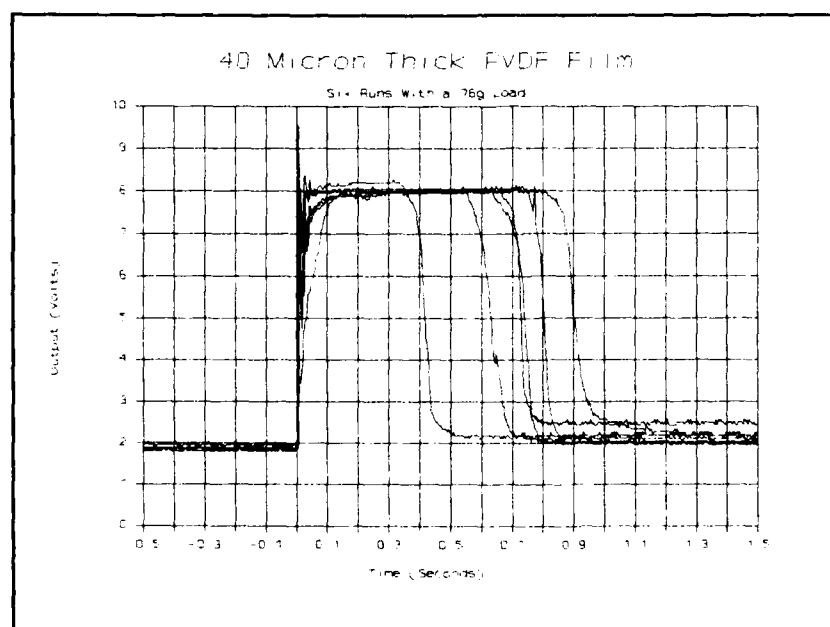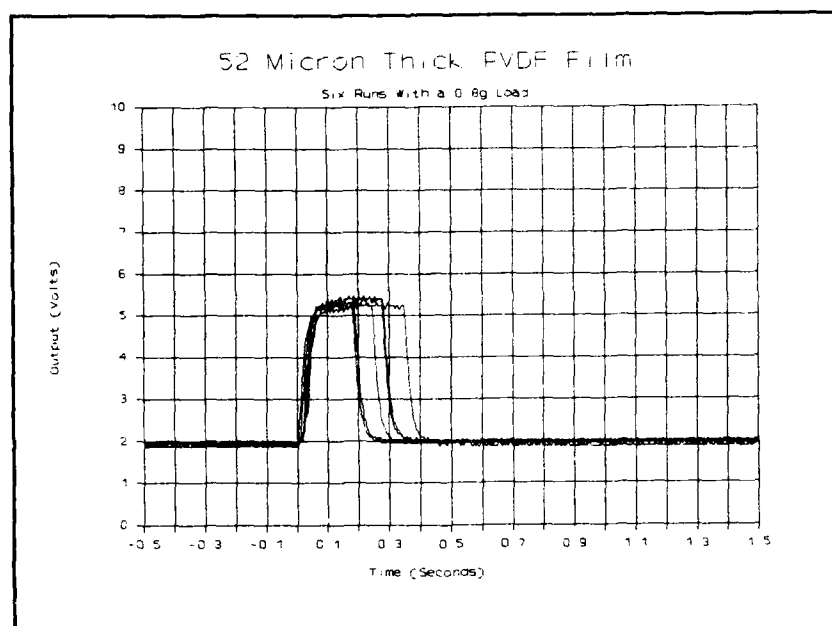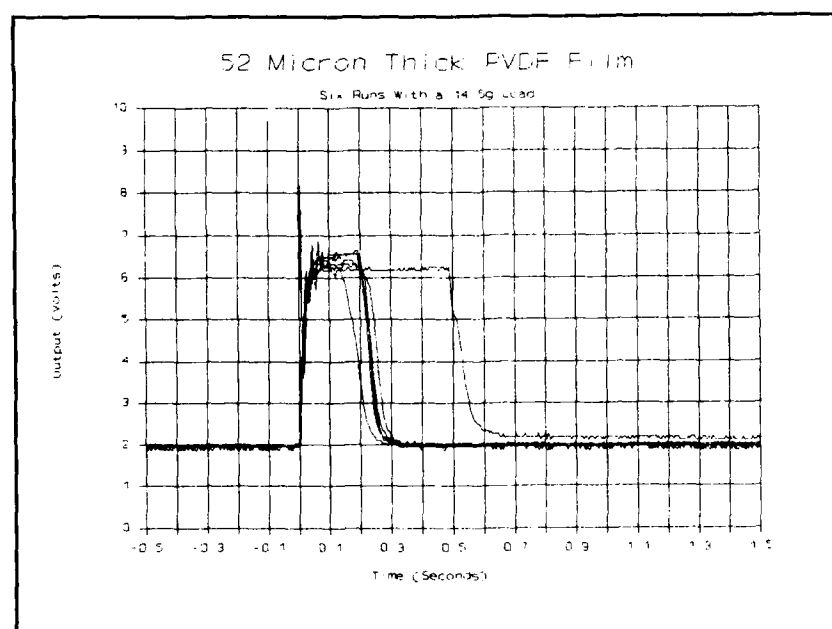

Figure F-8. 40μm Thick PVDF Film With a 14.5g Load.

F-4

Figure F-9. 40μm Thick PVDF Film With a 21g Load.

Figure F-10. 40μm Thick PVDF Film With a 37g Load.

F-5

Figure F-11. 40μm Thick PVDF Film With a 61g Load.

Figure F-12. 40μm Thick PVDF Film With a 76g Load.

Figure F-13. 52μm Thick PVDF Film With a 0.8g Load.
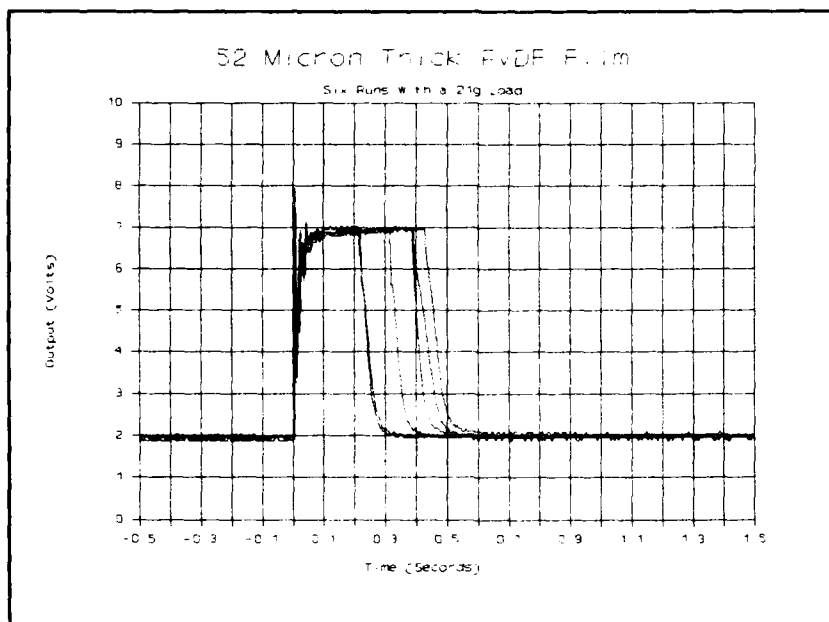

Figure F-14. 52μm Thick PVDF Film With a 14.5g Load.
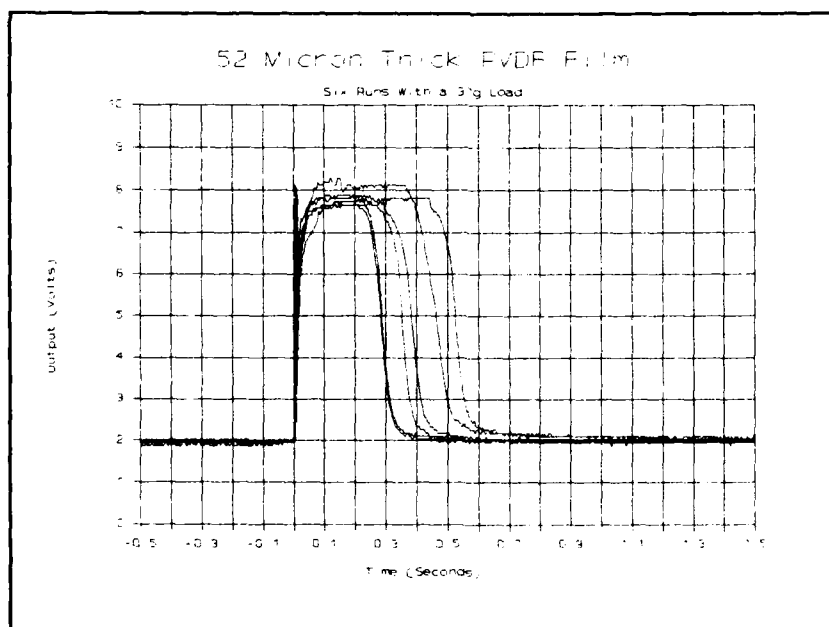
Figure F-15. 52μm Thick PVDF Film With a 21g Load.

Figure F-16. 52μm Thick PVDF Film With a 37g Load.

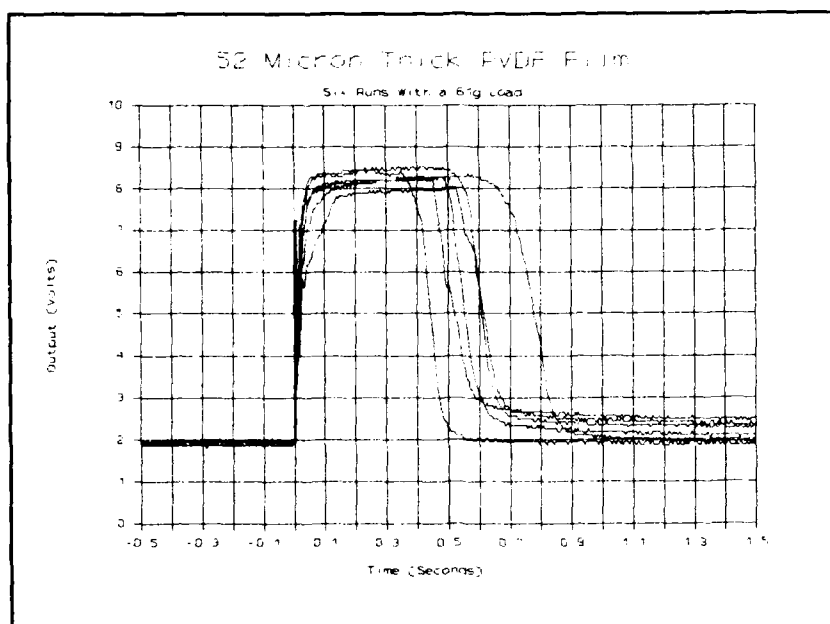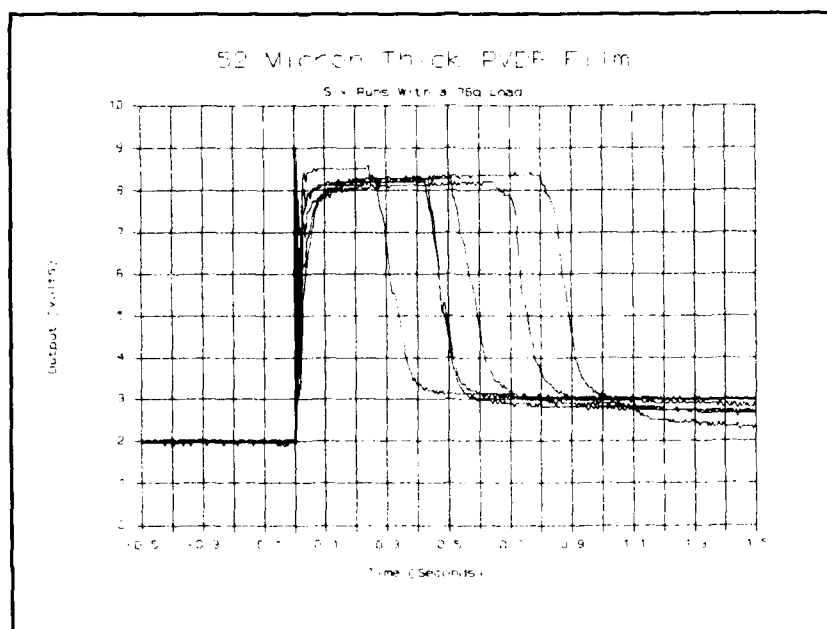F-8

Figure F-17. 52μm Thick PVDF Film With a 61g Load.

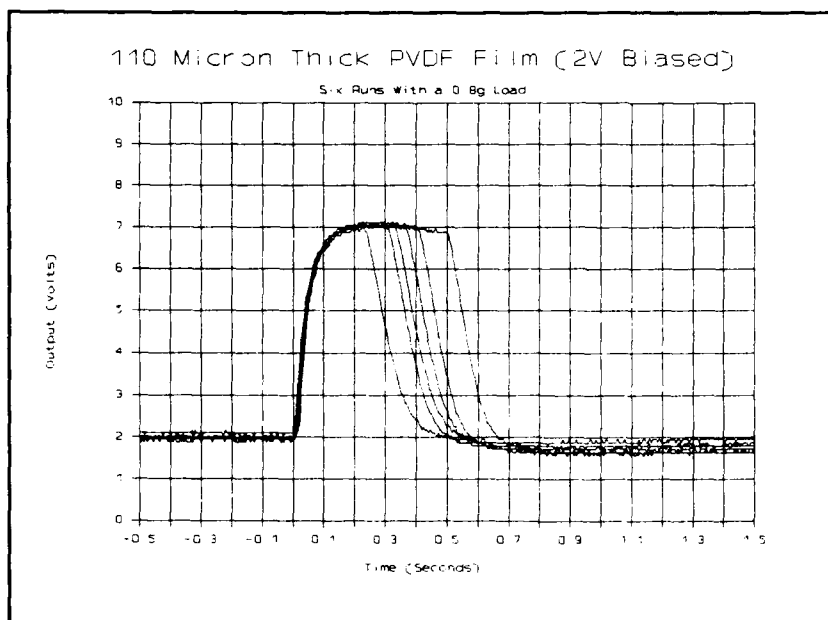
Figure F-18. 52μm Thick PVDF Film With a 76g Load.

F-9
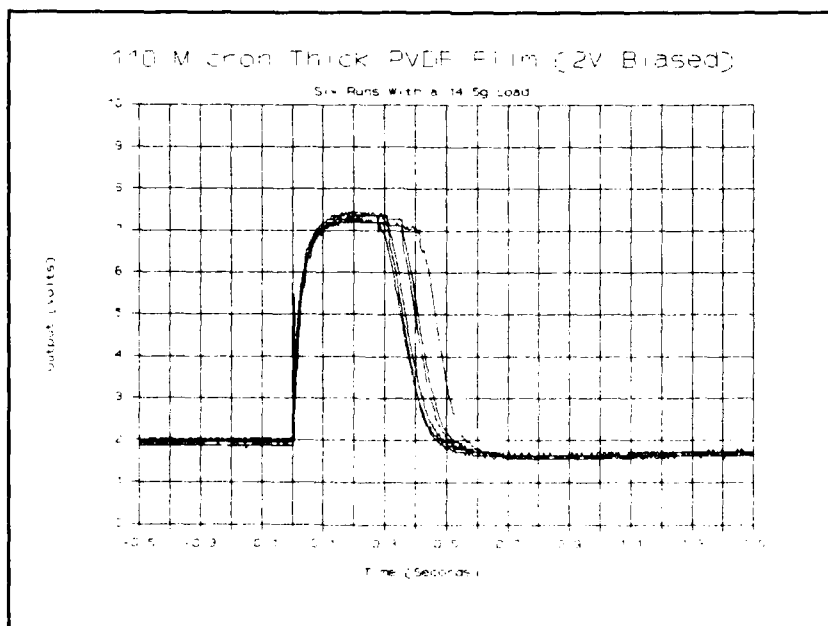
Figure F-19. 110μm Thick PVDF Film With a 0.8g Load.
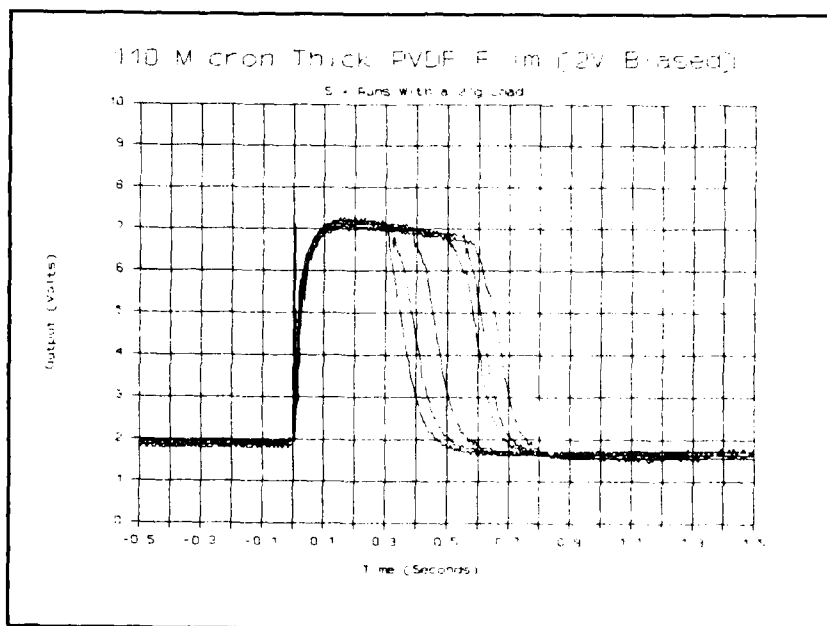

Figure F-20. 110μm Thick PVDF Film With a 14.5g Load.
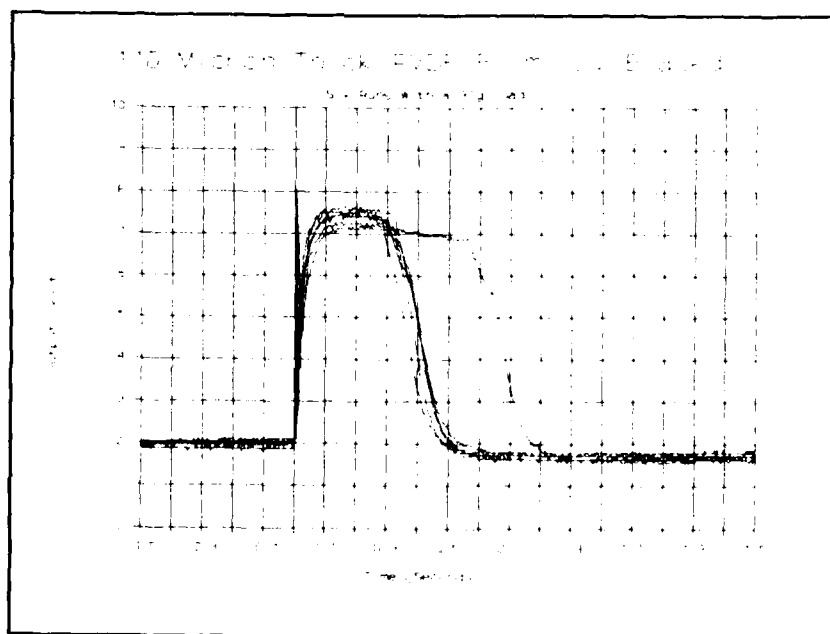
Figure F-21. 110μm Thick PVDF Film With a 21g Load.

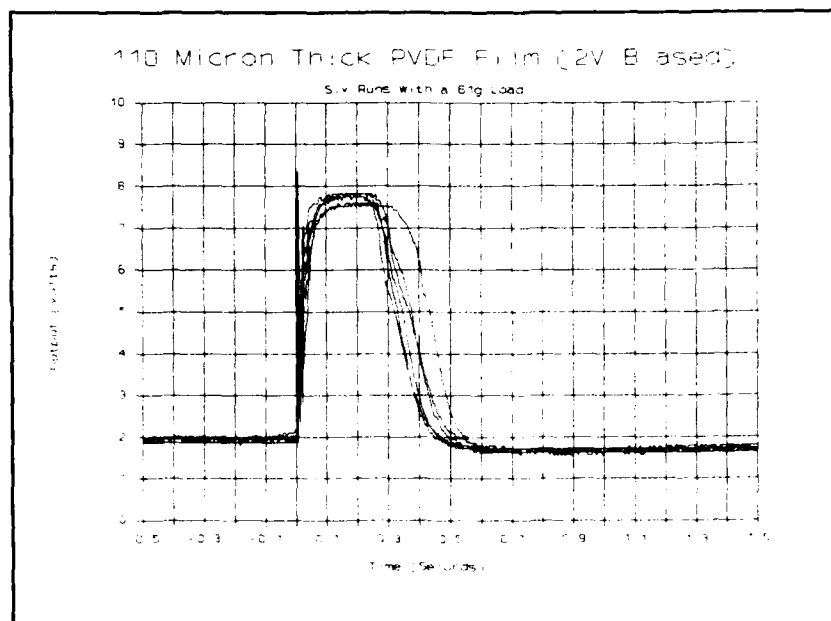Figure F-22. 110μm Thick PVDF Film With a 37g Load.

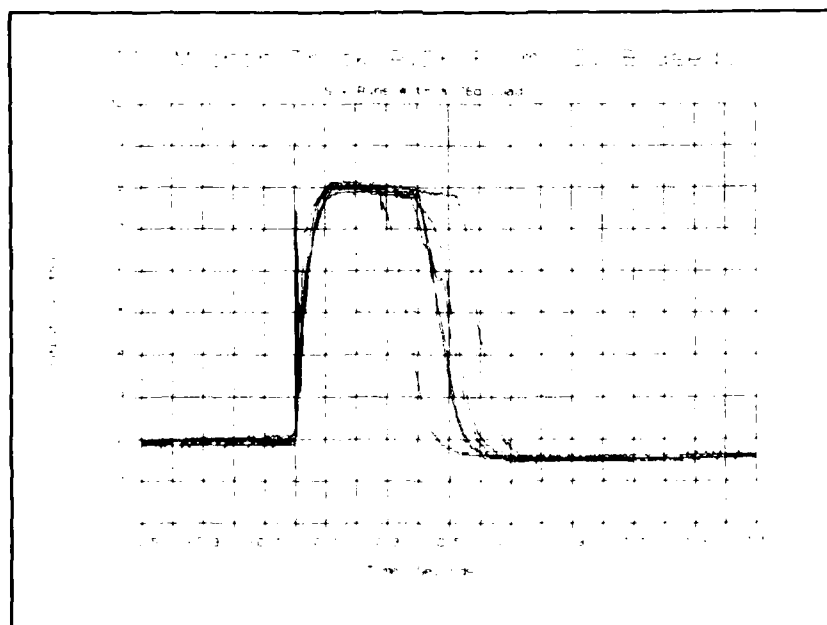Figure F-23. 110μm Thick PVDF Film With a 61g Load.

Figure F-24. 110μm Thick PVDF Film With a 76g Load.

Bibliography

1. Pennywitt Kirk E. "Robotic Tactile Sensing," Byte, 11: 177-200 (January 1986).

2. Barth, Philip W. "Sensor Applications in Robotics," Robotics Engineering: 17-20 (September 1986).

3. Chatigny, J. Victor and Lester E. Robb. "Piezo Film Sensors," Sensors: 50-55 (May 1986).

4. Dario, P. and D. De Rossi. "Tactile Sensors and the Gripping Challenge," IEEE Spectrum: 46-52 (August 1985).

5. McAlpine, George A. "Tactile Sensing," Sensors: 7-16 (April 1986).

6. Dario, P. and others. "Ferroelectric Polymer Tactile Sensors for Prostheses," Ferroelectrics, 60: 199-214 (1984).

7. Pirolo, Capt David G. Piezoelectric Polymer Tactile Sensor Arrays for Robotics. M.S. Thesis, AFIT/GE/ENG/87D-52. School of Engineering, Air Force Institute of Technology (AU), Wright-Patterson AFB OH, December 1987.

8. Osterhout, John K. "Magic: A VLSI Layout Editor," 1986 Berkeley CAD Tools User's Manual. Berkeley, (1986).

9. Mason, Warren P. Piezoelectric Crystals and Their Application to Ultrasonics. New York: D. Van Nostrand Company, Inc., 1950.

10. Cady, Walter G. Piezoelectricity, An Introduction to the Theory and Applications of Electromechanical Phenomena, Volumes I and II. New York: Dover Publications, Inc., 1964.

11. KYNAR Piezo Film Department. Kynar Piezo Film Technical Manual. Pennwalt Corporation, King of Prussia PA, 1987.

12. KYNAR Piezo Film Department. Kynar Piezo Film Technical Manual. Manual 10-M-11-83-M. Pennwalt Corporation, King of Prussia PA, 1983.

13. Kraus, John D. Electromagnetics (Third Edition). New York: McGraw-Hill, 1984.

14. van der Ziel, Aldert. Solid State Physical Electronics (Second Edition). Englewood Cliffs: Prentice-Hall, 1968.

15. Jaffe, Bernard and others. <u>Piezoelectric Ceramics</u>. New York: Academic Press, 1971.

16. Kawai, Heiji. "The Piezoelectricity of Poly (vinylidene Fluoride)," <u>Japan Journal of Applied Physics, 8</u>: 975-976 (May 1969).

17. KYNAR Piezo Film Department. <u>Appendix A, Human Tactile Capabilities</u>. Pennwalt Corporation, King of Prussia PA, 1984.

18. Weste, Neil and Kamran Eshraghian. <u>Principles of CMOS VLSI Design A Systems Perspective</u>. Reading MA: Addison-Wesley Publishing Company, 1985.

19. Tuinenga, Paul W. <u>SPICE: A Guide to Circuit Simulation & Analysis Using PSpice</u>. Englewood Cliffs NJ: Prentice-Hall, Inc., 1988.

20. Millman, Jacob. <u>Microelectronics</u>. New York: McGraw-Hill Book Company, 1979.

21. Solvay & Cie. <u>Solef Piezo Film Principal Properties</u>. Experimental Product Data Sheet. Solvay & Cie, Brussels, Belgium, 1987.

22. KYNAR Piezo Group. <u>Kynar Piezo Film</u>. TR-3M-8-86-PF101. Pennwalt Corporation, King of Prussia PA, undated.

23. KYNAR Plastics Department. <u>Kynar Polyvinylidene Fluoride Chemical Resistance Chart</u>. 25-M-8-85-TR. Pennwalt Corporation, King of Prussia PA, undated.

Vita

Captain Rocky R. Reston was born on ████████████████████ ████████ He graduated from Air Academy High School, Colorado Springs, Colorado in 1980, and immediately entered the United States Air Force Academy where he graduated in 1984 with a Bachelor of Science in Electrical Engineering and a commission in the United States Air Force. Upon graduation, he was assigned to the Radar Test Facility of the 4484th Test Squadron, Tyndall Air Force Base, Florida as an instrumentation engineer. In May of 1987, he entered the School of Engineering, Air Force Institute of Technology.
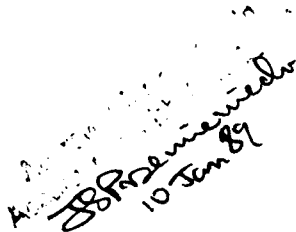
████████████████████████

████████████████

REPORT DOCUMENTATION PAGE		Form Approved OMB No. 0704-0188

1a. REPORT SECURITY CLASSIFICATION UNCLASSIFIED	1b. RESTRICTIVE MARKINGS

2a. SECURITY CLASSIFICATION AUTHORITY	3. DISTRIBUTION/AVAILABILITY OF REPORT Approved for public release; distribution unlimited.
2b. DECLASSIFICATION/DOWNGRADING SCHEDULE	

4. PERFORMING ORGANIZATION REPORT NUMBER(S) AFIT/GE/ENG/88D-41	5. MONITORING ORGANIZATION REPORT NUMBER(S)

6a. NAME OF PERFORMING ORGANIZATION School of Engineering	6b. OFFICE SYMBOL (If applicable) AFIT/ENG	7a. NAME OF MONITORING ORGANIZATION

6c. ADDRESS (City, State, and ZIP Code) Air Force Institute of Technology Wright-Patterson AFB OH 45433-6583	7b. ADDRESS (City, State, and ZIP Code)

8a. NAME OF FUNDING/SPONSORING ORGANIZATION AAMRL	8b. OFFICE SYMBOL (If applicable) CC	9 PROCUREMENT INSTRUMENT IDENTIFICATION NUMBER

8c. ADDRESS (City, State, and ZIP Code) Wright-Patterson AFB OH 45433-6583	10. SOURCE OF FUNDING NUMBERS			
	PROGRAM ELEMENT NO.	PROJECT NO.	TASK NO	WORK UNIT ACCESSION NO.

11. TITLE (Include Security Classification)

See Box 19

12. PERSONAL AUTHOR(S)
Rocky R. Reston, B.S.E.E., Captain, USAF

13a. TYPE OF REPORT MS Thesis	13b. TIME COVERED FROM _____ TO _____	14. DATE OF REPORT (Year, Month, Day) 1988 December	15. PAGE COUNT 123

16. SUPPLEMENTARY NOTATION

17. COSATI CODES			18. SUBJECT TERMS (Continue on reverse if necessary and identify by block number)
FIELD	GROUP	SUB-GROUP	Piezoelectric Materials, Sensors
09	01		Piezoelectric Transducers

19. ABSTRACT (Continue on reverse if necessary and identify by block number)

Title: Robotic Tactile Sensor Fabricated from Piezoelectric
         Polyvinylidene Fluoride Films (Unclassified)

Thesis Chairman: Edward S. Kolesar, Major, USAF

20. DISTRIBUTION/AVAILABILITY OF ABSTRACT ☐ UNCLASSIFIED/UNLIMITED ☒ SAME AS RPT. ☐ DTIC USERS	21. ABSTRACT SECURITY CLASSIFICATION UNCLASSIFIED
22a. NAME OF RESPONSIBLE INDIVIDUAL Edward S. Kolesar, Major, USAF	22b. TELEPHONE (Include Area Code) (513) 255-3576	22c. OFFICE SYMBOL AFIT/ENG

DD Form 1473, JUN 86   Previous editions are obsolete.   SECURITY CLASSIFICATION OF THIS PAGE

(Continued from Block 19)

The purpose of this research effort was to design, fabricate and test a robotic tactile sensor fabricated from polyvinylidene fluoride (PVDF) films coupled to a silicon substrate containing active amplification circuitry. The integrated circuit incorporated 25 sensor electrode pads (0.6mmx0.6mm each) arrayed in a 5x5 grid with a spacing of 0.6mm between electrodes (this corresponds to a spatial resolution four times greater than the human fingertip). The on-board amplification circuitry consisted of a dual MOSFET amplifier (with a gain of 5) for each sensor electrode.

Four different sensor configurations were fabricated and tested. The configurations varied only in the thickness of the PVDF film used (25 microns, 40 microns, 52 microns, and 110 microns). The individual elements of each of the sensor configurations were tested and the sensor based on the 25 micron thick film was considered the optimal sensor of the four. This decision was based on its superior biasing ability and its linear operation over the test loading range (0.8g to 76g). Additionally, there was essentially no coupling between nearest neighbors for all of the sensor configurations. A group loading test (where multiple elements were loaded) was also performed, but problems with obtaining a consistent no-load output across the entire array prevented a true picture of the performance of the sensor. Methods for improving the tactile sensor (including a means for obtaining a consistent no-load output across the entire array) are discussed in the final chapter.